Structural and functional connectivity in patients with glioma

Inaugural Dissertation

zur

Erlangung des Doktorgrades
philosophiae doctor (PhD) in Health Sciences
der Medizinischen Fakultät
der Universität zu Köln

vorgelegt von

Michel Sascha Friedrich

aus Mönchengladbach

Druckerei der Forschungszentrum Jülich GmbH, Jülich

2025

Erstbetreuer:	Univ.-Prof. Dr. med. Norbert Galldiks
Zweitbetreuer:	Prof. Dr. med. Martin Kocher
Gutachter:	Univ.-Prof. Dr. med. Peter Weiss-Blankenhorn
	Univ.-Prof. Dr. med. Thilo van Eimeren
Datum der Mündlichen Prüfung:	01.07.2025

Kurzfassung

Die funktionelle Organisation des menschlichen Gehirns basiert auf neuronalen Verbindungen (Kanten) zwischen kortikalen Regionen (Knoten), bekannt als strukturelle Konnektivität. Diese kann durch Tumorwachstum oder multimodale Behandlungen gestört werden, was zu kognitiven Beeinträchtigungen führen kann. Die funktionelle Konnektivität hingegen ist definiert als die zeitlich korrelierte Aktivität von Knoten, die durch mehrere oder alle anatomischen Kanten zwischen ihnen etabliert wird. Wir stellen die Hypothese auf, dass tumor- und therapiebedingte Läsionen die Integrität der weißen Substanz unterschiedlich beeinträchtigen, was zu einer reduzierten strukturellen Konnektivität und verminderter kognitiver Leistung führt. Darüber hinaus sollte der Grad der funktionellen Konnektivität zwischen tumorinfiltrierten Hirnregionen und betroffenen Hirnnetzwerken mit dem Gesamtüberleben assoziiert sein.

In 121 vorbehandelten Patienten mit rezidivierendem Gliom wurde zunächst die Integrität der weißen Substanz in verschiedenen kortikalen Läsionsgebieten untersucht. Dazu wurde die lokale neuronale Faserdichte mittels modernster Traktografieverfahren bestimmt. Die zugrundeliegenden Traktografien wurden dann zusammen mit den Ergebnissen einer Testbatterie zur kognitiven Leistungsfähigkeit verwendet, um mittels maschinellen Lernens einen Zusammenhang zwischen Kognition und Hirnkonnektivität herzustellen. Für die Untersuchung der funktionellen Konnektivität im Ruhezustand zwischen metabolisch aktiven Gliom-Regionen und Gehirnnetzwerken wurde eine Korrelationsanalyse in einer Untergruppe von 82 Patienten durchgeführt.

Die durch Ödeme und Gliose deutlich beeinträchtigte Integrität der weißen Substanz hatte einen ähnlichen negativen Einfluss auf den Leistungsstatus der Patienten wie die der kontrastmittel-aufnehmenden Gliomanteile. Die verringerte strukturelle Konnektivität zwischen Ruhezustandsnetzwerken erwies sich als kritischer Faktor für die kognitive Leistungsfähigkeit, wobei die Mehrzahl der betroffenen Knoten in der linken Hemisphäre lagen. Zudem blieb die funktionelle Konnektivität im Ruhezustand zu diesen Netzwerken innerhalb der metabolisch aktiven Gliom-Region erhalten, wobei die Konnektivität zu bestimmten Netzwerken mit einem besseren Gesamtüberleben assoziiert war.

Um die Leistungsfähigkeit von Patienten mit Gliomen zu bewahren und den kognitiven Abbau zu verringern, sollte die Behandlungsplanung einen eher netzwerkbasierten Ansatz verfolgen, wobei der Einfluss von Ödemen und Gliose zu berücksichtigen ist. Darüber hinaus liegt ein großes klinisches Potenzial für die Prognose in der funktionellen Konnektivität zwischen der Gliom-Region und dem umgebenden Hirngewebe.

Abstract

The functional organization of the human brain is based on neuronal connections (edges) between cortical regions (nodes), known as structural connectivity. This may become disrupted by tumor growth or multimodal treatments, leading to cognitive impairment. Functional connectivity, on the other hand, is defined as the temporally correlated activity of nodes, established by some or all of the anatomical edges between them. We hypothesize that tumor- and therapy-induced lesions differentially affect white matter integrity, resulting in reduced structural connectivity and impaired cognitive performance. Furthermore, the degree of functional connectivity between tumor-infiltrated brain regions and affected brain networks should be associated with overall survival.

In a cohort of 121 patients with recurrent glioma, the integrity of the white matter in various cortical lesions was initially assessed. For this purpose, the local neuronal fiber density was determined using state-of-the-art tractography methods. The underlying tractographies were then used together with the results of a cognitive performance test battery to establish a relationship between cognition and brain connectivity using a machine learning approach. To investigate resting-state functional connectivity between metabolically active glioma regions and brain networks, a correlation analysis was performed in a subset of 82 patients.

The significantly impaired integrity of the white matter due to edema and gliosis had a similar negative impact on the performance status of the patients as that of the contrast-enhancing tumor parts. Reduced structural connectivity between resting-state networks was identified as a critical factor in cognitive performance, with the majority of affected nodes located in the left hemisphere. Additionally, resting-state functional connectivity to these networks was preserved in the metabolically active glioma region, with connectivity to specific networks associated with improved overall survival.

In order to maintain the overall performance of glioma patients and reduce cognitive decline, treatment planning should adopt a more network-based approach, taking into account the influence of edema and gliosis. Additionally, a great clinical potential for prognostication lies in the functional connectivity between the glioma region and the surrounding brain tissue.

Contents

List of Figures

List of Abbreviations

^{18}F-FDG	2-[^{18}F]fluoro-2-deoxy-d-glucose
19q	long arm of chromosome 19
1p	short arm of chromosome 1
ACT	anatomically-constrained tractography
BOLD	blood-oxygen-level-dependent
CHARMED	composite hindered and restricted model of diffusion
CNS	central nervous system
CPM	connectome-based predictive modeling
CSD	constrained spherical deconvolution
DNA	deoxyribonucleic acid
DTI	diffusion tensor imaging
DW	diffusion-weighted
DWI	diffusion-weighted imaging
e.g.	Latin: exempli gratia, English: for example
ECOG	Eastern Cooperative Oncology Group
EEG	electroencephalogram
et al.	Latin: et alii, English: and others
FET	O-(2-^{18}F-Fluoroethyl)-L-Tyrosin
FLAIR	fluid-attenuated-inversion-recovery
fMRI	functional magnetic resonance imaging
FOD	fiber orientation distribution
HARDI	high angular resolution diffusion-weighted imaging
i.e.	Latin: id est, English: that is

IDH	isocitrate dehydrogenase
MEG	magnetoencephalography
MGMT	O^6-methylguanine-DNA-methyltransferase
MNI	Montreal Neurosciences Institute
MRI	magnetic resonance imaging
MSMT-CSD	Multi-Shell Multi-Tissue constrained spherical deconvolution
PET	positron emission tomography
ROI	region of interest
rs-fMRI	resting-state functional magnetic resonance imaging
RSN	resting-state network
SS3T-CSD	Single-Shell 3-Tissue constrained spherical deconvolution
ST-CSD	Single-Tissue constrained spherical deconvolution
WHO	World Health Organization

Due to copyright concerns, some figures in the introduction have been replaced with references to the corresponding figures in the original publication, compared to the original version of the dissertation.

1 Introduction

We live in an increasingly interconnected world. Roads, power grids and, above all, computer networks facilitate life as we know it today. In this context, connectivity describes the ability of different actors or structures to connect. This concept can also be applied to the human brain. Billions of neurons form a unique network via their axons, which is not yet fully understood in terms of its function. When describing brain connectivity, a distinction is usually made between the spatial and temporal connectivity of brain areas, the so-called structural and functional connectivity. Neurological disorders such as dementia, multiple sclerosis or stroke may affect connectivity in various forms that often lead to cognitive impairments[1]. Brain tumors are another type of disease with equally far-reaching consequences. In patients with brain tumors, the lesion pattern is typically heterogeneous due to the infiltrative growth of tumor cells and the effects of administered treatments. Thus, induced macroscopic structural brain alterations can be detected well with standard anatomical magnetic resonance imaging (MRI) and positron emission tomography (PET) using radiolabeled amino acids.

Nevertheless, microscopic changes in white matter fibers or altered functional organization cannot be detected by standard MRI. This requires special imaging techniques such as modern diffusion-weighted MRI (DWI) or functional MRI (fMRI) in combination with appropriate analysis methods. By means of the latest diffusion models and tractography techniques, it is possible to adequately identify individual fibers tracts of the white matter[2]. Among other measures, this allows to determine the local fiber density, which can be used as a measure of structural changes. Tractography can also be used to create whole brain connectomes that reflect structural connectivity between a wide range of different brain regions, based e.g., on a brain atlas. In combination with machine learning approaches and graph theory, these are powerful tools that can help unravel the effects of structural connectivity changes on cognition.

As repeatedly shown before, brain tumors also affect functional connectivity[3,4]. Here, the emerging field of *Cancer Neuroscience*, focusing on the interaction between tumor cells and the normal brain, is becoming increasingly important. Recent studies focus specifically on resting-state functional connectivity between the tumor region and cortical areas or brain networks and have found an association with survival[5,6]. Different aspects

of the above-mentioned approaches to brain connectivity research have been combined in this work to provide a more detailed picture of the effects of brain tumors on structural and functional connectivity. The newly gained insights contribute significantly to the overall understanding of tumor- and treatment-induced changes in brain connectivity and have the potential to improve treatment planning and prognosis assessment.

1.1 Principles of brain connectivity organization

The brain can be considered as a complex branched network with a hierarchical structure, starting with individual neurons that merge into cortical columns and finally form distinct brain regions. The interactions between these neuronal elements can be described by their structural and functional connectivity at various scales. The physical connection of cortical regions via white matter fiber tracts (groups of axons) is generally referred to as structural connectivity, where the strength of connection can e.g., be quantified by the number of connecting fibers. On the basis of tracing studies, it is additionally possible to assess excitatory or inhibitory postsynaptic effects or the directional strengths of structural connectivity[7]. Functional connectivity, on the other hand, is characterized by the magnitude of correlation of temporal signal fluctuations between two cortical regions as measured by e.g., fMRI, electroencephalogram (EEG) or magnetoencephalography (MEG).

The structural architecture of large-scale brain networks underlying brain functions has been characterized to a certain extent by graph theory, a branch of discrete mathematics and theoretical computer science which is often used to characterize these networks[8] (see Figure 1 in Sporns et al., 2016 Annu Rev Psychol[9]). According to this framework, structural brain connections are defined as edges and interconnected brain areas as nodes. The number of edges connected to a node is indicated by its node degree. The structural connectivity pattern follows a “small-world” behavior with short average path lengths and strong clustering of edges[10]. In addition, groups of nodes are assigned to network communities, so-called modules. The general concept of structural and functional organization of these subnetworks has been described in various publications[7,9,11-13] and can be summarized as follows: Modules are highly connected internally (local integration) and only weakly interconnected via certain critical nodes, the hubs (global integration). In this way, functionally distinct areas are segregated from each other. Considering the hierarchical structure of the brain, the degree of segregation can be further increased by submodules, allowing brain functions to be specified in more detail. Overall, specialized brain functions are represented by local modular integration within an arbitrary scale, whereby functional processing is ensured by short-range edges.

In contrast, perception, cognition and action are associated with the global integration of the modules[7]. Thereby, the neural information flow is mediated via network hubs, which are characterized by a high node degree. These connector hubs are different from provincial hubs, which only support connectivity within a module. Intermodal exchange is further optimized by certain highly interconnected connector hubs. This phenomenon is called rich-club organization and is usually established via long-range structural connectivity. In this way, the functional global integration of the modules is regulated and cognitive processes are optimized[11]. Rich-club nodes were found predominantly in the cingulate and peri-cingulate regions, the medial aspect of the occipital areas, the precuneus as well as in important and specialized brain regions such as the orbitofrontal cortex, the caudate nucleus, and the hippocampus[14].

1.1.1 Relationship between structural and functional brain connectivity

Large-scale brain networks can be either characterized as structural or functional, where connectivity is either represented by the anatomical neuronal connections or by the time series of neuronal activity. The structural and functional connectivity of these network types depends considerably on each other and form the basis for the segregation and integration of brain functions. Nevertheless, there is no simple relation between brain functions, their underlying functional connectivity patterns and the invariant structural brain structure. In this context, convergences and divergences between functional and structural connectivity can be assessed by means of so-called resting-state networks (RSNs)[7,13].

Distinct functional connectivity is not only measurable when the brain is engaged in a specific task, but also when it is supposedly at rest. Based on spatially organized coherent blood-oxygen-level-dependent (BOLD) signal fluctuations of different nodes during a fMRI measurement, circumscribed regions of the whole cerebral cortex can be assigned to different large-scale RSNs[15]. Although different nomenclatures and network definitions exist, the most commonly known networks are the default mode, salience, visual, control, somatomotor and dorsal attention networks. The topography of the RSNs is closely related to the functional specialization of nodes that resemble groups of regions co-activated in a variety of cognitive and behavioral tasks[16,17]. There is also a robust relationship between the structural and functional connectivity of individual components of the multiple RSNs[18-20], whereby the functional connectivity of two nodes correlates with the presence and strength of their structural connectivity[21]. In addition, further analysis suggests a similar hierarchical modularity of RSNs compared to the anatomy of the brain at different scales[22]. Their individual modules consist of synchronously active voxels with a strong, temporally stable coupling, while the RSNs exhibit a less strong

coupling among each other, expressed by a more dynamic and context-sensitive functional connectivity[7,23,24]. The first observation can be attributed to the structural local integration and the second to the global integration of these modules[7], including a rich-club organization based on network hubs that form a coherent sub-network between RSNs[25,26], whereby the participation of networks in the rich-club varies[27].

In addition to a strong convergence between structural and functional networks, there is also a divergence that manifests itself in the dynamic nature of functional connectivity. The relationships between structural and functional networks are less pronounced when looking at the short-term averages of the correlations among spontaneous or resting-state fluctuations compared to the long-term averages[28]. Consequently, the spatial pattern of functional connectivity changes over time, giving it a dynamic character[29]. In addition, functional connectivity can change depending on individual tasks[19] and functional networks can slowly remodel during learning[28]. Various functional connectivity patterns can also be observed depending on how directly functionally connected nodes are structurally connected. For example, the functionally directly connected left motor cortex[30] is only indirectly structurally connected to the right cerebellum. In general, anatomically directly connected nodes have strong functional connectivity, while nodes that are indirectly connected via multiple polysynaptic connections show a wide range of functional connectivity patterns[21,31]. Taken together, different functional connectivity patterns can arise from the invariant structural architecture. Therefore, functional correlation between brain regions is mainly the result of functional relationships along multiple or all anatomical edges that exist between the two nodes[28,32]. In this case, functional connectivity depends not only on the structural presence but also synaptic efficiency of these edges, whereby, e.g., the frequent performance of a task can increase the correlation between co-activated nodes[28,33,34]. This divergence between structure and function throughout the brain enables the emergence of a variety of functional responses and thus flexible cognition[31].

1.1.2 Neurological disorders affecting structural and functional connectivity

The functional organization of the brain that enables cognition is based on a hierarchical-modular architecture in which functional connectivity is constrained by its structural anatomy. Brain dysfunctions due to neurological disorders are therefore also reflected in connectivity disturbances of structural and functional networks. In principal, disorders may be localized due to brain lesions in the affected region, or diffuse causing interruption of the connections between many areas[35]. Of note, the brain provides mechanisms to respond to brain injuries. This phenomenon is known as neuroplasticity

and occurs in various forms, ranging from functional changes in existing structures to the formation and proliferation of new structures[35,36].

Neurological diseases such as Alzheimer's, multiple sclerosis, traumatic brain injury, schizophrenia, depression or autism are clearly associated with disorders in brain connectivity[11,35]. For example, patients with multiple sclerosis exhibit structural changes in network topology in conjunction with an altered structure of “small-world” networks[35,37]. This impairs the efficiency of information transmission and leads to a significant reduction in the efficiency of the network[35,38]. In addition, changes in brain activation and functional connectivity have also been observed in multiple sclerosis[35,39,40]. Another example is Alzheimer's disease, in which the degree of cognitive impairment in later stages was found to be correlated with the disconnection of various brain regions[35,41]. The disconnection was caused by a decrease in the density of dendritic spines in the cortical pyramidal cells and structural changes in the inhibitory circuits[35]. Additionally, the deposition of β-amyloid peptide leads to progressive neurodegeneration, which was associated with a reduced connectivity of the default-mode network[35,42].

In particular, rich-clubs are of great importance in psychiatric and neurological disorders and are mostly affected by altered functional and structural connectivity[11]. Also, pathological lesions occur more frequently in rich-club regions than in peripheral node regions, indicating that brain disorders are more strongly associated with damage to central brain regions[11].

1.2 Primary tumors of the central nervous system

The term cancer is used for a broad spectrum of diseases that can also affect the human brain. It is characterized by the development of a solid tumor consisting of a cluster of cells with uncontrolled cell proliferation that displaces, infiltrates and destroys the adjacent healthy tissue. In general, primary tumors are classified according to their growth characteristics into benign, malignant and semi-malignant tumors. In contrast to malignant tumors, benign tumors exhibit slow, non-invasive cell proliferation, are well delineated and do not penetrate the basal membrane. Nevertheless, displacement of the surrounding tissue and compression of e.g., nerves may cause symptoms. Malignant tumors destroy the surrounding tissue through their rapid invasive growth, whereby nearby blood vessels may be infiltrated. In this way, individual tumor cells can enter the bloodstream and spread throughout the body, forming secondary tumors (metastases) at distant sites. In order to ensure the supply of nutrients for unrestricted proliferation, malignant tumors are able to form their own blood vessels (angiogenesis). Semi-

malignant tumors share most of the characteristics of malignant tumors but rarely develop distant metastases.

A diverse group of tumors arise from the cells of the central nervous system (CNS). Primary CNS tumors are the eighth most common cancer in older adults and the second most common in adolescents and young adults[43,44]. In adults, gliomas are the most frequent primary malignant brain tumor, accounting for 78% of malignant brain tumors. They remain one of the most difficult cancers to treat, with a 5-year overall survival rate of 35% or less[45]. Apart from ionizing radiation[46,47], no other environmental exposure or behavior has been identified as a clear risk factor[48], including the use of cell phones[45,49]. In adults, primary brain tumors can develop as a result of genetic predisposition syndromes (in less than 5% of patients)[45], and there is some evidence that an increased risk may be associated with hereditary factors[50]. The symptoms of patients with brain tumors can be diverse and include headaches (30%), seizures (35%), cognitive decline (36%) and neurological deficits such as aphasia (20%) and motor deficits (20%)[44]. Their occurrence and severity depend on the size, location and growth rate of the tumor[51].

In addition to clinical factors, the prognosis of brain tumors depends on molecular changes such as mutation in specific genes, histologic appearance and cell type of origin. Most of these features are now integrated into the World Health Organization (WHO) CNS tumor classification. The WHO tumor grade ranges from grade 1 to 4, reflecting the potential aggressiveness of the tumor type with increasing grade. Overall survival is inversely related to tumor grade. Other important tumor features relevant to prognosis and classification are molecular changes such as *IDH* (*isocitrate dehydrogenase*) mutational status and 1p/19q co-deletion in gliomas (see also next section). *IDH* is an enzyme that is part of the citrate cycle. It plays a key role in this aerobic pathway and is important for cellular energy metabolism. The *IDH* mutational status comprises two types, the *IDH*-wildtype with a normal enzyme structure and the *IDH*-mutant with a structure altered by mutation. The combined loss of alleles on the short arm of chromosome 1 (1p) and the long arm of chromosome 19 (19q) is known as a 1p/19q co-deletion, which is a form of loss of heterozygosity.

Gliomas arise from glial cells of the brain or spine. The majority of gliomas fall into the category of diffuse gliomas (WHO grade 2-4) with *IDH*-mutant astrocytoma, *IDH*-mutant and 1p19q-codeleted oligodendroglioma and *IDH*-wildtype glioblastoma being the predominant types. Diffuse gliomas are usually characterized by progressive, infiltrative growth and are incurable. The average annual age-adjusted incidence rate in the United States is 5.95 per 100,000 people, with the majority being glioblastomas (3.23 per 100,000 people)[44,52]. They are the most aggressive and deadliest form of glioma with a

median survival time of 14-17 months[53-55] despite aggressive treatment. In contrast, the estimated age-adjusted incidence of *IDH*-mutant gliomas (astrocytoma or oligodendroglioma) is 0.80 per 100,000 people, with astrocytomas slightly dominating[43,44]. Gliomas with mutations in the *IDH* gene (*IDH*-mutant gliomas) grow less aggressively[56], and the 1p/19q co-deletion is associated with a better response to radiotherapy and chemotherapy[57]. Both of these molecular features are therefore associated with a longer overall survival. Meanwhile, *IDH*-mutated gliomas with histopathological grade 3 are also considered lower grade gliomas in addition to grade 1 and 2 tumors due to the long survival time of more than nine years of many patients[44,58].

1.2.1 Brain tumor diagnosis and classification

The diagnosis of patients with brain tumors is usually based on a combination of different imaging techniques and biopsy, where the specimen is analyzed by histological examination including molecular testing. For this purpose, structural MRI with pre- and post-contrast T1- and T2-weighted sequences is the gold standard. Its diagnostic value can be further enhanced by advanced imaging techniques such as perfusion/diffusion MRI and PET[44]. Overall, these modalities enable a better physiological, cellular and microstructural representation[44,59]. As shown in the review by Galldiks et al. (2024 *Neuro Oncol*)[60], which I co-authored, amino acid PET in particular offers considerable added value in the clinical management of patients with gliomas. Unlike contrast-enhanced MRI, the uptake of radiolabeled amino acids does not rely on a disruption of the blood-brain barrier, thus enabling the identification of non-enhancing tumor regions[60]. It is therefore increasingly used to guide invasive diagnostic procedures and treatment planning, e.g., to guide biopsies or to define the target volume for radiotherapy and resection in patients with non-enhancing gliomas[60]. Especially the amino acid O-(2-^{18}F-Fluoroethyl)-L-Tyrosin (FET) developed at Forschungszentrum Jülich[61] is nowadays an established PET tracer for brain tumor imaging[62]. In contrast to 2-[^{18}F]fluoro-2-deoxy-d-glucose (^{18}F-FDG), which is widely used in oncology, FET shows a low uptake in the normal brain tissue, which leads to a considerably improved tumor-to-brain contrast[60]. The most common clinical application of amino acid PET in patients with glioma is the differentiation between relapse and treatment-related changes[63]. Brain metastases are beyond the scope of this work; a detailed discussion on the topic of diagnosis and assessment of post-treatment relapse in brain metastases using PET can be found in another collaboration of mine in the review by Galldiks et al. (2022 *Expert Rev Neurother*)[64]. Amino acid PET also proved to be useful for the differential diagnosis of newly diagnosed brain lesions especially to identify high-grade gliomas[65,66].

The basis for CNS tumor diagnosis is the current WHO classification, which was fundamentally revised in 2021 compared to the previous 2016 edition. The definition of CNS tumor classes relies on various criteria such as age, mutations, tumor location, histology and DNA (deoxyribonucleic acid) methylation. In particular, molecular markers, like the *IDH* mutational status and 1p/19q co-deletion, gained in importance[67]. Specific point mutations are now crucial for the diagnosis of some CNS tumor types, but more often patterns of mutations or other alterations are necessary for diagnostic conclusions[44]. Furthermore, DNA methylation-based classification of CNS tumors enables a histology-independent tumor classification of CNS tumors and has been adopted for a variety of tumor types, especially for unexplained cases[44]. With regard to the present work, the most important aspects of tumor classification are mainly the differences in glioma type grouping between the 2016 and the current 2021 classification (see Figure 2A in van den Bent et al., 2023 Lancet[44]). In the initial classification, gliomas were divided into “diffuse astrocytic and oligodendroglial tumors”, “other astrocytic tumors” and “other gliomas”, which were then reclassified into four new main groups[44]. Therefore, individual tumor types have been removed and several new ones have been introduced, for which molecular characteristics are a prerequisite for diagnosis[44]. The new glioma groups include “circumscribed astrocytic gliomas” and a subdivision of diffuse gliomas into adult-type and pediatric-type (low-grade and high-grade), each with a distinct spectrum of molecular alterations[68]. The three predominant types of diffuse gliomas - *IDH*-mutant astrocytoma, *IDH*-mutant and 1p19q-codeleted oligodendroglioma and *IDH*-wildtype glioblastoma - now represent the adult-type diffuse gliomas. On the other hand, diffuse gliomas of the pediatric type are mostly newly introduced tumor types based on molecular characteristics, and the old groups of “other astrocytic tumors” and “other gliomas” were mostly reclassified as “circumscribed astrocytic gliomas”. Overall, the revised classification reflects the fact that molecular profiling is nowadays essential for determining the biological behavior of a CNS tumor in addition to morphological features from histopathology, immunohistochemistry and radiological imaging[68]. Thus, many brain tumors that morphologically exhibit no features of a higher tumor grade are now diagnosed as high-grade tumors on the basis of a molecular examination[68].

1.2.2 Brain tumor treatment

The histopathological and molecular diagnostic classification of brain tumors is the foundation for the selection of an effective tumor therapy, whereby additional risk factors such as tumor size, residual tumor, age or tumor-related deficits are also taken into account. In general surgery, radiotherapy, chemotherapy, or a combination thereof are applied. The aim of brain tumor resection is to obtain a maximum safe resection of the

tumor to create an optimal starting point for further therapy. This can be achieved, for example, using mapping techniques and intraoperative fluorescence-guided surgery with 5-aminolevulinic acid[44,69]. Moreover, tumor tissue is also obtained during surgery for histological assessment and classification of the degree of malignancy[70]. Radiotherapy is often combined with tumor resection, especially in cases where complete resection is not possible, such as in diffuse gliomas due to their infiltrative growth. Radiotherapy is based on the principle of radiation-induced mitotic death, initiated by breakage of DNA strands in the cell nucleus. This may result in cell death after the next cell cycle. In this way, cell proliferation can be slowed down or stopped, causing the tumor to shrink or disappear completely. Radiotherapy can be applied in two forms, teletherapy and brachytherapy. In teletherapy, cancer cells are irradiated from the outside the body by ionizing radiation, produced for instance by a linear electron accelerator that emits photons or electrons with different energies. In brachytherapy, radiation is administered from inside the body by implanting or inserting encapsulated radionuclides. It should be noted that radiotherapy bears the risk of acute cerebral edema mainly due to blood-brain-barrier damage and late radiation necrosis caused by an inflammatory reaction of the surrounding tissue triggered by tumor cell death. Besides surgery and radiotherapy, chemotherapy is applied using mainly alkylating agents, such as temozolomide or lomustine, that further reduce the tumor burden by eliminating dividing tumor cells.

The decision to combine radiotherapy and chemotherapy is not always trivial, depending among other factors on the *O^6-methylguanine-DNA-methyltransferase* (*MGMT*) promoter methylation status and whether the adverse effects of radiotherapy predominate. The *MGMT* promoter methylation status in patients with brain tumors serves as a clinical biomarker that predicts the efficacy of temozolomide, which is greater in patients with a methylated *MGMT* promoter[44]. Particularly in the case of combined treatment (chemoradiation with temozolomide) with maximum safe resection, the standard-of-care treatment for glioblastomas, treatment-related changes such as pseudoprogression or radiation necrosis must be expected[71]. Pseudoprogression characterized by an increase of contrast enhancement on MRI, which resolves spontaneously without any change of treatment. Unawareness of this phenomenon may lead to considerable misinterpretation of further treatment planning. For example, my contribution to the publication of Flies et al. (2024 *Neuro Oncol*)[71] showed a higher rate of treatment-related changes in *MGMT*-promoter methylated glioblastomas additionally treated with the antiangiogenic drug cilengitide than in glioblastomas treated with the standard-of-care.

Beyond the standard therapies, experimental therapies such as immunotherapy and various targeted therapy options are also available. Ongoing research is focused on a better understanding of factors that are important to overcome treatment resistance, such as the immunosuppressive tumor microenvironment, the molecular heterogeneity of tumors, and the role of microtube network connections between cells in the tumor microenvironment[44]. In addition, studies on immunotherapy of CNS tumors with checkpoint inhibitors and vaccination studies have been performed but have so far shown no improvement in treatment outcomes for patients with glioblastoma[44].

1.3 Tumor effects on brain connectivity

Considering the hierarchical structure of the human brain, tumors can affect connectivity at different levels, leading to disruptions of structural and functional connectivity. In particular, the white matter tracts, which play a decisive role in neurological functions, can be spatially and functionally affected by brain tumors. Therefore, pre- and intraoperative mapping of the tumor and white matter tracts is frequently performed to avoid neurological deficits during tumor treatment.

1.3.1 Structural effects

Disturbances of white matter tract integrity may appear in four general patterns: displacement, edematous affection, tumorous infiltration and disruption of neural fibers[72] (see Figure 18 in Jellison et al., 2004 Am J Neuroradiol[72]). Displacement of otherwise intact fiber tracts occurs most frequently in all types of gliomas[73]. In contrast, the edematous pattern describes the widening of fiber tracts that run partially through or around the tumor without a change in their position and orientation. This is most common for metastasis[73]. White matter tracts can also pass directly through the tumor, either remaining identifiable or being completely disrupted, patterns associated with astrocytomas and glioblastomas[73].

Diffuse gliomas in particular spread continuously along the white matter tracts and recur even after complete resection[74]. This pathophysiological mechanism has been found to rely on various mechanisms of tumor cell migration and invasion[74-77]. The evaluation of structural connectomes, which reflect the white matter architecture, revealed that glioblastoma-related connectivity disturbances extend beyond the focal lesion into the normal-appearing brain up to the contralateral side[74]. Pathways connecting distant cortical brain regions are most likely to be disrupted and the amount of disruption correlates with overall survival[74,78]. In the case of diffuse gliomas of all grades, a recurrence may also develop far from the primary tumor in distant brain regions[74]. Thus, the far-reaching white matter tracts in particular offer the possibility of long-distance

migration of tumor cells. Furthermore, brain regions with high tract density are involved in long-range white matter tracts (e.g., arcuate and superior longitudinal fasciculus and callosum), and glioblastoma-related lesions in these areas were found to result in reduced survival, consistent with the finding that tumors spread along white matter tracts[74].

1.3.2 Functional effects

Brain tumors also have an impact at the functional level and lead to connectivity alterations in individual resting-state networks (e.g., default mode network), accompanied by an impairment of the associated functional domain (e.g., language or attention)[79,80]. Multi-network approaches also showed that functional networks far away from the tumor site up to the contralateral hemisphere can be functionally altered[81-84]. There was also evidence of functional connectivity between tumor-infiltrated regions and resting-state networks, whereby the level of preserved functional connectivity was associated with better overall survival[85]. Specifically, in remote brain regions, functional connectivity correlated positively or negatively with overall survival depending on the remote brain region[6,83]. Furthermore, white matter tracts and functional brain networks impaired by tumor- and treatment-related brain lesions affect health-related quality of life in patients with glioma, as the paper I co-authored by Heinzel et al. (2023 *J Neurooncol*)[86] showed. Here, especially T2/fluid-attenuated-inversion-recovery (T2/FLAIR) signal alterations affecting structural and functional networks in the right hemisphere were associated with reduced health-related quality of life scores in most functional domains, with the exception of communication ability.

Beyond that, brain tumors also show functional interactions with neurons at the synaptic level. For instance, glioma cells integrate themselves electrically into neuronal circuits via synaptic connections[87-89]. Through a bidirectional neuron-to-glioma interconnection, glioblastoma might enhance synaptic activity resulting in an increase (if excitatory pathways) or decrease (if inhibitory pathways) functional connectivity[74]. Moreover, tumor proliferation is promoted by membrane depolarization of excitatory electrochemical neuron-glioma synapses, and paracrine signaling, depending on neuronal activity, which may also contribute to glioma progression[89-92]. It was also shown that brain regions with many synapses have a higher metabolic demand and a higher turnover of glial cells, which affects the risk of brain cancer[74]. This observation was derived from the significant spatial relationship between connectivity hubs, gene expression in terms of metabolic activity, synaptic signaling and development of gliomas[93-96]. Glioblastomas preferentially occur in functional networks, with a higher frequency in associative networks or more

specifically in connector hubs[93,94] that are generally important for the integration of cognitive functions[74].

1.4 Brain connectivity imaging and analysis

The measurement of brain connectivity is primarily based on special MRI techniques that, in contrast to simple structural MRI, take into account molecular processes in order to resolve the cortical microstructures and functions. DWI in particular is well established for the non-invasive assessment of structural connectivity and fMRI for functional connectivity. Other frequently used functional measurement techniques are electrophysiological methods such as EEG, and MEG. In conjunction with adequate data analysis approaches, e.g., based on tractography, machine learning or correlation, it is possible to detect tumor and treatment effects on brain connectivity.

1.4.1 Diffusion-weighted imaging and diffusion models

DWI is an established technique in medicine and neuroscience that enables the mapping of neuronal fiber orientations on the basis of water molecule diffusion. According to Brownian motion, the change in the position of the water proton spins results in a loss of signal intensity due to their molecular movement measured by diffusion-sensitizing gradients[97]. The diffusion-weighted signal intensity S_i with the diffusion-sensitizing gradients applied along direction i can be described for each voxel in the most straightforward manner by the following exponential equation (Equation 1)[97]:

$$\boldsymbol{S_i = S_0 \cdot e^{-b \cdot D_i}} \qquad \text{(Equation 1)}$$

S_0 represents the signal intensity measured without the diffusion-sensitizing gradients, D_i denotes the diffusion coefficient in direction i, and b defines the b-value, which is a measure of the diffusion weighting[97]. The latter depends on the strength, duration and time interval of the diffusion-sensitizing gradients. Water molecules diffuse mainly in and along the structures of the white matter tracts. Their behavior differs significantly from unrestricted Brownian motion due to interactions with various tissue components in the body. As a result, the diffusion rate along the fibers is faster than perpendicular to them. This directed diffusion is called anisotropic diffusion. In contrast, isotropic diffusion, which is characterized by uniform diffusion in all directions, occurs in the cerebrospinal fluid and gray matter. In DWI, these various diffusion patterns provide information that makes it possible to characterize the structural organization of the brain on a microscopic level.

There are several mathematical models for estimating white matter fiber orientation from DWI data. The most popular model is the diffusion tensor model, which serves as the

basis for diffusion tensor imaging (DTI), a technique widely used in clinical practice due to its ability to map fiber orientation in several major white matter structures[98,99]. The diffusion tensor corresponds to an ellipsoid whose diameter in each direction describes the anisotropic diffusion of water molecules along the white matter fibers in that direction (see Figure 1 in Jellison et al., 2004 Am J Neuroradiol[72]): It is based on a symmetric 3 × 3 matrix derived from diffusion measurements in at least six non-collinear directions[72]. The eigenvectors (ε_1, ε_2, ε_3,) from the diagonalization transformation of the diffusion matrix (D) denote the major, middle and minor principal axes of the tensor and the related eigenvalues (λ_1, λ_2, λ_3) indicate the diffusivities along the three axes[72].

Despite its broad clinical application, the diffusion tensor is fundamentally limited a priori by the fact that it can only resolve a single dominant fiber orientation within an image voxel[100-102] (see Figure 1B in Farquharson et al., 2013 J Neurosurg[103]). At current scanner resolutions of 2-3 mm, at least 90% of white matter voxels contain multiple fiber orientations[104], leading to erroneously missing or anatomically implausible fiber tracts during the fiber mapping[103,104]. A much preferable approach is to estimate fiber orientation directly from high angular resolution diffusion-weighted imaging (HARDI) data[105,106]. In contrast to the six gradient directions required by DTI, HARDI is based on at least 50 directions, which allows a much more accurate representation of the fibers in a voxel. To determine the relative proportion of fibers passing through the voxel in different directions, an advanced diffusion model based on rotational and spherical harmonics, called spherical deconvolution, can be used[106,107]. Spherical harmonic are special functions defined on the surface of a sphere, while spherical deconvolution is a mathematical operation that recovers the original signal from a measurement that is the result of a known modification (convolution) of that signal.

Accordingly, the fiber orientations of an image voxel, expressed by the fiber orientation distribution function (FOD), can be calculated under the following assumption (Equation 2): The measured diffusion-weighted signal (S) is given by the spherical convolution of the signal expected from a voxel containing a single coherent fiber bundle (response function, R) with the FOD (f) of a given voxel[105,106].

$$\boldsymbol{S} = \boldsymbol{R} \otimes \boldsymbol{f} \qquad \text{Equation 2}$$

Finally, the FOD is derived by an inverse convolution operation known as spherical deconvolution (Equation 3), in which the response function is used as a kernel to extract the white matter FOD from the measured diffusion-weighted signal within each voxel[105,106]. For this purpose, the response function can be estimated directly from the diffusion-weighted image data.

$$\boldsymbol{f = R \otimes^{-1} S}$$ Equation 3

In advanced diffusion models, a modified Tikhonov regularization method is usually applied to minimize the susceptibility of the spherical deconvolution to noise[108]. This is called constrained spherical deconvolution (CSD) since the false negative lobes caused by noise at the FODs are not completely removed, but constrained[108]. In this way, angular resolution is maintained, allowing fiber orientations separated by a smaller angle to be resolved. In contrast to other advanced diffusion models, such as Q-ball imaging[100], this also enables the use of lower b-values around 1000 s/mm^2 [106]. CSD also does not require a wide range of b-values like diffusion spectrum imaging[109] or the composite hindered and restricted model of diffusion (CHARMED)[110]. Both of these requirements are difficult to achieve on clinical systems and would result in impractically long scan times[106]. In addition, these models are based on the q-space formalism, which, among other shortcomings, does not allow the resolution of fibers with a crossing angle greater than 90 degrees[111]. There are also several tensor matching algorithms[112-114] but they can only resolve up to two different fiber orientations[105].

1.4.2 Tractography

Tractography enables non-invasive mapping of white matter fiber tracts derived from DWI data that have been processed by a diffusion model. In the case of an advanced CSD model, the resolution of complex fiber architectures during tractography is based on the FODs, which represent the estimated fiber orientations in each image voxel. This is much more accurate than simple DTI-based tractography, which results in a significant underestimation of actual white matter fibers due to its inability to resolve multiple fiber orientations (see Figure 4 in Farquharson et al., 2013 J Neurosurg[103]). In general, a tractography algorithm begins by identifying suitable starting points for the fibers to be computed, called seeds. Fibers are then propagated along the estimated fiber orientations of each voxel and terminated according to certain criteria, such as the FOD amplitudes. These depend on the tissue properties and decrease in comparison to the white matter within the cerebrospinal fluid or gray matter.

Fiber mapping is either deterministic or probabilistic, which determines how a connection between two brain regions is established. Most tractography algorithms use a deterministic approach, in which only a single fiber is propagated per seed. In contrast, probabilistic algorithms are generally an extension of this approach, which is in principle no more accurate, since they are based on the same underlying concept and constraints. However, the advantage lies in the intended use. Connections between any two brain regions are much less likely to be identified by deterministic approaches, so they are

often applied to investigate the status of known prominent tracts according to region of interest (ROI) based mapping protocols[115]. In contrast, probabilistic tractography can identify tracts at any distance from the seeds[115]. Instead of estimating a single path for each seed, the probabilistically estimated fibers are based on probability distributions where the direction of each step within the propagation is randomly selected from a set of probable orientations[115]. The estimation of the distribution of probable connections results from the generation of many fibers from the same starting point[115]. The connection between a brain region and the seed point is finally determined on the basis of the density of the resulting fibers, whereby a higher density is associated with a higher connection probability[115].

To increase the accuracy of a tractography, an advanced approach is to take into account the biological characteristics of the brain tissue, which enables even more precise termination and propagation of the neural fibers. This can be achieved with a specialized tractography algorithm called anatomically-constrained tractography (ACT)[116]. It allows the identification of predominantly biologically plausible fibers based on anatomical information about brain tissue types (see Section 3.2.3).

1.4.3 Structural connectomes and fiber density images

For subsequent evaluation, the tractography images can be converted into brain connectomes. This requires them to be combined with a parcellation, which divides the brain into individual parcels (regions). It is provided, e.g., by a brain atlas or can be self-generated. In this way, the calculated fibers (edges) between the individual brain regions (nodes) of the parcellation can be analyzed. For this purpose, graph theory offers a large repertoire of indicators that describe the structural connectivity of such networks, including degree (number of edges connected to a node), shortest path length (measure for integration), clustering coefficient (measures for segregation), etc.[117]. The most common approach in connectome analysis is to quantify the connection strength between all brain regions and, for example, to correlate them with the location of lesions such from tumors or strokes or to compare structural connectivity between two groups, e.g., patients with healthy controls. The quantification usually takes the form of a connectivity matrix, which is mirrored on a diagonal of zeros and plotted as a square divided into four quadrants (Figure 1). The upper left quadrant corresponds to the strength of the connections within the left hemisphere, and the lower right one to those of the right hemisphere. The other quadrants show the strength of inter-hemispheric connections. The connection strength can be specified both relatively or as an absolute number of edges between two nodes.

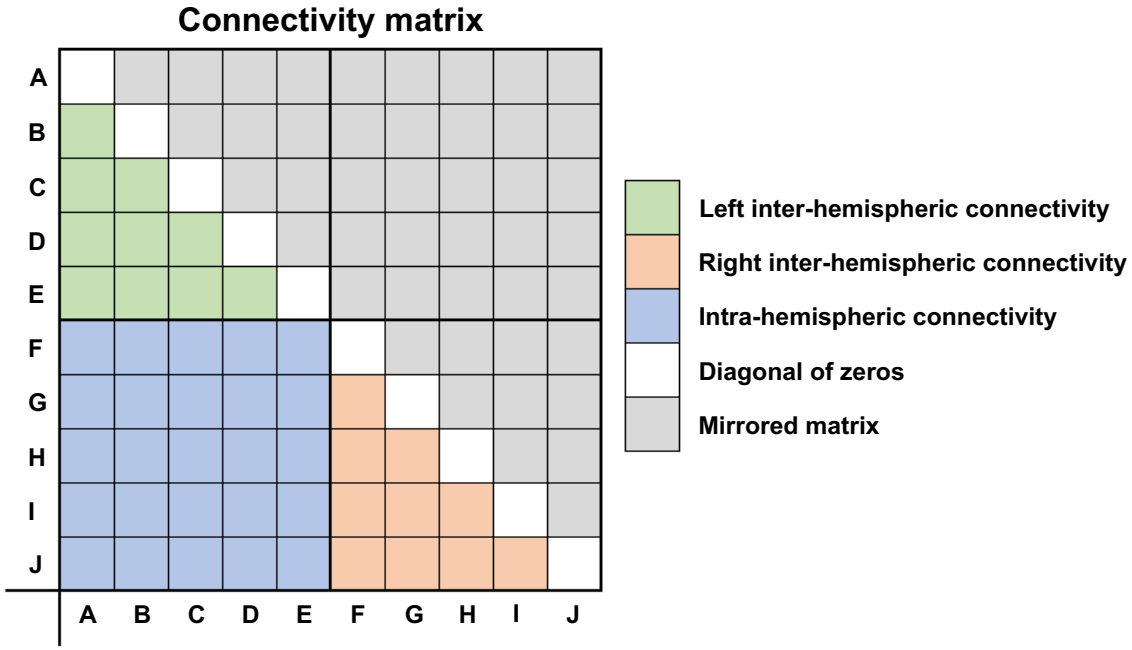

Figure 1: Schematic 10x10 connectivity matrix.
Nodes are labelled from A to J. Each field contains the edge weight of the respective node pair, e.g., expressed by the number of fibers (structural connectivity) or the correlation quotient (functional connectivity).

There are also binary connectivity matrices that only indicate whether a connection exists. Another approach for analyzing tractographies is to convert them into tract density images[118,119] (Figure 2). This allows the integrity of local structural connectivity to be measured. The pseudo-colorized image contrast in these images is based on the number of fibers per voxel.

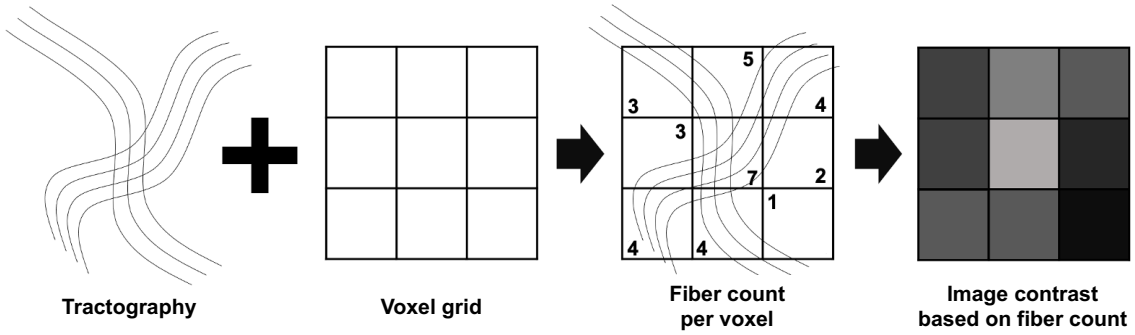

Figure 2: Generation of white matter fiber density images.
For this purpose, a tractography is superimposed on a voxel grid with a freely selectable resolution. Subsequently, the fibers per voxel are counted and color-coded accordingly, resulting in a fiber density image where the image contrast is based on the number of fibers.

1.4.4 Predictive models from structural connectomes

In addition, an important goal of modern neuroscience is to establish relationships between individual differences in behavior and brain structure[120]. Accordingly, correlations between measurements of individual structural differences and cognitive functions can be established on the basis of tractography data and cognitive

performance tests, for example. Often, the high dimensionality of the data requires the application of machine learning methods, including cross-validation of correlation or similar regression models, which tend to overfit the data and render generalization difficult[120]. Cross-validation, in contrast to simple correlation, is a conservative approach in which the strength of a relationship is validated in an independent sample which has not been used for training the model[120]. A robust machine learning approach with built-in cross-validation to relate individual behavior to brain connectivity is the “connectome-based predictive modeling” (CPM) approach published by Shen and colleagues[120]. According to the published protocol, the method can be summarized as follows (see Figure 1 in Shen et al., 2017 Nat Protoc[120]): The behavioral measurements of each subject and their connectivity matrices, which can be derived from structural connectomes, serve as input. These input data must be split into a training and test set. For feature selection, each edge in the connectivity matrices is related to the behavioral measures of all training subjects to determine the significant edges that are relevant to the behavior. These features are summed up to a single connectivity value in each subject. Afterwards, a prediction model is created that assumes a linear relationship between the single subject value and the behavioral score of the training set. Following the cross-validation approach, the connectivity values of the individual subjects from the test set are inserted into the model to predict their behavioral scores.

1.4.5 Functional magnetic resonance imaging

fMRI enables the measurement of brain activity in vivo and represents another essential non-invasive imaging method alongside DWI that can be used to investigate brain connectivity. It provides further insight into the basic mechanisms of brain function and can expand our understanding of how the brain generates behavior, as well as offering the opportunity to study pathological changes in brain activation[121]. In patients with glioma, fMRI is often used for preoperative planning to determine the individual functional anatomy of the motor and language network so that these functionally eloquent areas can be preserved[121].

fMRI is based on the BOLD signal, describing the dependence of the MRI signal on the blood oxygen level. Accordingly, neuronal activity and the associated synaptic potentials at the microscopic level trigger a local increase in blood flow to meet the neurons' oxygen demand for the transmission of action potentials and generation synaptic potentials. This leads to an increase in the blood oxygen level, as more oxygen is supplied than is consumed. In contrast to the paramagnetic deoxygenated state of haemoglobin, its oxygenated state is diamagnetic, which leads to a deviating behaviour in a magnetic field. In this way, neuronal activity can be measured indirectly via the altered oxygen

level of the blood, which is expressed by the BOLD signal in the MRI[122]. In its measurement, two different methods are applied, task-related and resting-state fMRI (rs-fMRI). The task-based fMRI generates a statistical map of the localization of neuronal activation by comparing the BOLD activity during the task with the activity at rest. This allows, for example, to assess the functional integrity of the neural networks involved in the information processing of the task being performed[121]. Similar BOLD activity of brain regions may also be used as an indicator for functional connectivity, which is often investigated by measuring the spontaneous BOLD fluctuations when the subject is at rest and not performing any task[122]. These fluctuations were found to be spatially organized in RSNs[15], where their location was found to be closely associated with the functional specialization of cognitive and behavioral tasks[16,17]. Resting-state fMRI enables the simultaneous assessment of multiple functional networks, whereas task-based fMRI uses a measurement with a specific task in order to capture a specific functional system[121].

The easiest way to determine similarities between two BOLD signals is to use Pearson correlation to check whether their time series correlate with each other. Beside this, many other more advanced analysis methods exist that fall into two broad categories: voxel based and node-based functional connectivity methods[122]. The latter is again based on graph theory and is comparable to the generation of structural connectivity matrices. This includes the definition of nodes via atlas parcellations or directly from the functional data, the definition of edges based on correlation similarities between two nodes, and the generation of a functional connectivity matrix with edge weights (correlation strengths) between each node combination[122] (Figure 1). Various other node-based analyses can be applied to the matrix, including those already known from structural connectivity analysis, such as graph-theoretical analyses or the CPM approach to relate functional connectivity to behavioral data. The voxel-based methods, on the other hand, generate a connectivity map of the brain with functional connectivity values for each voxel. Most common here is the seed-based correlation analysis in which the functional connectivity between a brain region (seed) and all voxels in the brain is considered[122]. This analysis is based on three steps (Figure 3): First, a seed region is defined, e.g., a prominent cortical region such as an RSN or a lesion in the form of a tumor or stroke. Secondly, the mean BOLD time series is extracted from the seed region and finally correlated voxel by voxel with each time series of the brain to obtain a connectivity map. This map describes the strength of the functional connectivity of each brain voxel in relation to the seed region. Or in other words, in this way connectivity between each voxel in the brain and the seed region can be characterized.

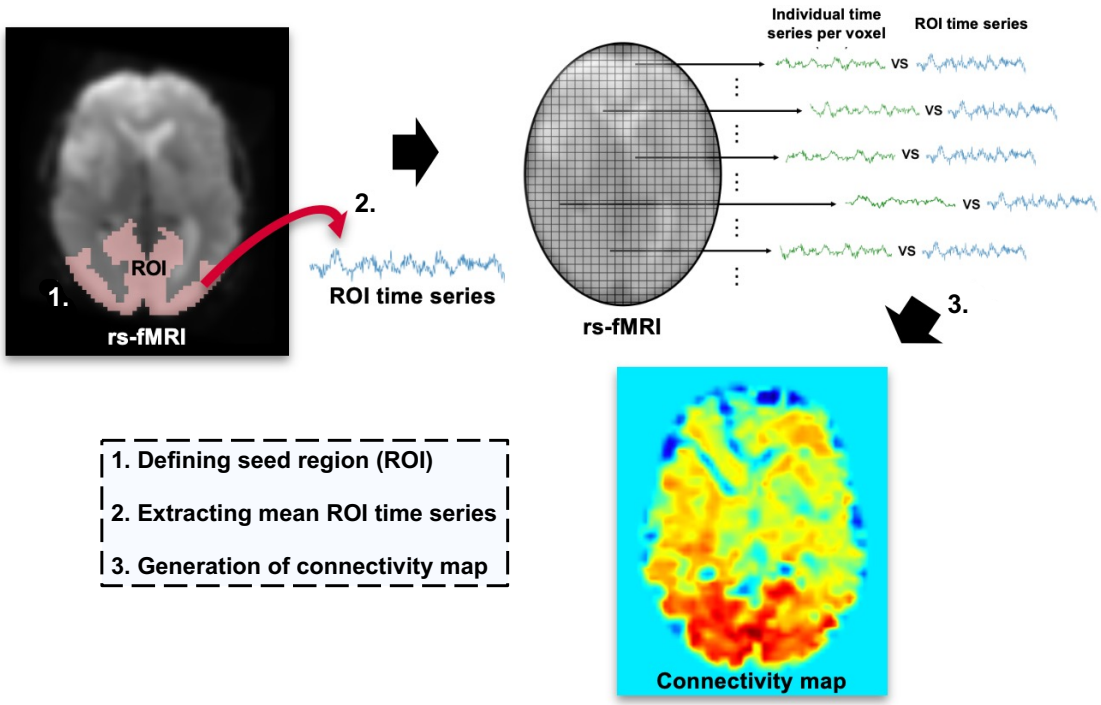

Figure 3: Workflow of a seed-based correlation analysis.
First, a seed region (ROI, region of interest) is defined, e.g., a prominent cortical region such as a node or an entire resting-state network (1.). Then, the mean ROI time series is extracted from the seed region (2.) and correlated voxel-wise with each resting-state functional magnetic resonance imaging (rs-fMRI) time series (3.). This results in a connectivity map that describes the strength of functional connectivity of each brain voxel in relation to the seed region.

1.5 Objective

The aim of this dissertation is to further explore tumor- and treatment-induced changes in structural and functional connectivity and the resulting effects on cognition and survival in patients with recurrent gliomas. We hypothesize that the various tumor- and treatment-induced structural brain lesions, as indicated by pathological MRI and FET PET findings, have a differential impact on white matter integrity. Furthermore, we expect that the resulting altered structural connectivity between cortical regions impairs cognitive function. In addition, we assume that preserved or absent functional connectivity between the tumor infiltrated parts of the brain and the main affected resting-state networks can be used as an imaging biomarker for overall survival.

In the future, these and other insights that further decipher the mechanisms of cognitive changes and their underlying altered connectivity profiles may allow a more accurate assessment of treatment efficacy through more detailed evaluation of the impact of therapeutic procedures on cognition and prognosis. This could be of particular relevance when planning local treatments, such as surgery and radiotherapy, where healthy brain tissue frequently needs to be damaged to access the treatment site. It would be a significant advance to understand exactly which areas need to be spared to avoid functional consequences. Preoperative planning for certain medical procedures already

includes DTI-based identification of vulnerable structural connections that are susceptible to neurological or cognitive impairment[103,123,124]. However, DTI proved to be inherently unable to adequately map complex fiber courses[104], resulting in anatomically invalid or erroneously missing fiber tracts[103,104]. This may lead to misjudgments that may affect survival[125] and result in long-term neurological impairment[126]. To avoid this, we here used state-of-the-art tractography methods based on an advanced diffusion model with CSD[105,106] that is easy to implement in clinical practice[106].

In contrast to previous clinical research in neuro-oncology that focused on identifying selected structures at risk, such as the motor and language tracts (neurosurgery) or the hippocampus (radiotherapy)[103], a growing body of evidence suggests that the long-term outcome of higher-order cognitive function in patients with glioma is related to the maintained integrity of a variety of distributed networks, instead of single nodes or edges[124,127,128]. Therefore, we investigated the relationship between cognitive performance and structural connectivity in gliomas on a network basis using CPM, a robust and easy-to-implement machine learning approach to generate generalizable results that allow easy translation into clinical application[120].

Furthermore, the preserved functional connectivity between tumor-infiltrated brain regions and resting-state networks of primary gliomas has the potential to be used as a novel prognostic imaging biomarker. Initial findings in newly diagnosed glioblastomas already support this hypothesis[5], and we aimed to further substantiate these findings in patients who had been treated for recurrent gliomas of various types. This is of particular interest because common therapeutic interventions such as resection, radiotherapy and alkylating chemotherapy, usually undergone by patients at recurrence, involve interactions with glioma cells, neurons and immunogenic/inflammatory cells, which may further complicate the establishment of a prognosis[129-131].

2 Publications

2.1 Alterations in white matter fiber density associated with structural MRI and metabolic PET lesions following multimodal therapy in glioma patients

Attribution and license information for the following PDF:

Included publication: *Alterations in white matter fiber density associated with structural MRI and metabolic PET lesions following multimodal therapy in glioma patients*
Michel Friedrich, Ezequiel Farrher, Svenja Caspers, Philipp Lohmann, Christoph Lerche, Gabriele Stoffels, Christian P. Filss, Carolin Weiss Lucas, Maximilian I. Ruge, Karl-Josef Langen, Nadim J. Shah, Gereon R. Fink, Norbert Galldiks and Martin Kocher
Originally published in Frontiers in Oncology, Section Neuro-Oncology and Neurosurgical Oncology, Volume 12, 2022
Available at: https://doi.org/10.3389/fonc.2022.998069

frontiers | Frontiers in Oncology

TYPE Original Research
PUBLISHED 14 November 2022
DOI 10.3389/fonc.2022.998069

OPEN ACCESS

EDITED BY
Roberta Rudà,
University Hospital of the City of Health and Science of Turin, Italy

REVIEWED BY
Konstantinos Gousias,
St. Marien Hospital, Germany
Markus Fahlström,
Uppsala University, Sweden

*CORRESPONDENCE
Martin Kocher
martin.kocher@uk-koeln.de

†These authors share senior authorship

SPECIALTY SECTION
This article was submitted to Neuro-Oncology and Neurosurgical Oncology, a section of the journal Frontiers in Oncology

RECEIVED 19 July 2022
ACCEPTED 17 October 2022
PUBLISHED 14 November 2022

CITATION
Friedrich M, Farrher E, Caspers S, Lohmann P, Lerche C, Stoffels G, Filss CP, Weiss Lucas C, Ruge MI, Langen KJ, Shah NJ, Fink GR, Galldiks N and Kocher M (2022) Alterations in white matter fiber density associated with structural MRI and metabolic PET lesions following multimodal therapy in glioma patients. *Front. Oncol.* 12:998069. doi: 10.3389/fonc.2022.998069

Alterations in white matter fiber density associated with structural MRI and metabolic PET lesions following multimodal therapy in glioma patients

Michel Friedrich[1], Ezequiel Farrher[1], Svenja Caspers[1,2], Philipp Lohmann[1,3], Christoph Lerche[1], Gabriele Stoffels[1], Christian P. Filss[1,4], Carolin Weiss Lucas[5,6], Maximilian I. Ruge[3,5], Karl-Josef Langen[1,4,5], Nadim J. Shah[1,7,8], Gereon R. Fink[1,5,9], Norbert Galldiks[1,5,9†] and Martin Kocher[1,3,5*†]

[1]Institute of Neuroscience and Medicine (INM-1, -3, -4, -11), Research Center Juelich, Juelich, Germany, [2]Institute for Anatomy I, Medical Faculty and University Hospital Duesseldorf, Heinrich Heine University Duesseldorf, Duesseldorf, Germany, [3]Department of Stereotaxy and Functional Neurosurgery, Center for Neurosurgery, Faculty of Medicine and University Hospital Cologne, Cologne, Germany, [4]Department of Nuclear Medicine, University Hospital Aachen, Rheinisch-Westfaelische Technische Hochschule (RWTH) Aachen University, Aachen, Germany, [5]Center of Integrated Oncology (CIO), Universities of Aachen, Bonn, Cologne, and Duesseldorf, Cologne, Germany, [6]Department of General Neurosurgery, Faculty of Medicine and University Hospital Cologne, University of Cologne, Cologne, Germany, [7]Juelich-Aachen Research Alliance (JARA), Section JARA-Brain, Juelich, Germany, [8]Department of Neurology, University Hospital Aachen, Rheinisch-Westfaelische Technische Hochschule (RWTH) Aachen University, Aachen, Germany, [9]Department of Neurology, Faculty of Medicine and University Hospital Cologne, University of Cologne, Cologne, Germany

Background: In glioma patients, multimodality therapy and recurrent tumor can lead to structural brain tissue damage characterized by pathologic findings in MR and PET imaging. However, little is known about the impact of different types of damage on the fiber architecture of the affected white matter.

Patients and methods: This study included 121 pretreated patients (median age, 52 years; ECOG performance score, 0 in 48%, 1-2 in 51%) with histomolecularly characterized glioma (WHO grade IV glioblastoma, n=81; WHO grade III anaplastic astrocytoma, n=28; WHO grade III anaplastic oligodendroglioma, n=12), who had a resection, radiotherapy, alkylating chemotherapy, or combinations thereof. After a median follow-up time of 14 months (range, 1-214 months), anatomic MR and O-(2-[^{18}F]fluoroethyl)-L-tyrosine (FET) PET images were acquired on a 3T hybrid PET/MR scanner. Post-therapeutic findings comprised resection cavities, regions with contrast enhancement or increased FET uptake and T2/FLAIR hyperintensities. Local fiber density was determined from high angular-resolution diffusion-weighted imaging and advanced tractography methods. A cohort of 121 healthy subjects selected from the 1000BRAINS study matched for age, gender and education served as a control group.

10.3389/fonc.2022.998069

Results: Lesion types differed in both affected tissue volumes and relative fiber densities compared to control values (resection cavities: median volume 20.9 mL, fiber density 16% of controls; contrast-enhanced lesions: 7.9 mL, 43%; FET uptake areas: 30.3 mL, 49%; T2/FLAIR hyperintensities: 53.4 mL, 57%, p<0.001). In T2/FLAIR-hyperintense lesions caused by peritumoral edema due to recurrent glioma (n=27), relative fiber density was as low as in lesions associated with radiation-induced gliosis (n=13, 48% vs. 53%, p=0.17). In regions with pathologically increased FET uptake, local fiber density was inversely related (p=0.005) to the extent of uptake. Total fiber loss associated with contrast-enhanced lesions (p=0.006) and T2/FLAIR hyperintense lesions (p=0.013) had a significant impact on overall ECOG score.

Conclusions: These results suggest that apart from resection cavities, reduction in local fiber density is greatest in contrast-enhancing recurrent tumors, but total fiber loss induced by edema or gliosis has an equal detrimental effect on the patients' performance status due to the larger volume affected.

KEYWORDS

glioma, multimodal therapy, PET/MR hybrid imaging, high-angular resolution diffusion-weighted imaging, white matter damage, tractography, fiber density imaging, constrained spherical deconvolution

Introduction

There is broad evidence that brain functions depend critically on the integrity of structural connections between cortical regions (1–6). These connections are built by axon bundles in the brain's white matter and can be identified as single fibers or tracts composed of fiber groups using modern diffusion-weighted magnetic resonance imaging (DWI) techniques (7–9). Following multimodal treatment in glioma patients, fiber connections may become disrupted by structural tissue damage resulting from tumor resection, radiotherapy, alkylating chemotherapy, or combinations thereof (10–13), or by recurrent tumor growth (14). Apart from the fiber tracts originating in the primary, eloquent cortical regions, tissue damage may affect larger and wider distributed white matter areas (15–17) involving structural connections of multiple functional networks (18). Therefore, glioma patients often develop deficits in cognition, general performance (19), and quality of life that increase with the duration of survival and intensity of therapy (15, 20).

While the gross structural tissue changes induced by neurosurgical tumor resection, radiation, local tumor recurrence and edema can be readily made visible by standard magnetic resonance imaging (MRI) and amino acid positron emission tomography (PET) such as O-(2-[^{18}F]fluoroethyl)-L-tyrosine (FET) PET, the resulting damage to white matter microstructural integrity remains to be elucidated (21, 22). In principle, fiber tractography methods, based on DWI aiming to identify individual interconnecting fibers at the submillimeter level, are best suited to answer this question. Diffusion tensor imaging (DTI), used to model the MR signal behavior in DWI, is based on a simple diffusion tensor model and is widely established in clinical practice, aiding to estimate white matter fiber orientation (23). However, the model is *a priori* unable to resolve multiple fiber orientations, which are present in approximately 90% of the voxels, causing missing or false positive fibers (23, 24). Advanced methods that can overcome the former limitations use DWI data acquired within the so-called high-angular resolution diffusion-weighted MR imaging (HARDI) framework. Amongst these methods, constrained spherical deconvolution (CSD) (25) has been shown to improve the assessment of complex, intra-voxel fiber configuration significantly. Thus, fiber-tracking procedures based on advanced DWI methods allow a more accurate estimation of complex fiber architectures (7) and are increasingly used for planning the extent of resection in brain tumors adjacent to eloquent areas (23, 26–32).

We hypothesize here that, apart from resection, structural brain damage due to radiation or tumor recurrence, as indicated by pathologic MRI and FET PET findings, has a differential impact on local fiber density and affects the patient's overall performance status to varying degrees.

10.3389/fonc.2022.998069

Patients and methods

Patient characteristics

The patient group consisted of 121 patients (73 males, 48 females; mean age, 51.6 ± 11.6 years) with histomolecularly characterized glioma (World Health Organization (WHO) grade IV glioblastoma, n=81; WHO grade III anaplastic astrocytoma, n=28; WHO grade III anaplastic oligodendroglioma, n=12) according to the WHO classification of 2016 (33), who underwent resection, radiotherapy, alkylating chemotherapy, or combinations thereof (Table 1). Most of the patients (77, 64%) received their primary treatment between 2016 and 2019 in one of the 4 university hospitals of the comprehensive cancer center 'Center for Integrative Oncology Aachen-Bonn-Cologne-Duesseldorf', and another 21 (17%) were treated at another university hospital (Frankfurt). Complete resection as determined from early postoperative contrast-enhanced MR was achieved in 88 patients (73%), while the others had partial resection or stereotactic biopsy only. At time of imaging, adjuvant radiotherapy (60 Gy in most cases) had been applied in 112 (93%) and simultaneous and/or adjuvant chemotherapy comprising temozolomide, temozolomide and lomustine (CCNU) or procarbacine/CCNU/vincristine (PCV) in 108

TABLE 1 Patient characteristics.

	n	%
Gender (male/ female)	73/ 48	60/ 40
ECOG score (0/ 1/ 2/ 3)	58/ 56/ 6/ 1	48/ 46/ 5/ 1
Tumor type		
GBM: IDH-wt/ IDH-mut/ NOS	67/ 10/ 4	56/ 8/ 3
AA: IDH-wt/ IDH-mut/ NOS	5/ 16/ 7	4/ 13/ 6
AOD: IDH-mut-1p-19q-codel	12	10
Glioma Grade 3/ Grade 4	40/ 81	33/ 67
IDH-wt or NOS/ IDH-mut	88/ 37	69/ 31
Tumor location		
Left frontal/ parietal/ temporal/ occipital	30/ 8/ 22/ 5	25/ 7/ 18/ 4
Right frontal/ parietal/ temporal/ occipital	28/ 8/ 16/ 4	23/ 7/ 13/ 3
Primary treatment[#]		
Biopsy/ partial/ complete resection	19/ 14/ 88	16/ 11/ 73
Radiotherapy yes/ no	112/ 9	93/ 7
Temozolomide	76	63
Temozolomide + CCNU	27	22
PC/ PCV	5	4
Number of treatment interventions[#]		
Surgery* (1/ 2/ 3/ 4)	101/ 17/ 2/ 1	83/ 14/ 2/ 1
Radiotherapy series (0/ 1/ 2)	7/ 100/ 14	6/ 83/ 12
Chemotherapy courses (0/ 1/ 2/ 3)	10/ 91/ 16/ 4	8/ 76/ 13/ 3
Neurological symptoms		
None	40	33
Paresis	29	24
Aphasia	17	14
Visual field/ diplopia	12	10
Other symptoms	23	19
	mean ± SD	**median (range)**
Age (years)	51.6 ± 11.6	51.9 (28.1 - 73.8)
Radiation dose (Gy)	59.3 ± 2.6	60.0 (40.1 - 62.0)
of first radiation series (n=114)		
Interval (months)	30.4 ± 43.0	14.4 (0.6 - 213.7)
between therapy and imaging		

ECOG, Eastern Cooperative Oncology Group; GBM, glioblastoma multiforme; AA, anaplasticastrocytoma; AOD, anaplastic oligodendroglioma; IDH-wt/-mut, mutation status in the isocitrate dehydrogenase gene (wildtype/mutant); 1p-19q-codel, 1p/19q-codeletion; NOS, not otherwise specified; CCNU, lomustine; PCV, procarbacine/CCNU/vincristine; [#]received prior to imaging; *including biopsy and resection.

(89%). Where ever possible, the final diagnosis was based on the presence of a IDH (isocitrate-dehydrogenase) mutation and the 1p-19q loss-of-heterozygosity status. Of note, therapy was initiated between 2000 and 2015 in some patients, so molecular characteristics were not available. Between 2018 and 2020, structural MRI and metabolic PET findings after treatment were evaluated in all patients using anatomical MRI and FET PET acquired on a 3T hybrid PET/MR scanner (Siemens Trim-TRIO/BrainPET, Siemens Medical Systems, Erlangen). The median interval between treatment initiation and imaging was 14 months (range, 1-214 months). Of note, 14 patients were examined more than 60 months (5 years) after therapy initiation. Regarding general performance status, 58 patients (48%) had an ECOG score of 0 (fully active, able to carry on all pre-disease performance without restriction), 56 (46%) were grade 1 (restricted in physically strenuous activity, but ambulatory and able to carry out work of a light or sedentary nature), and 6 (5%) were grade 2 (ambulatory, capable of all self-care, up and about more than 50% of waking hours, but unable to work) (19). All patients were free from major depression and seizures. A total of 81 patients (67%) had mild neurological (48%) or other symptoms (fatigue, vertigo, 19%) without requiring assistance for personal needs.

A control group of 121 healthy subjects was obtained from the 1000BRAINS cohort study (34) that investigates environmental and genetic influences on inter-individual variability in brain structure, function, and connectivity in the aging brain. Controls were matched for gender (males, n=75; females, n=46), age (mean 51.7 ± 11.5 years), and educational status using propensity score matching (35). Both cohorts have been analyzed in an earlier study presented by our group (36).

Hybrid PET/MR imaging

In all patients, FET PET, as well as anatomical and diffusion-weighted MR images, were obtained from the 3T hybrid PET/MR scanner equipped with a birdcage-like quadrature transmitter head coil mounted on the couch, an 8-channel receiver coil and a PET insert consisting of 72 rings (axial field-of-view, 19.2 cm; center spatial resolution, 3 mm FWHM). The PET image data were corrected for random and scatter coincidences as well as for dead time, attenuation (based on a T1-weighted anatomical MRI scan), and motion before OPOSEM (Ordered Poisson Ordinary Subset Expectation Maximization) reconstruction (2 subsets, 32 iterations), with software provided by the manufacturer (37).

The MRI protocol comprised a 3D high-resolution T1-weighted magnetization prepared rapid acquisition gradient echo (MPRAGE) native scan (176 slices; TR=2250 ms; TE=3.03 ms; FoV=256×256 mm^2; flip angle=9°; voxel size=1×1×1 mm^3), a contrast-enhanced MPRAGE scan recorded after injection of gadolinium-based contrast agent, a T2-weighted sampling perfection with application optimized contrasts (SPACE) scan (176 slices; TR=3.2 ms; TE=417 ms; FoV=256×256 mm^2; voxel size=1×1×1 mm^3), and a T2-weighted fluid-attenuated inversion recovery (T2/FLAIR) scan (25 slices; TR=9000 ms; TE=3.86 ms; FoV=220×220 mm^2; flip angle=150°; voxel size=0.9×0.9×4 mm^3).

The HARDI measurements were performed with a double-echo diffusion-weighted echo-planar imaging (EPI) sequence. The protocol parameters were: 55 slices, TR=8 s; TE=112 ms; *b*-values (gradient directions)=0 (13, interleaved) and 2700 s/mm^2 (120); voxel size=2.4×2.4×2.4 mm^3). An additional non-diffusion-weighted volume was acquired with the same settings but a reverse phase-encoding direction for the purpose of EPI distortion correction. The healthy subjects were measured on a stand-alone MRI scanner (3T Siemens Tim-TRIO), identical to the MR component of the hybrid PET/MR system. The body coil was used for transmission and a 32-channel receive-only head coil for signal reception. Before the *in vivo* measurements, a phantom study was performed as a control that confirmed an equal signal level, quality and signal-to-noise ratio values between both scanners.

Lesion segmentation

The local fiber density was evaluated in four different types of imaging findings: i) hypointense resection cavities, ii) contrast-enhancing lesions, iii) T2/FLAIR hyperintense regions, and iv) lesions with pathologically increased FET uptake defined by a tumor-to-brain ratio (TBR) >1.6. A fully automated software based on deep-learning algorithms (HD_GLIO-AUTO) was used to segment T2/FLAIR hyperintense regions and contrast-enhancing lesions (38).

Resection cavities were manually contoured using the medical 3D segmentation software ITK-SNAP (http://www.itksnap.org, vs. 3.8.0, Universities of Pennsylvania and Utah, USA). The resection cavities were mostly filled with cerebrospinal fluid but sometimes also comprised complex, intermingled structures of undeterminable origin. The mask of areas with increased FET uptake originated from a semi-automatic segmentation that identified all voxels with a TBR above 1.6, which was histologically validated and is highly predictive for glioma tissue (39). Finally, all masks were visually examined and manually corrected by i) removing spurious small-segmented regions that were not connected to the primary lesion, and ii) padding of necrotic areas surrounded by contrast-enhancing or FET-enhancing tissue.

T2/FLAIR lesions can be caused by both peritumoral edema and radiation-induced gliosis which may be present simultaneously and difficult to distinguish. Therefore, the prevailing characteristics were used to assign a single classification to a selection of patients. Such, T2/FLAIR lesions were classified as perifocal edema in n=27 patients with recurrent tumors >10 mL in both the contrast-enhancing and

FET images. In opposite, T2/FLAIR hyperintensities were classified as radiation-induced gliosis in n=13 patients in the almost complete absence of contrast enhancement and FET uptake (<0.1 mL) and a time interval >6 months from local irradiation.

Tractography and local fiber density

Advanced DWI and tractography methods have rarely been used to characterize or quantify brain tissue damage caused by infiltrative tumor growth or treatment effects other than surgery (40). This reluctance might be related to the observation that most fiber tracking methods in brain regions affected by recurrent tumor or other structural changes yield inconsistent or biased results, usually leading to a severe underestimation of fiber density (28, 32, 41, 42). Therefore, we applied a recently developed modification of a widely used fiber-tracking method that allows for reasonable identification of the fibers passing through and near tumorous tissue and the surrounding brain structures (43). In short, the applied constrained spherical deconvolution (CSD) method (25) assumes that the diffusion-weighted MRI signal results from the spherical convolution of a response function with the underlying fiber orientation distribution function (FOD). The response functions are tissue-type specific and describe the expected MR signal of a pure white matter (single oriented white matter fiber bundle), gray matter, or cerebrospinal fluid image voxel. The estimated white matter FODs in the original, single-shell CSD model (25) are usually distorted by signal contributions from different tissue types within the voxels. This problem has been addressed by the advanced multi-shell multi-tissue CSD (MSMT-CSD) method, which also considers the signal contributions of gray matter and cerebrospinal fluid and exploits their different response properties at different *b*-values (44). However, it has also been shown that MSMT-CSD underestimates or excludes white matter FODs in tumor tissue, since such areas are often misclassified as gray matter-like tissue (43). In contrast, the novel single-shell 3-tissue CSD (SS3T-CSD) method considers different tissue types from single-shell (single *b*-value plus non-diffusion weighted images) HARDI data and estimates white matter FODs as bias-free as possible, even within different compartments of a tumor (43, 45, 46). The method is implemented in the toolkit MRtrix3Tissue (https://3tissue.github.io, accessed on 1.3.2021), a fork of the widely used fiber tracking toolkit MRtrix3 [https://www.mrtrix.org, accessed on 1.3.2020 (47)].

The MRtrix3Tissue toolkit steps were embedded in the following processing pipeline. The image corrections were passed from MRtrix to the FSL toolbox [FSL version 5.0, https://fsl.fmrib.ox.ac.uk/fsl (48)] and the ANTs software suite (https://github.com/ANTsX/ANTs, accessed on 3.1.2020). First, the HARDI data were subjected to EPI distortion correction using the script "topup". Second, eddy-current and motion distortion correction were performed using the FSL tool "eddy", both scripts available in FSL. Afterwards, a bias field correction based on the N4ITK algorithm was executed by the ANTs software suite. The white matter, gray matter, and cerebrospinal fluid response functions were estimated from the preprocessed HARDI data using an unsupervised method (46). Afterwards, SS3T-CSD was performed to obtain white matter-, gray matter- and cerebrospinal fluid-like FODs in all voxels (45). The response functions for each tissue compartment were averaged across all patients and subjects in order to ensure that the FODs were comparable within the group study. In addition, the FODs were subjected to a global intensity normalization (49).

Finally, in order to increase the biological plausibility of the fiber tractograms, the method called Anatomically-Constrained Tractography (available as part of MRtrix) which makes several assumptions about the behavior of healthy neuronal fibers in terms of their propagation and termination was applied to the obtained fiber tractograms (50). These assumptions were relaxed in all areas of segmented pathological tissue using a compound lesion mask containing all segmented lesion types. Apart from the default settings, the option "backtrack" was activated, the number of seed points was fixed at 4 million and restricted to a brain mask, and the cutoff value for the FOD amplitude was set to 0.01. Lastly, the tractography data were converted into fiber density images with an isotropic voxel size of 1 mm^3. All image processing steps were also performed for the control group, except for the EPI distortion correction due to the lack of the corresponding sequence with reversed phase-encoding. In Figures 1, 2, representative results for the applied tractography methods and lesion segmentation are depicted. Although the lack of the EPI distortion correction could theoretically have led to an inward-facing deformation mainly of the frontal tracts in the healthy subjects, there was no indication that this happened in the fiber density images, probably due to the successful application of the spatial normalization to the MNI template (see next section).

Effect of lesion type on local fiber density

The tractography methods supplied by MRtrix support the determination of the voxel-wise fiber density [also termed track density by the developers (51, 52)], which we here used to measure the integrity of local structural connectivity. For this purpose, all structural and fiber density images of the patients and healthy subjects as well as all lesion masks of the patients were registered from the individual patient space to the standard MNI space by the unified segmentation method of the SPM12 toolbox (Statistical Parametric Mapping Toolbox, https://www.fil.ion.ucl.ac.uk/spm/software/spm12/, Matlab R2017b,

10.3389/fonc.2022.998069

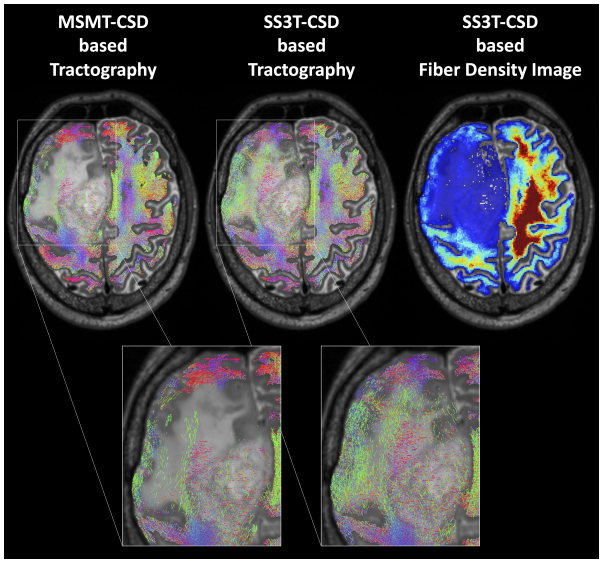

FIGURE 1
Probabilistic whole-brain tractography and fiber density image in a patient with recurrent glioma and perifocal edema. In normal brain tissue, a method that increases the biological plausibility is applied (Anatomically-Constrained Tractography), while this condition is relaxed in pathologically altered brain regions. In contrast to the standard multi-shell multi-tissue constrained spherical deconvolution (CSD) based tractography of MRtrix3 (MSMT), the advanced MRtrix3tissue method using the single-shell 3-tissue CSD algorithm (SS3T) detected an adequate number of fibers also within the tumorous or edematous tissue.

MathWorks, Natick, MA, USA). This method combines tissue segmentation with elastic registration (53). All further analyses were done in the MNI standard space. A map of the average fiber density in the control group (n=121) was computed from the individual fiber density images of the healthy subjects. Then, the mean fiber density within the lesion segments of the patients was computed and compared to the mean fiber density in the corresponding region of the average normal fiber density map. In order to check the validity of the fiber density estimation, it was also evaluated for the manually segmented resection cavities and later used for calculation of the total fiber loss and its impact on the ECOG performance status (see next section).

In order to analyze a possible correlation between FET PET uptake and local fiber density, TBR values were divided into 4 bins, starting from the histologically validated cut-off value for glioma tissue of 1.6 (binning thresholds, 1.6-2.6; 2.6-3.6; 3.6-4.6; >4.6). As the tumors also extended into fiber-free areas (gray matter and ventricles), the following measures were undertaken to make the resulting TBR-binned lesion segments comparable. Only patients with pathologically increased FET uptake located in a region with a reasonable homogenous underlying fiber density in the reference fiber density image (control group) were included. Thus, only patients for whom the standard deviation of the fiber density in the reference region was smaller than the mean fiber density itself were considered. Besides, tiny TBR-binned segments (i.e., <0.25 mL) were excluded within the patients, and one patient was discarded for whom the displaced fibers probably caused the fiber density to exceed the reference value. In the remaining 43 patients, the mean TBR within the TBR-binned segments was computed, and the mean relative fiber density was expressed as the ratio to the reference region.

Impact of reduced fiber density on the ECOG performance status

The effect of reduced fiber density on performance status was examined to evaluate the clinical impact of reduced structural connectivity induced by different types of lesions.

10.3389/fonc.2022.998069

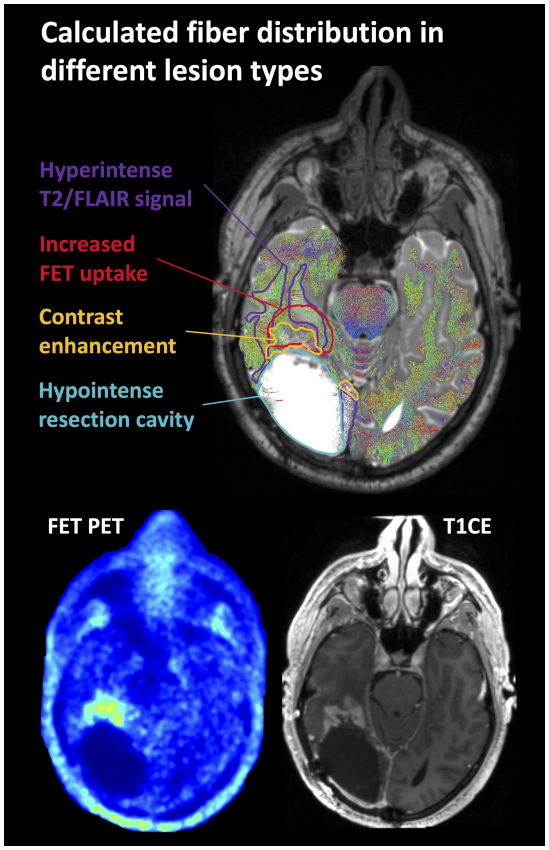

FIGURE 2
Representative case of lesion segmentation superimposed on a tractography image in a patient who had undergone surgery and radiochemotherapy and developed local recurrence near the resection cavity. FET, O-(2-[^{18}F]fluoroethyl)-L-tyrosine; T2/FLAIR, T2-weighted fluid-attenuated inversion recovery; T1CE, T1-weighted contrast-enhancing image.

The total fiber loss caused by each lesion type was calculated from the relative reduction in fiber density [1 – (patient fiber density/reference fiber density)] of each segment multiplied by the corresponding segment volume. In patients where one or more lesion types were not present, the respective volumes were set to zero. The patient's performance status was classified as either normal/unaffected (i.e., ECOG score of 0) or impaired (i.e., ECOG≥1).

Statistical analysis

Statistical analysis was performed using the SPSS statistical software package (version 27, IBM Corporation, Armonk, New York, USA). All fiber density values were also converted to fractions relative to the reference values in the corresponding regions of the healthy subjects. To compare the absolute and relative fiber densities between patients and healthy subjects, the

Mann-Whitney U test and one-sample Wilcoxon signed-rank tests (2-sided) were applied. For 3 lesion types (FET PET, T1CE and resection cavity), 1-2 outliers were each excluded from analysis. For evaluation of the differential effect of lesion types in the patients, the Kruskal-Wallis test (2-sided) and a post-hoc comparison by the Mann-Whitney U-test (2-sided) were applied. The relationship between FET uptake and relative fiber density was determined using linear regression analysis and a mixed linear model using the TBR as fixed effect and allowing for random variation of the constant term in each individual patient. The influence of the total fiber loss caused by different lesion types on performance status was examined using univariate and multivariate logistic regression analysis including a set of clinical variables as potential confounders. In all analyses, a p-value <0.05 was considered statistically significant.

Results

The probability of lesion location is shown in Figure 3. Most lesions were located in the frontal and temporal lobes. Average fiber densities in the healthy subjects and in the unaffected brain regions of the patients are illustrated in Figure 4, indicating that the overall pattern of fiber tracts outside the lesions was maintained in the patients. However, as expected, some of the main tracts showed a reduced fiber density which we did not further evaluate here. As shown in Table 2, the median volume of resection cavities, contrast-enhancing regions, regions with increased FET uptake, and T2/FLAIR hyperintense regions amounted to 20.9, 7.9, 30.3, and 53.4 mL, respectively. A significant decrease in absolute fiber density was observed in all four major lesion types ($p<0.001$ in all cases).

The relative fiber densities (fraction of fiber density compared to the corresponding region in the healthy subjects) in different lesion types are shown in Table 2 and Figure 5. The relative fiber density was most decreased in the resection cavities (resulting mean density 16%, $p<0.001$), followed by T1-weighted contrast-enhancing lesions (43%, $p<0.001$), lesions with pathologically increased FET uptake (49%, $p<0.001$) and T2/FLAIR hyperintense regions (57%, $p<0.001$) and depended significantly on lesion type (Kruskal-Wallis-test, $p<0.001$). A post-hoc analysis revealed that the contrast-enhancing lesions and FET uptake regions were associated with a significantly larger decrease in relative fiber density than the T2/FLAIR lesions (both $p<0.001$) and that the relative fiber density in contrast enhancing regions was significantly lower than in regions with pathologic FET uptake ($p<0.01$). Also, the relative fiber densities found in T1-enhancing lesions and in lesions with pathologic FET uptake did not differ significantly between grade 3 and grade 4 gliomas.

T2/FLAIR lesions, predominantly related to radiation-induced gliosis, were identified in n=13 patients (Table 2). Within these lesions, the mean relative fiber density amounted to 53% which was not significantly different from that measured in lesions dominated by tumor-related edema (n=27, 48%, $p=0.17$). Representative cases are presented in Figure 6. With regard to the FET uptake versus fiber density, a significant ($p=0.005$, $R^2= 0.076$) inverse linear dependence (constant term 0.59, slope -0.074) of fiber density on the level of FET uptake (tumor-to-brain ratio, Figure 7) was observed. The mixed linear model confirmed the highly significant dependency of fiber density on TBR ($p<0.001$) and the inverse relationship (mean constant term 0.61, slope -0.084).

The regression analysis on general performance revealed a significant influence of the total fiber loss in contrast-enhancing lesions ($p=0.006$) and T2/FLAIR hyperintense areas ($p=0.013$) on the performance status (ECOG score) of the patients (Table 3; Figure 8). None of the clinical variables comprising age, gender, type of resection, grade 3 vs. 4, number of surgical procedures, number of radiotherapy series, number of chemotherapy courses and follow-up interval had a significant impact on the ECOG score. In a multivariate logistic regression analysis that included the total fiber loss caused by the 4 different lesion types, only the effect of contrast-enhancing lesions on the ECOG performance status kept its significant impact ($p=0.04$).

Discussion

Main findings

This study shows that structural and metabolic imaging changes after multimodal therapy in glioma patients are associated with a significant reduction in local white matter fiber density, as assessed using the DWI single-shell 3-tissue CSD algorithm. Compared to a matched cohort of healthy subjects, the reduction was almost total in resection cavities, strong in contrast-enhancing lesions and regions with pathologically increased FET PET uptake, and still pronounced in regions with T2/FLAIR hyperintensity. For lesions with an increased FET uptake, an inverse linear relationship between the TBR and a reduced fiber density was observed. The total fiber loss in contrast-enhancing lesions and T2/FLAIR hyperintense regions was associated with a significant risk of lowered performance status as assessed by the ECOG score, while the total fiber loss caused by resection and regions with increased FET uptake did not impact general performance. The methodological issues and clinical implications of these results are discussed below.

Reliability of CSD-based tractography and fiber density estimation

All tractography methods are based on assumptions that relate the observed non-isotropic diffusion-weighted MRI signal to the expected local fiber architecture. The main prerequisites of

10.3389/fonc.2022.998069

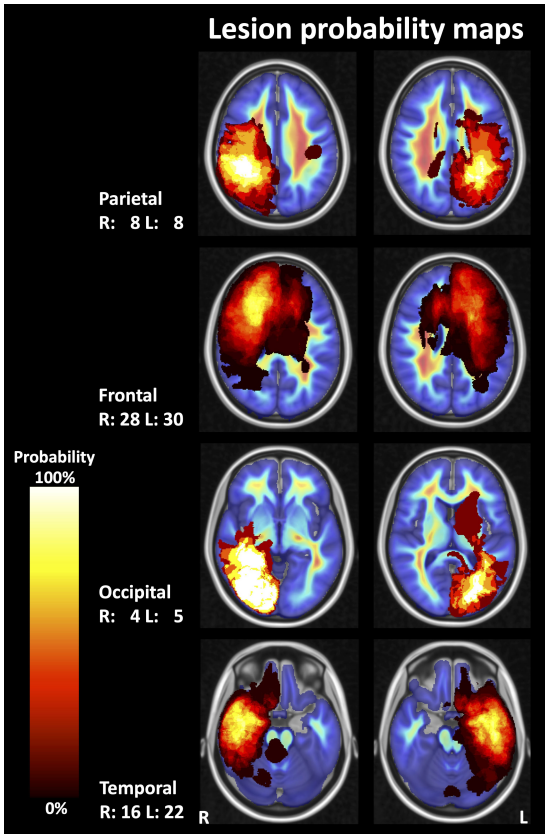

FIGURE 3
Probability maps for lesion localization. Compound lesion maps comprising T2-weighted fluid-attenuated inversion recovery (FLAIR) hyperintense lesions, contrast-enhancing lesions, resection cavities, and lesions with pathologically increased FET (O-(2-[^{18}F]fluoroethyl)-L-tyrosine) uptake on PET images are shown superimposed on images depicting the mean fiber density in a control group (representative sections of the MNI-152 standard brain template). R, right; L, left; numbers, number of patients.

these models for reliable performance are a high angular resolution of the diffusion-weighted signal and low confounding of the fiber-associated signal by other sources, e.g., the presence of freely diffusing water (54, 55) or isotropic diffusion such as present in grey matter. The HARDI scheme applied here comprised 120 directions at a high b-value of 2700 s/mm^2, which ensures optimal contrast-to-noise properties within the shell and between the single shell and the b=0 data as detailed in (43). From these diffusion-weighted data, the composition of every voxel in terms of grey-matter-like, cerebrospinal fluid-like and white-matter-like tissue was computed and the respective response functions were determined from the experimental data themselves (45). Then, the FODs of the white-matter-like compartments of normal and pathological brain tissue and the contamination of each voxel by freely diffusing water as found in cerebrospinal fluid or edema (48) were calculated by the 3-tissue CSD algorithm (56, 57) for

10.3389/fonc.2022.998069

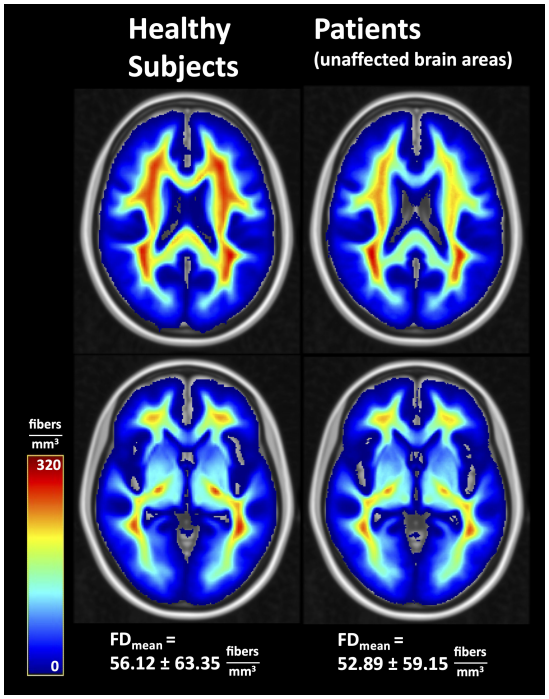

FIGURE 4
Average fiber densities in healthy subjects and in unaffected brain regions of the patients. FD, fiber density; FD_{mean}, whole-brain mean fiber density.

subsequent tractography. Thus, effective measures have been taken to avoid underestimation of fiber density in brain regions affected by tumor, edema, or other pathological tissue (28, 32, 41, 42).

Due to the inhomogeneous distribution of the fiber tracts in the normal brain, reference regions for fiber density have to be carefully selected. This is probably why in a comparable study on fiber density in different tumor compartments of glioblastoma (58) reported in due course after the publication of the method (51, 52), a paradoxical positive correlation between the extent of tumor infiltration and the fiber density was observed. In the present paper, the spatially co-registered data of healthy subjects served as reference, and all procedures were equally applied to the patient and healthy subject data, resulting in reasonable fiber density distributions in both groups. In summary, the methods applied here can be expected to provide a solid estimate of the local and relative fiber density in pathologically altered brain tissue.

Fiber density in glioma tissue

Several groups investigated the impact of tumor cell density in gliomas' core or infiltration zone on local fiber density. For this purpose, Stadlbauer et al. (59) applied DTI-based fiber density mapping in patients with non-enhancing WHO grade II or III glioma and evaluated 38 biopsies taken from the tumor center, transition zone, and tumor border. A steep decrease in the fiber density from the periphery into the tumor center was observed. However, the fiber loss in the tumor core was probably overestimated mainly due to the above-mentioned methodological limitations to detect fibers in pathologically altered brain tissue. In a subsequent study, the choline concentration in the tissue (determined by MR spectroscopy), which is a marker of membrane turnover and cellular density, was also inversely related to the fiber density (60). It is worth mentioning that fiber density maps have also been applied to evaluate tumor infiltration of the corticospinal tract in motor-eloquent WHO

TABLE 2 Volume and fiber density in lesions of different type.

Lesion type	n#	Lesion size (mL) mean ± SD (median)	Fiber density Healthy (fibers/mm^3)	Patients (fibers/mm^3)	Patients (% of reference)
Resection cavity	90	35.8 ± 40.3 (20.9)	45.1 ± 23.0	5.9 ± 7.3***	15.5 ± 21.1***
T1CE	99	17.2 ± 23.3 (7.9)	76.3 ± 43.5	26.9 ± 19.9***	42.9 ± 31.7***
FET PET (TBR>1.6)	79	39.5 ± 35.2 (30.3)	62.3 ± 30.6	27.8 ± 17.5***	49.3 ± 26.1***
T2/FLAIR	121	70.1 ± 55.5 (53.4)	107.6 ± 39.6	60.9 ± 29.1***	56.9 ± 16.3***
T2/FLAIR (edema)	27	121.1 ± 58.0 (131.8)	88.3 ± 23.2	40.7 ± 12.8***	48.1 ± 15.5***
T2/FLAIR (gliosis)	13	52.3 ± 45.7 (33.3)	120.4 ± 41.3	62.6 ± 24.8***	52.7 ± 12.5**

T1CE, T1-weighted contrast-enhancing; FET, O-(2-[^{18}F]fluoroethyl)-L-tyrosine; FLAIR, fluidattenuated inversion recovery; TBR, tumor-to-brain ratio; #patients affected; **p<0.01, ***p<0.001, Mann-Whitney U test (fibers/mm^3), one-sample Wilcoxon signed-rank test (% of reference).

grade III or IV gliomas, where a significant reduction in fiber density was found in the peritumoral region as well as in the cortico-spinal tract itself (61). The observation that an increase in FET uptake is associated with a decrease in fiber density fits well into these findings, as the FET signal was found to correlate with the tumor cell density in glioma (62, 63). A particular effort was undertaken in the present study to generate reliable reference regions by using spatially registered normal brains and excluding patients with tumor localizations distributed over brain regions with strongly varying physiological fiber density.

Fiber density in peritumoral edema and gliosis

It is commonly believed that malignant brain tumors disrupt the blood-brain barrier, causing intravascular fluid to leak into the interstitial space and leading to what has been termed as vasogenic edema (64, 65). This process leads to an increased interstitial pressure, which can displace, compress, or disrupt the axons that pass through the affected edematous region (66). In the preoperative setting, several methodological attempts have been made to reliably identify the major fibers tracts in the perilesional tissue of gliomas, including techniques such as free-water modeling (48) and local connectivity mapping (28), which seem to recover more fibers in the tracts than the standard methods based on DTI. We have attempted here for the first time to quantify the relative fiber loss caused by edema and found it to be in the range of 50%.

Late side effects of radiotherapy have been found to mainly affect white matter, leading to demyelination, axonal degeneration, and astrogliosis (15), which, in the absence of other tissue changes, may be readily detected by a signal increase in T2-weighted or FLAIR images (67). In order to quantify radiation-induced white matter damage, surrogate markers for structural connectivity such as cortical atrophy, fractional anisotropy, and mean, axial and radial diffusivity determined from DTI have been applied (22, 68–72). However, in most of these studies, the analysis was performed on the whole brain or confined to anatomically predefined regions or tracts. In contrast, we attempted here to quantify the relative fiber loss

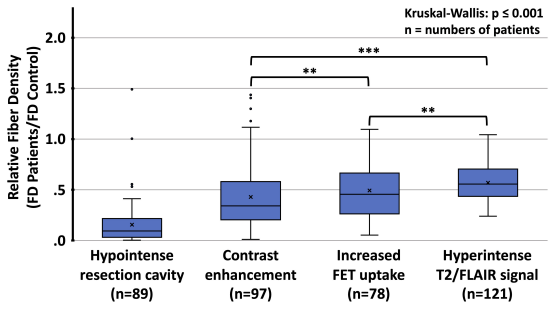

FIGURE 5
Distribution of relative fiber densities (fraction of fiber density (FD) of the corresponding region in healthy controls) for the respective imaging findings. FET, O-(2-[^{18}F]fluoroethyl)-L-tyrosine; T2/FLAIR, T2-weighted fluid-attenuated inversion recovery (FLAIR) hyperintense lesions; **p<0.01, ***p<0.001, Mann-Whitney U test for comparison between different types of lesions.

10.3389/fonc.2022.998069

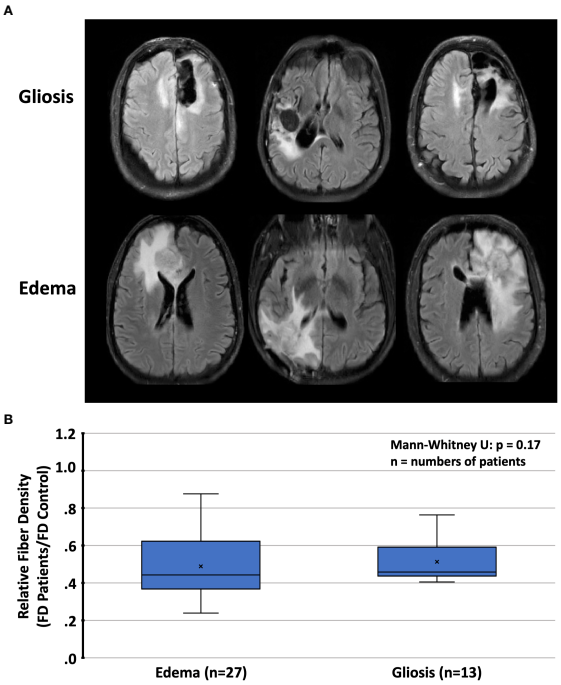

FIGURE 6
(A) Representative cases with T2/FLAIR hyperintense regions and **(B)** relative fiber densities (FD) in patients with radiation-induced gliosis or peritumoral edema. T2/FLAIR, T2-weighted fluid-attenuated inversion recovery.

in brain regions affected by radiation-induced damage, which was also approximately 50%; the same order of magnitude as the loss caused by edema. However, as the distinction between edema and radiation-induced gliosis proved difficult, these numbers have to be taken as largely provisional.

Clinical impact of fiber loss

It remains unclear how the apparent loss of fiber density detected by MRI tractography methods is related to neuronal function, e.g., the propagation of action potentials along the axons in the affected tracts. At least in the case of edema, axons are still present but may become nonfunctional, for example, because of compression. However, our data show that the overall extent of fiber loss in the volumes affected by different lesion types significantly affects the global performance status. The differential impact of the lesion types can be explained, at least in part, by the study population. Most patients had recovered from surgery without permanent neurological deficits but were at constant risk of developing radiation-induced damage or recurrent tumor, the latter diagnosed early enough by FET PET before it led to performance loss.

Limitations of the study

In the present study, regular follow-up data were available for only a few patients. Consequently, each patient was examined only once, resulting in a wide dispersion of intervals between the initiation of therapy and imaging. Because multiple types of lesions were present simultaneously in almost all patients, uncertainties remained regarding the nature and boundaries of each segment, despite all efforts to achieve a distinct and well-circumscribed segmentation. Often, the contrast-enhancing and FET uptaking lesions partially overlapped. However, in a small set

10.3389/fonc.2022.998069

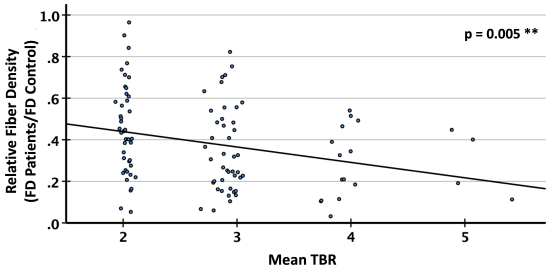

FIGURE 7
Relative fiber density (FD) in PET lesion segments with different tumor-to-brain ratio (TBR) of FET (O-(2-[^{18}F]fluoroethyl)-L-tyrosine) uptake. Linear regression, R^2=0.076, **p<0.01.

of non-overlapping contrast enhancing (n=24) or FET uptake lesions (n=9), a relative fiber density in the same order of magnitude as found before (56% and 54%) was observed. Also, the distinction between edema and radiation-induced gliosis proved difficult, such that a substantial proportion of patients could not be classified. Nevertheless, the relative fiber densities in these two lesion types did not differ significantly. In addition, hyperintense T2/FLAIR lesions could result from tumor infiltration not leading to contrast enhancement or pathologic FET uptake.

The minimal remaining fiber density within the resection cavity can be explained in part by the difficulty of unambiguous segmentation of the resection cavity boundaries. Therefore, it is possible that individual voxels that still contained tissue were part of the segmented area. On the other hand, it should be kept in mind that no model perfectly reflects reality, which in this case obviously resulted in a small number of false positive fibers inside the resection cavity. These problems are illustrated in Figure 2.

Conclusions

In summary, we interpret this study as follows: i) The almost complete fiber loss in the resection cavities was mainly the result of carefully planned neurosurgical interventions based on neuroanatomic and neuro-functional expertise, avoiding neurological deficits in most patients. ii) Most contrast-enhancing lesions were caused by recurrent tumor growth, which severely disrupted fiber tracts in deliberate localizations and thus impacted general performance significantly. iii) Most regions with increased FET uptake also resulted from recurrent tumor growth; however, due to the higher sensitivity of amino acid PET compared to MRI for detecting early tumor infiltration, the associated fiber density loss was less pronounced and did not impair general performance. iv) T2/FLAIR-hyperintense lesions mainly resulted from radiation injury or peritumoral edema or a

TABLE 3 Results of logistic regression analyses for the impact of total fiber loss on general performance status (normal ECOG=0 vs. impaired ECOG ≥ 1).

Imaging finding[#]	Total fiber loss median (range)	p-value univariate	p-value multivariate
Resection cavity	7506 (0 - 171033)	0.906	0.692
Increased FET uptake	3977 (0 - 204533)	0.054	0.462
Contrast enhancement	1774 (0 - 102088)	0.006**	0.040*
T2/FLAIR hyperintensities	20265 (0 - 168450)	0.013*	0.310

FET, O-(2-[^{18}F]fluoroethyl)-L-tyrosine; T2/FLAIR, T2-weighted fluid-attenuated inversion recovery; *p<0.05; **p<0.01; [#]including patients not affected by respective lesion type (lesion-specific volume/total fiber loss set to zero).

10.3389/fonc.2022.998069

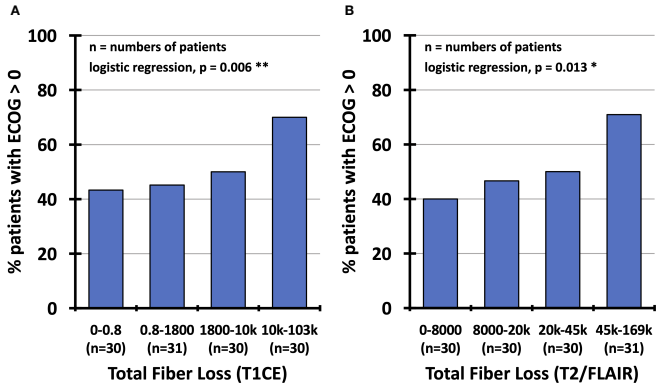

FIGURE 8
Percentage of patients with impaired performance status (ECOG score≥1) depending on total fiber loss (1 – (patient fiber density/reference fiber density) multiplied by lesion volume), partitioned into quartiles of observed values confined to contrast-enhancing lesions **(A)** and hyperintense T2/FLAIR regions **(B)**. ECOG, Eastern Cooperative Oncology Group; T1CE, T1-weighted contrast-enhancing; T2/FLAIR, T2-weighted fluid-attenuated inversion recovery.

combination thereof and affected larger brain areas. Although the reduction in fiber density was less pronounced, the larger affected brain volume likely led to dysfunction in many brain regions, resulting in impaired general performance.

Data availability statement

Data that support the findings of this study are available on reasonable request from the corresponding author. The data are not publicly available due to privacy or ethical restrictions.

Ethics statement

The study protocol was approved by the ethics committee of the University of Cologne, protocol no. 17-365. Informed written consent according to the Declaration of Helsinki was obtained from all patients and healthy subjects.

Author contributions

MF and MK analysed and interpreted most of the data. EF, PL, CL, and NJS developed the MR and PET imaging techniques. SC provided the control group data. GS and CPF performed the patient examinations. CWS, MIR, KJL, GRF, NG and MK recruited the patients and conceptualized the study. All authors contributed to the article and approved the submitted version.

Funding

This project was partially funded by the German National Cohort and the 1000BRAINS-Study of the Institute of Neuroscience and Medicine, Research Centre Juelich, Germany. We thank the Heinz Nixdorf Foundation (Germany) for the generous support of the Heinz Nixdorf Study. We thank the investigative group and the study staff of the Heinz Nixdorf Recall Study and 1000BRAINS. This project has received funding from the European Union's Horizon 2020 Research and Innovation Programme under Grant Agreement No. 945539 (HBP SGA3; SC) as well as from the Initiative and Networking Fund of the Helmholtz Association (SC). Open access publication is funded by the Deutsche Forschungsgemeinschaft (DFG, German Research Foundation, contract number 491111487).

Acknowledgments

The technical assistance of N. Judov, S. Frensch, T. Plum, S. Schaden, and L. Tellmann is gratefully acknowledged.

Conflict of interest

The authors declare that the research was conducted in the absence of any commercial or financial relationships that could be construed as a potential conflict of interest.

Publisher's note

References

1. Bullmore E, Sporns O. Complex brain networks: graph theoretical analysis of structural and functional systems. *Nat Rev Neurosci* (2009) 10(3):186–98. doi: 10.1038/nrn2575

2. Jung J, Cloutman LL, Binney RJ, Lambon Ralph MA. The structural connectivity of higher order association cortices reflects human functional brain networks. *Cortex* (2017) 97:221–39. doi: 10.1016/j.cortex.2016.08.011

3. Jung J, Visser M, Binney RJ, Lambon Ralph MA. Establishing the cognitive signature of human brain networks derived from structural and functional connectivity. *Brain Struct Funct* (2018) 223(9):4023–38. doi: 10.1007/s00429-018-1734-x

4. Power JD, Cohen AL, Nelson SM, Wig GS, Barnes KA, Church JA, et al. Functional network organization of the human brain. *Neuron* (2011) 72(4):665–78. doi: 10.1016/j.neuron.2011.09.006

5. van den Heuvel MP, Kahn RS, Goni J, Sporns O. High-cost, high-capacity backbone for global brain communication. *Proc Natl Acad Sci USA* (2012) 109 (28):11372–7. doi: 10.1073/pnas.1203593109

6. Luo N, Sui J, Abrol A, Chen J, Turner JA, Damaraju E, et al. Structural brain architectures match intrinsic functional networks and vary across domains: A study from 15 000+ individuals. *Cereb Cortex* (2020) 30(10):5460–70. doi: 10.1093/cercor/bhaa127

7. Zhang F, Daducci A, He Y, Schiavi S, Seguin C, Smith R, et al. Quantitative mapping of the brain's structural connectivity using diffusion MRI tractography: a review. *Neuroimage* (2022) 2021:118870. doi: 10.1016/j.neuroimage.2021.118870

8. Yeh FC, Irimia A, Bastos DCA, Golby AJ. Tractography methods and findings in brain tumors and traumatic brain injury. *Neuroimage* (2021) 245:118651. doi: 10.1016/j.neuroimage.2021.118651

9. Rosen BQ, Halgren E. A whole-cortex probabilistic diffusion tractography connectome. *eNeuro* (2021) 8(1). doi: 10.1523/ENEURO.0416-20.2020

10. Kazmi F, Soon YY, Leong YH, Koh WY, Vellayappan B. Re-irradiation for recurrent glioblastoma (GBM): a systematic review and meta-analysis. *J Neurooncol* (2019) 142(1):79–90. doi: 10.1007/s11060-018-03064-0

11. Salvati M, Pesce A, Palmieri M, Floriana Brunetto GM, Santoro A, Frati A. The role and real effect of an iterative surgical approach for the management of recurrent high-grade glioma: An observational analytic cohort study. *World Neurosurg* (2019) 124:e480–8. doi: 10.1016/j.wneu.2018.12.118

12. Weller M, Reifenberger G. Beyond the world health organization classification of central nervous system tumors 2016: what are the new developments for gliomas from a clinician's perspective? *Curr Opin Neurol* (2020) 33(6):701–6. doi: 10.1097/WCO.0000000000000871

13. Weller M, van den Bent M, Preusser M, Le Rhun E, Tonn JC, Minniti G, et al. EANO guidelines on the diagnosis and treatment of diffuse gliomas of adulthood. *Nat Rev Clin Oncol* (2021) 18(3):170–86. doi: 10.1038/s41571-020-00447-z

14. Bosma I, Vos MJ, Heimans JJ, Taphoorn MJ, Aaronson NK, Postma TJ, et al. The course of neurocognitive functioning in high-grade glioma patients. *Neuro Oncol* (2007) 9(1):53–62. doi: 10.1215/15228517-2006-012

15. Greene-Schloesser D, Robbins ME, Peiffer AM, Shaw EG, Wheeler KT, Chan MD. Radiation-induced brain injury: A review. *Front Oncol* (2012) 2:73. doi: 10.3389/fonc.2012.00073

16. Xi L, Moron F. Treatment-related MR imaging findings in patients with glioma after radiotherapy, chemotherapy, and biological therapy. *Clin Oncol* (2016) 1(1103).

17. Terziev R, Psimaras D, Marie Y, Feuvret L, Berzero G, Jacob J, et al. Cumulative incidence and risk factors for radiation induced leukoencephalopathy in high grade glioma long term survivors. *Sci Rep* (2021) 11(1):10176. doi: 10.1038/s41598-021-89216-1

18. Aerts H, Fias W, Caeyenberghs K, Marinazzo D. Brain networks under attack: robustness properties and the impact of lesions. *Brain* (2016) 139(Pt 12):3063–83. doi: 10.1093/brain/aww194

19. Oken MM, Creech RH, Tormey DC, Horton J, Davis TE, McFadden ET, et al. Toxicity and response criteria of the Eastern cooperative oncology group. *Am J Clin Oncol* (1982) 5(6):649–55. doi: 10.1097/00000421-198212000-00014

20. Gilbert MR, Dignam JJ, Armstrong TS, Wefel JS, Blumenthal DT, Vogelbaum MA, et al. A randomized trial of bevacizumab for newly diagnosed glioblastoma. *N Engl J Med* (2014) 370(8):699–708. doi: 10.1056/NEJMoa1308573

21. Witzmann K, Raschke F, Troost EGC. MR image changes of normal-appearing brain tissue after radiotherapy. *Cancers (Basel)* (2021) 13(7). doi: 10.3390/cancers13071573

22. Ding Z, Zhang H, Lv XF, Xie F, Liu L, Qiu S, et al. Radiation-induced brain structural and functional abnormalities in presymptomatic phase and outcome prediction. *Hum Brain Mapp* (2018) 39(1):407–27. doi: 10.1002/hbm.23852

23. Farquharson S, Tournier JD, Calamante F, Fabinyi G, Schneider-Kolsky M, Jackson GD, et al. White matter fiber tractography: why we need to move beyond DTI. *J Neurosurg* (2013) 118(6):1367–77. doi: 10.3171/2013.2.JNS121294

24. Jeurissen B, Leemans A, Tournier JD, Jones DK, Sijbers J. Investigating the prevalence of complex fiber configurations in white matter tissue with diffusion magnetic resonance imaging. *Hum Brain Mapp* (2013) 34(11):2747–66. doi: 10.1002/hbm.22099

25. Tournier JD, Calamante F, Connelly A. Robust determination of the fibre orientation distribution in diffusion MRI: non-negativity constrained super-resolved spherical deconvolution. *Neuroimage* (2007) 35(4):1459–72. doi: 10.1016/j.neuroimage.2007.02.016

26. Abhinav K, Yeh FC, Mansouri A, Zadeh G, Fernandez-Miranda JC. High-definition fiber tractography for the evaluation of perilesional white matter tracts in high-grade glioma surgery. *Neuro Oncol* (2015) 17(9):1199–209. doi: 10.1093/neuonc/nov113

27. Mato D, Velasquez C, Gomez E, Marco de Lucas E, Martino J. Predicting the extent of resection in low-grade glioma by using intratumoral tractography to detect eloquent fascicles within the tumor. *Neurosurgery* (2021) 88(2):E190–202. doi: 10.1093/neuros/nyaa463

28. Schult T, Hauser TK, Klose U, Hurth H, Ehricke HH. Fiber visualization for preoperative glioma assessment: Tractography versus local connectivity mapping. *PLoS One* (2019) 14(12):e0226153. doi: 10.1371/journal.pone.0226153

29. Becker D, Scherer M, Neher P, Jungk C, Jesser J, Pfluger I, et al. Q-ball - high resolution fiber tractography of language associated tracts-quantitative evaluation of applicability for glioma resections. *J Neurosurg Sci* (2019). doi: 10.23736/S0390-5616.19.04782-9

30. Caverzasi E, Hervey-Jumper SL, Jordan KM, Lobach IV, Li J, Panara V, et al. Identifying preoperative language tracts and predicting postoperative functional recovery using HARDI q-ball fiber tractography in patients with gliomas. *J Neurosurg* (2016) 125(1):33–45. doi: 10.3171/2015.6.JNS142203

31. Kupper H, Groeschel S, Alber M, Klose U, Schuhmann MU, Wilke M. Comparison of different tractography algorithms and validation by intraoperative stimulation in a child with a brain tumor. *Neuropediatrics* (2015) 46(1):72–5. doi: 10.1055/s-0034-1395346

32. Mormina E, Longo M, Arrigo A, Alafaci C, Tomasello F, Calamuneri A, et al. MRI Tractography of corticospinal tract and arcuate fasciculus in high-grade gliomas performed by constrained spherical deconvolution: Qualitative and quantitative analysis. *AJNR Am J Neuroradiol* (2015) 36(10):1853–8. doi: 10.3174/ajnr.A4368

33. Louis DN, Perry A, Reifenberger G, von Deimling A, Figarella-Branger D, Cavenee WK, et al. The 2016 world health organization classification of tumors of the central nervous system: a summary. *Acta Neuropathol* (2016) 131(6):803–20. doi: 10.1007/s00401-016-1545-1

34. Caspers S, Moebus S, Lux S, Pundt N, Schutz H, Muhleisen TW, et al. Studying variability in human brain aging in a population-based German cohort-rationale and design of 1000BRAINS. *Front Aging Neurosci* (2014) 6:149. doi: 10.3389/fnagi.2014.00149

35. Baek S, Park SH, Won E, Park YR, Kim HJ. Propensity score matching: a conceptual review for radiology researchers. *Korean J Radiol* (2015) 16(2):286–96. doi: 10.3348/kjr.2015.16.2.286

36. Kocher M, Jockwitz C, Lohmann P, Stoffels G, Filss C, Mottaghy FM, et al. Lesion-function analysis from multimodal imaging and normative brain atlases for prediction of cognitive deficits in glioma patients. *Cancers (Basel)* (2021) 13(10). doi: 10.3390/cancers13102373

37. Herzog H, Langen KJ, Weirich C, Rota Kops E, Kaffanke J, Tellmann L, et al. High resolution BrainPET combined with simultaneous MRI. *Nuklearmedizin* (2011) 50(2):74–82. doi: 10.3413/Nukmed-0347-10-09

38. Kickingereder P, Isensee F, Tursunova I, Petersen J, Neuberger U, Bonekamp D, et al. Automated quantitative tumour response assessment of MRI in neuro-oncology with artificial neural networks: a multicentre, retrospective study. *Lancet Oncol* (2019) 20(5):728–40. doi: 10.1016/S1470-2045(19)30098-1

39. Pauleit D, Floeth F, Tellmann L, Hamacher K, Hautzel H, Muller HW, et al. Comparison of O-(2-18F-fluoroethyl)-L-tyrosine PET and 3-123I-iodo-alpha-methyl-L-tyrosine SPECT in brain tumors. *J Nucl Med* (2004) 45(3):374–81.

40. Wu C, Ferreira F, Fox M, Harel N, Hattangadi-Gluth J, Horn A, et al. Clinical applications of magnetic resonance imaging based functional and structural connectivity. *Neuroimage* (2021) 244:118649. doi: 10.1016/j.neuroimage.2021.118649

41. Chen Z, Tie Y, Olubiyi O, Rigolo L, Mehrtash A, Norton I, et al. Reconstruction of the arcuate fasciculus for surgical planning in the setting of peritumoral edema using two-tensor unscented kalman filter tractography. *NeuroImage Clin* (2015) 7:815–22. doi: 10.1016/j.nicl.2015.03.009

42. Liao R, Ning L, Chen Z, Rigolo L, Gong S, Pasternak O, et al. Performance of unscented kalman filter tractography in edema: Analysis of the two-tensor model. *NeuroImage Clin* (2017) 15:819–31. doi: 10.1016/j.nicl.2017.06.027

43. Aerts H, Dhollander T. Marinazzo d: Evaluating the performance of 3-tissue constrained spherical deconvolution pipelines for within-tumor tractography. *bioRxiv preprint* (2019). doi: 10.1101/629873

44. Jeurissen B, Tournier JD, Dhollander T, Connelly A, Sijbers J. Multi-tissue constrained spherical deconvolution for improved analysis of multi-shell diffusion MRI data. *Neuroimage* (2014) 103:411–26. doi: 10.1016/j.neuroimage.2014.07.061

45. Dhollander T, Connelly A. A novel iterative approach to reap the benefits of multi-tissue CSD from just single-shell (+b=0) diffusion MRI data. *Proc Intl Soc Mag Reson Med* (2016) 24:3010.

46. Dhollander T, Raffelt D, Connelly A. Unsupervised 3-tissue response function estimation from single-shell or multi-shell diffusion MR data without a co-registered T1 image. *ISMRM Workshop Breaking Barriers Diffusion MRI* (2016) 2016:5.

47. Tournier JD, Smith R, Raffelt D, Tabbara R, Dhollander T, Pietsch M, et al. MRtrix3: A fast, flexible and open software framework for medical image processing and visualisation. *Neuroimage* (2019) 202:116137. doi: 10.1016/j.neuroimage.2019.116137

48. Gong S, Zhang F, Norton I, Essayed WI, Unadkat P, Rigolo L, et al. Free water modeling of peritumoral edema using multi-fiber tractography: Application to tracking the arcuate fasciculus for neurosurgical planning. *PLoS One* (2018) 13 (5):e0197056. doi: 10.1371/journal.pone.0197056

49. Dhollander T, Tabbara R, Rosnarho-Tornstrand J, Tournier JD, Raffelt D, Connelly A. Multi-tissue log-domain intensity and inhomogeneity normalisation for quantitative apparent fibre density. *Proc Intl Soc Mag Reson Med* (2021) 29:2472.

50. Smith RE, Tournier JD, Calamante F, Connelly A. Anatomically-constrained tractography: improved diffusion MRI streamlines tractography through effective use of anatomical information. *Neuroimage* (2012) 62(3):1924–38. doi: 10.1016/j.neuroimage.2012.06.005

51. Calamante F, Tournier JD, Heidemann RM, Anwander A, Jackson GD, Connelly A. Track density imaging (TDI): validation of super resolution property. *Neuroimage* (2011) 56(3):1259–66. doi: 10.1016/j.neuroimage.2011.02.059

52. Calamante F, Tournier JD, Jackson GD, Connelly A. Track-density imaging (TDI): super-resolution white matter imaging using whole-brain track-density mapping. *Neuroimage* (2010) 53(4):1233–43. doi: 10.1016/j.neuroimage.2010.07.024

53. Ashburner J, Friston KJ. Unified segmentation. *Neuroimage* (2005) 26 (3):839–51. doi: 10.1016/j.neuroimage.2005.02.018

54. Farrher E, Grinberg F, Kuo LW, Cho KH, Buschbeck RP, Chen MJ, et al. Dedicated diffusion phantoms for the investigation of free water elimination and mapping: insights into the influence of T2 relaxation properties. *NMR BioMed* (2020) 33(4):e4210. doi: 10.1002/nbm.4210

55. Pasternak O, Sochen N, Gur Y, Intrator N, Assaf Y. Free water elimination and mapping from diffusion MRI. *Magn Reson Med* (2009) 62(3):717–30. doi: 10.1002/mrm.22055

56. Newman BT, Dhollander T, Reynier KA, Panzer MB, Druzgal TJ. Test-retest reliability and long-term stability of three-tissue constrained spherical deconvolution methods for analyzing diffusion MRI data. *Magn Reson Med* (2020) 84(4):2161–73. doi: 10.1002/mrm.28242

57. Dhollander T, Mito R, Raffelt D, Connelly A. Improved white matter response function estimation for 3-tissue constrained spherical deconvolution. *Proc Intl Soc Mag Reson Med* (2019) 27:555.

58. Barajas RFJr., Hess CP, Phillips JJ, Von Morze CJ, Yu JP, Chang SM, et al. Super-resolution track density imaging of glioblastoma: histopathologic correlation. *AJNR Am J Neuroradiol* (2013) 34(7):1319–25. doi: 10.3174/ajnr.A3400

59. Stadlbauer A, Buchfelder M, Salomonowitz E, Ganslandt O. Fiber density mapping of gliomas: histopathologic evaluation of a diffusion-tensor imaging data processing method. *Radiology* (2010) 257(3):846–53. doi: 10.1148/radiol.10100343

60. Stadlbauer A, Hammen T, Buchfelder M, Bachmair J, Dorfler A, Nimsky C, et al. Differences in metabolism of fiber tract alterations in gliomas: a combined fiber density mapping and magnetic resonance spectroscopic imaging study. *Neurosurgery* (2012) 71(2):454–63. doi: 10.1227/NEU.0b013e318258e332

61. Fekonja LS, Wang Z, Aydogan DB, Roine T, Engelhardt M, Dreyer FR, et al. Detecting corticospinal tract impairment in tumor patients with fiber density and tensor-based metrics. *Front Oncol* (2020) 10:622358. doi: 10.3389/fonc.2020.622358

62. Liesche-Starnecker F, Prokop G, Yakushev I, Preibisch C, Delbridge C, Meyer HS, et al. Visualizing cellularity and angiogenesis in newly-diagnosed glioblastoma with diffusion and perfusion MRI and FET-PET imaging. *EJNMMI Res* (2021) 11(1):72. doi: 10.1186/s13550-021-00817-3

63. Stadlbauer A, Polking E, Prante O, Nimsky C, Buchfelder M, Kuwert T, et al. Detection of tumour invasion into the pyramidal tract in glioma patients with sensorimotor deficits by correlation of (18)F-fluoroethyl-L: -tyrosine PET and magnetic resonance diffusion tensor imaging. *Acta Neurochir (Wien)* (2009) 151 (9):1061–9. doi: 10.1007/s00701-009-0378-2

64. Nag S, Manias JL, Stewart DJ. Pathology and new players in the pathogenesis of brain edema. *Acta Neuropathol* (2009) 118(2):197–217. doi: 10.1007/s00401-009-0541-0

65. Dubois LG, Campanati L, Righy C, D'Andrea-Meira I, Spohr TC, Porto-Carreiro I, et al. Gliomas and the vascular fragility of the blood brain barrier. *Front Cell Neurosci* (2014) 8:418. doi: 10.3389/fncel.2014.00418

66. Jellison BJ, Field AS, Medow J, Lazar M, Salamat MS, Alexander AL. Diffusion tensor imaging of cerebral white matter: a pictorial review of physics, fiber tract anatomy, and tumor imaging patterns. *AJNR Am J Neuroradiol* (2004) 25(3):356–69.

67. Szerlip N, Rutter C, Ram N, Yovino S, Kwok Y, Maggio W, et al. Factors impacting volumetric white matter changes following whole brain radiation therapy. *J Neurooncol* (2011) 103(1):111–9. doi: 10.1007/s11060-010-0358-7

68. Duan F, Cheng J, Jiang J, Chang J, Zhang Y, Qiu S. Whole-brain changes in white matter microstructure after radiotherapy for nasopharyngeal carcinoma: a diffusion tensor imaging study. *Eur Arch Otorhinolaryngol* (2016) 273(12):4453–9. doi: 10.1007/s00405-016-4127-x

69. Chapman CH, Zhu T, Nazem-Zadeh M, Tao Y, Buchtel HA, Tsien CI, et al. Diffusion tensor imaging predicts cognitive function change following partial brain radiotherapy for low-grade and benign tumors. *Radiother Oncol* (2016) 120 (2):234–40. doi: 10.1016/j.radonc.2016.06.021

70. Chen W, Qiu S, Li J, Hong L, Wang F, Xing Z, et al. Diffusion tensor imaging study on radiation-induced brain injury in nasopharyngeal carcinoma during and after radiotherapy. *Tumori* (2015) 101(5):487–90. doi: 10.5301/tj.5000348

71. Ravn S, Holmberg M, Sorensen P, Frokjaer JB, Carl J. Differences in supratentorial white matter diffusion after radiotherapy–new biomarker of normal brain tissue damage? *Acta Oncol* (2013) 52(7):1314–9. doi: 10.3109/0284186X.2013.812797

72. Chapman CH, Nazem-Zadeh M, Lee OE, Schipper MJ, Tsien CI, Lawrence TS, et al. Regional variation in brain white matter diffusion index changes following chemoradiotherapy: A prospective study using tract-based spatial statistics. *PLoS One* (2013) 8(3):e57768. doi: 10.1371/journal.pone.0057768

2.2 Structural connectome-based predictive modeling of cognitive deficits in treated glioma patients

Attribution and license information for the following PDFs:

Included publication with supplementary data: *Structural connectome-based predictive modeling of cognitive deficits in treated glioma patients*
Michel Friedrich, Christian P Filss, Philipp Lohmann, Felix M Mottaghy, Gabriele Stoffels, Carolin Weiss Lucas, Maximilian I Ruge, N Jon Shah, Svenja Caspers, Karl-Josef Langen, Gereon R Fink, Norbert Galldiks, Martin Kocher
Originally published in Neuro-Oncology Advances, Volume 6, Issue 1, January-December 2024, vdad151
Available at: https://doi.org/10.1093/noajnl/vdad151

Modifications: A black border has been added to each page of the included PDFs.

Neuro-Oncology Advances

1

6(1), 1–13, 2024 | https://doi.org/10.1093/noajnl/vdad151 | Advance Access date 15 November 2023

Structural connectome-based predictive modeling of cognitive deficits in treated glioma patients

Michel Friedrich, Christian P. Filss, Philipp Lohmann, Felix M. Mottaghy, Gabriele Stoffels, Carolin Weiss Lucas, Maximilian I. Ruge, N. Jon Shah, Svenja Caspers, Karl-Josef Langen, Gereon R. Fink, Norbert Galldiks[†,‡], and Martin Kocher[†,‡]

Institute of Neuroscience and Medicine (INM-1, INM-3, INM-4, INM-11), Forschungszentrum Juelich, Juelich, Germany (M.F, C.P.F, P.L., G.S., N.J.S., S.C., K.-J.L., G.R.F, N.G., M.K.); Department of Nuclear Medicine, RWTH University Hospital Aachen, RWTH University Aachen, Aachen, Germany (F.M.M., K.-J.L.); Department of General Neurosurgery, Center for Neurosurgery, Faculty of Medicine and University Hospital Cologne, University of Cologne, Cologne, Germany (C.W.L.); Center of Integrated Oncology (CIO), Universities of Aachen, Bonn, Cologne, and Duesseldorf, Germany (C.W.L., M.I.R., K.-J.L., N.G., M.K.); Department of Stereotaxy and Functional Neurosurgery, Center for Neurosurgery, Faculty of Medicine and University Hospital Cologne, Cologne, Germany (M.I.R., M.K.); Juelich-Aachen Research Alliance (JARA), Section JARA-Brain, Juelich, Germany (N.J.S.); Department of Neurology, RWTH University Hospital Aachen, RWTH University Aachen, Aachen, Germany (N.J.S.); Institute for Anatomy I, Medical Faculty and University Hospital Duesseldorf, Heinrich Heine University Duesseldorf, Duesseldorf, Germany (S.C.); Department of Neurology, Faculty of Medicine and University Hospital Cologne, University of Cologne, Cologne, Germany (G.R.F, N.G.)

Corresponding Author: Martin Kocher, MD, Institute of Neuroscience and Medicine, Forschungszentrum Juelich, Wilhelm-Johnen-Str., 52428 Juelich, Germany (m.kocher@fz-juelich.de).

[†]These authors contributed equally to this work.
[‡]These authors are co-senior authors.

Abstract

Background. In glioma patients, tumor growth and subsequent treatments are associated with various types of brain lesions. We hypothesized that cognitive functioning in these patients critically depends on the maintained structural connectivity of multiple brain networks.

Methods. The study included 121 glioma patients (median age, 52 years; median Eastern Cooperative Oncology Group performance score 1; CNS-WHO Grade 3 or 4) after multimodal therapy. Cognitive performance was assessed by 10 tests in 5 cognitive domains at a median of 14 months after treatment initiation. Hybrid amino acid PET/MRI using the tracer O-(2-[^{18}F]fluoroethyl)-L-tyrosine, a network-based cortical parcellation, and advanced tractography were used to generate whole-brain fiber count-weighted connectivity matrices.The matrices were applied to a cross-validated machine-learning model to identify predictive fiber connections (edges), critical cortical regions (nodes), and the networks underlying cognitive performance.

Results. Compared to healthy controls ($n = 121$), patients' cognitive scores were significantly lower in 9 cognitive tests. The models predicted the scores of 7/10 tests (median correlation coefficient, 0.47; range, 0.39–0.57) from 0.6% to 5.4% of the matrix entries; 84% of the predictive edges were between nodes of different networks. Critically involved cortical regions (≥10 adjacent edges) included predominantly left-sided nodes of the visual, somatomotor, dorsal/ventral attention, and default mode networks. Highly critical nodes (≥15 edges) included the default mode network's left temporal and bilateral posterior cingulate cortex.

Conclusions. These results suggest that the cognitive performance of pretreated glioma patients is strongly related to structural connectivity between multiple brain networks and depends on the integrity of known network hubs also involved in other neurological disorders.

Key Points

- Cognitive performance is closely related to structural connectivity between multiple brain networks.
- Critically affected cortical nodes are mainly located in the left hemisphere.
- Involvement of bilateral cortical hubs known from other neurological disorders.

Graphical Abstract

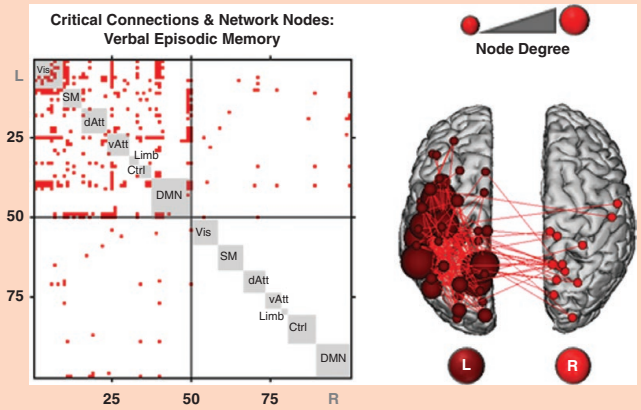

Importance of the Study

We here studied the association of whole-brain structural connectivity with cognitive performance in pretreated CNS WHO Grade 3 or 4 glioma patients through a network-based approach that included a recent cortical parcellation, advanced tractography methods, and a well-established method for connectome-based predictive modeling. We found that reduced fiber numbers in subsets of connections between different brain networks were significantly related to performance in various cognitive domains. Critical cortical regions, identified by their adjacency to predictive connections, were mainly located in the left hemisphere but also included bilateral cortical hubs, such as the precuneus and posterior cingulate cortex, which also play a significant role in other neurological diseases such as Alzheimer's disease. This finding implies that cognitive decline in treated brain tumor patients shares a common mechanism with other psychiatric and neurological disorders.

Gliomas are the most common malignant primary brain tumors in adults.[1] The prognosis of patients with gliomas mainly depends on molecular and histomorphologic tumor features that determine the growth rate and pattern of invasion into the normal brain tissue.[2] Apart from a reduced survival time, glioma patients frequently experience disturbances of cognitive function[3] that are potentially related to the structural damage imposed on the brain by the tumor itself or therapeutic interventions. Compared to other neurological disorders, such as stroke, multiple sclerosis, or dementia, the pattern of brain lesions in glioma patients is more heterogeneous, as it may comprise brain infiltration by residual or recurrent tumor growth, disruption of the blood-brain barrier, neurosurgical resection of cortical or subcortical brain tissue, or radiation- or chemotherapy-induced damage of white matter.[4]

So far, clinical research in neuro-oncology has primarily aimed at identifying selected vulnerable structures at risk of neurologic or cognitive deficits, such as the motor or language pathways (neurosurgery) or the hippocampus

(radiation therapy),[5] which in turn are preferably spared from treatment-related damage. The relationship between white matter alterations and cognitive deficits in glioma patients has been mainly established in the perioperative setting where single, anatomically defined tracts and their associated functions were identified. These include, among others, the right frontal aslant tract (executive functions, attention shift, verbal fluency),[6] the right superior longitudinal fascicle/frontostriatal tract/orbitofrontal cortex (mentalizing/visuospatial function),[7–10] and the right inferior frontostriatal tract/inferior frontal gyrus (inference control processes).[11] Moreover, radiation-induced alterations in the parahippocampal cingulum of the medial temporal lobes correlated with a decline in verbal memory and verbal fluency.[12]

However, a growing body of evidence indicates that the long-term outcome of higher-order cognitive functioning in glioma patients depends on the preserved integrity of several distributed networks rather than individual nodes or tracts,[13–16] which has led several groups to investigate the relation between cognitive outcome and structural connectivity in glioma on a more network-oriented level.[17–19] We also took this approach here and hypothesized that the various structural brain lesions in treated glioma patients impair cognitive functions through a common mechanism, namely the reduced structural connectivity between cortical regions, resulting from altered integrity of the cortical gray matter or the adjacent white matter fiber tracts. Therefore, we constructed whole-brain structural connectomes in pretreated patients with CNS WHO Grade 3 or 4 gliomas characterized according to the 2021 WHO classification of Tumors of the CNS,[2] and used advanced structural and diffusion-weighted MRI[20] as well as amino acid PET[21] imaging techniques to identify fiber tracts and structural brain lesions. In addition, a recent functional parcellation of the cortex[22] and tractography tools capable of reasonable fiber tracking within or close to tumor- or treatment-related lesions were applied.[23,24] The individual connectomes were used to develop a predictive machine-learning-based model[25] that identified networks, nodes, and connecting fiber tracts critical for performance in different cognitive domains.

Patients and Methods

Patient Characteristics

From February, 2018 to September, 2020, we prospectively evaluated 121 pretreated glioma patients (73 men, 48 women; mean age, 51.6 ± 11.6 years) who had undergone multimodal therapy, including resection, radiotherapy, alkylating chemotherapy, or combinations thereof (Supplementary Table 1). Patients were referred for follow-up from main academic institutions that had regular access to the 3T hybrid PET/MR imaging facility where simultaneous PET/MR imaging was performed using the radiolabeled amino acid O-(2-[^{18}F]fluoroethyl)-L-tyrosine (^{18}F-FET) at different time points after first-line therapy (median time, 14 months; range, 1–214 months). ^{18}F-FET PET is a sensitive method for early assessment of residual metabolically active tumors after surgery, evaluation of response to adjuvant chemotherapy using alkylating agents, and differentiation of tumor relapse from treatment-related changes.[26]

The inclusion criteria comprised a favorable general condition defined by a performance score of 0 or 1 according to the Eastern Cooperative Oncology Group[27] criteria, absence of major depression, and fluency in the German language. In case of a history of seizures, appropriate anticonvulsive medication was mandatory. Patients were screened and registered for the study by phone calls, reviewed on the day of imaging, and were included in the study after providing informed written consent following the Declaration of Helsinki. The local ethics committee approved the protocol (17–365). Of the 121 patients included, 104 (86%) had completed primary treatment according to the guidelines at the time of diagnosis. As shown in Supplementary Table 1, patients had either received tumor resection (n = 108) or biopsy (n = 13), and the majority (n = 100) had undergone at least 1 series of local radiotherapy (60 ± 2 Gy in 92% of patients) at a median interval of 13 months (range, 2–213 months) between the start of radiotherapy and imaging. Fourteen patients had 2 radiotherapy series. In 6 patients, planned postoperative radiotherapy/chemo-radiotherapy was pending; in 11 patients, adjuvant chemotherapy was incomplete. In order to quantify treatment intensity, the number of different types of oncologic interventions was assessed and analyzed about cognitive outcome.

The study included patients with adult-type diffuse glioma of Grades 3 and 4 according to the 2021 WHO classification.[2] All original neuropathological reports were re-classified mainly based on the isocitrate dehydrogenase (IDH)-gene mutation and 1p/19q loss-of-heterozygosity status. Most of the patients suffered from an IDH-wildtype glioblastoma (60%), but CNS WHO Grade 3 IDH-mutant astrocytomas (12%) and CNS WHO Grade 3 IDH-mutant 1p/19q co-deleted oligodendrogliomas (11%) were also prevalent. A total of 72 patients (60%) had anticonvulsive medication, and 81 patients (67%) had mild neurological (48%) or other symptoms (19%) without requiring assistance for personal needs. All patients except 1 were right-handed. Based on clinical deterioration, MRI findings, and ^{18}F-FET PET results, the diagnosis of glioma relapse was obtained in 58 of 121 patients.

Imaging Protocols

Simultaneous MR/PET imaging was performed on a 3T hybrid scanner (Siemens Trim-TRIO/BrainPET, Siemens Medical Systems, Erlangen, Germany) equipped with a PET insert. ^{18}F-FET PET images were obtained as described in detail before.[28] The presence or absence of metabolic active residual/recurrent tumor sites was assessed by a nuclear medicine physician (K.-J.L.) from the summed activity from 20 to 40 min post-injection and the time-activity curves according to established protocols.[26]

The MRI protocol comprised a 3D high-resolution T1-weighted magnetization-prepared rapid acquisition gradient echo (MPRAGE) native scan (176 slices;TR = 2250 ms; TE = 3.03 ms; field of view (FoV) = 256 × 256 mm^2; flip angle = 9°; voxel size = 1 × 1 × 1 mm^3), a contrast-enhanced MPRAGE scan recorded after injection of

gadolinium-based contrast agent, a T2-weighted sampling perfection with application-optimized contrasts using different flip angle evolution (SPACE) scan (176 slices; repetition time TR = 3.2 ms; echo time TE = 417 ms; FoV = 256 × 256 mm^2; voxel size = 1 × 1 × 1 mm^3), and a T2-weighted fluid-attenuated inversion recovery (T2/FLAIR) scan (25 slices; TR = 9000 ms; TE = 3.86 ms; FoV = 220 × 220 mm^2; flip angle = 150°; voxel size = 0.9 × 0.9 × 4 mm^3).

High-angular-resolution diffusion imaging (HARDI) measurements were acquired using a diffusion-weighted double-echo echo-planar imaging (EPI) sequence (55 slices; TR = 8000 ms; TE = 112 ms; b-values (gradient directions) = 0 (13, interleaved) and 2700 s/mm^2 (120); voxel size = 2.4 × 2.4 × 2.4 mm^3). Afterward, a nondiffusion-weighted ($b = 0$) volume was acquired with the same parameters but with a reversed phase-encoding direction needed for the EPI distortion correction.

Cognitive Performance

Cognitive performance was assessed on the day of imaging and based on 10 cognitive tests selected from a more extensive test battery developed for the 1000BRAINS study, a population-based cohort study that included over 1300 older subjects and investigated environmental and genetic influences on the interindividual variability of brain structure, function, and connectivity in the aging brain.[20] The applied test and the respective cognitive domains are shown in Supplementary Table 2. They included tests for attention/processing speed (Trail-making Test A [TMT-A]), executive function/concept shifting (Trail-making Test B [TMT-B]), semantic word fluency (Imagined Shopping Tour) and language processing (Number Transcoding), as well as tests for verbal working memory (Digit Span forward/backward), verbal episodic memory (Word List, immediate and delayed recall) and visuospatial working memory (Corsi Block Tapping test forward/backward).

For the generation of a control group, 121 healthy subjects who had performed the same cognitive tests were selected from the 1000BRAINS study. Propensity score matching[29] (R software package, https://www.r-project.org/) was applied to build a cohort that matched the patient population in terms of sex, age, and educational level according to the International Standard Classification of Education (ISCED) classification (http://uis.unesco.org/sites/default/files/documents/international-standard-classification-of-education-1997-en_0.pdf). This procedure resulted in a control group that broadly resembled the patient group (age 51.7 ± 11.5 vs 51.6 ± 11.6 years, 2-sided *t*-test $P = .96$; men/women 75/46 vs 73/48, 2-sided Chi-square test $P = .90$; ISCED-level 7.4 ± 1.7 vs 7.1 ± 2.1, 2-sided Mann–Whitney U-test $P = .41$). The cognitive deficits of the patients were classified as clinically relevant if their scores were lower than the mean−1.5× standard deviation of the control group.

Whole-brain Structural Connectome

The main steps for determining the whole-brain structural connectome and prediction modeling of cognitive performance are shown in Figure 1. We used the tractography imaging pipeline based on the GitHub-fork MRtrix3Tissue (https://3tissue.github.io), a recently developed modification of the widely accepted fiber-tracking software MRtrix3 (https://www.mrtrix.org). The novel single-shell 3-tissue constrained spherical deconvolution (SS3T-CSD) method generates estimates of white matter fiber orientation distribution functions (FODs) as bias-free as possible, even within different compartments infiltrated by the tumor.[23,30,31] This is mainly achieved by estimating the composition of each voxel in terms of white-matter-like, gray-matter-like, and cerebrospinal fluid-like tissue components, which are computed from single-shell HARDI data (single *b*-value 2700 s/mm^2 and nondiffusion-weighted images). CSD-based fiber mapping assumes that the diffusion-weighted MRI signal results from the spherical convolution of a response function with the underlying FOD function.[32] The response function, which is determined from the diffusion-weighted data itself, represents the expected MR signal from a pure white matter (a single-oriented white matter fiber bundle), gray matter, or cerebrospinal fluid voxel. Unlike the clinically widely used diffusion tensor model, CSD models can resolve multiple fiber orientations within an image voxel.

The HARDI data underwent image preprocessing following published recommendations (https://osf.io/ht7zv) and comprised corrections for EPI distortion, eddy current, motion distortion, and bias field. An unsupervised method was used to estimate the tissue-specific white matter, gray matter, and cerebrospinal fluid response functions from the preprocessed HARDI data. The response functions for each tissue compartment were averaged across all patients, and the tissue component fractions were corrected for the effects of residual intensity inhomogeneities by global intensity normalization[33] to ensure that FODs estimated by SS3T-CSD[30] were comparable within this group study. The subsequent fiber mapping was based on Anatomically Constrained Tractography, which poses physiological restrictions on the behavior of healthy neuronal fibers in terms of their propagation and termination.[24] These assumptions were lifted in the area of pathologic tissue by masking out the entire lesioned areas. For this purpose, resection cavities were manually contoured by a radiation oncologist (M.K.), the T1-contrast-enhancing lesions and T2/FLAIR hyperintensities were automatically segmented using the deep-learning-based software HD-GLIO-AUTO (https://github.com/NeuroAI-HD/HD-GLIO-AUTO), and ^{18}F-FET PET segmentation was implemented by an FSL (https://fsl.fmrib.ox.ac.uk/fsl/fslwiki) custom script using a tumor-to-brain ratio of 1.6 (20–40 min summed activity) as the lower threshold.[34] All segmentations were visually inspected, manually corrected, and added to form a composite lesion mask. Besides the default settings of MRtrix3Tissue, the number of seed points was set to a constant of 4 million seeds randomly placed in a whole-brain mask, the backtrack option was enabled, and the cutoff value for FOD amplitude was set to 0.01. In a former study,[4] we found that this setup could reasonably identify fibers passing through and near tumor tissue and the surrounding brain structures.

In order to obtain structural whole-brain connectivity matrices for each patient, the resulting set of fibers was combined with the functional cortical Schaefer-Yeo Atlas,[22]

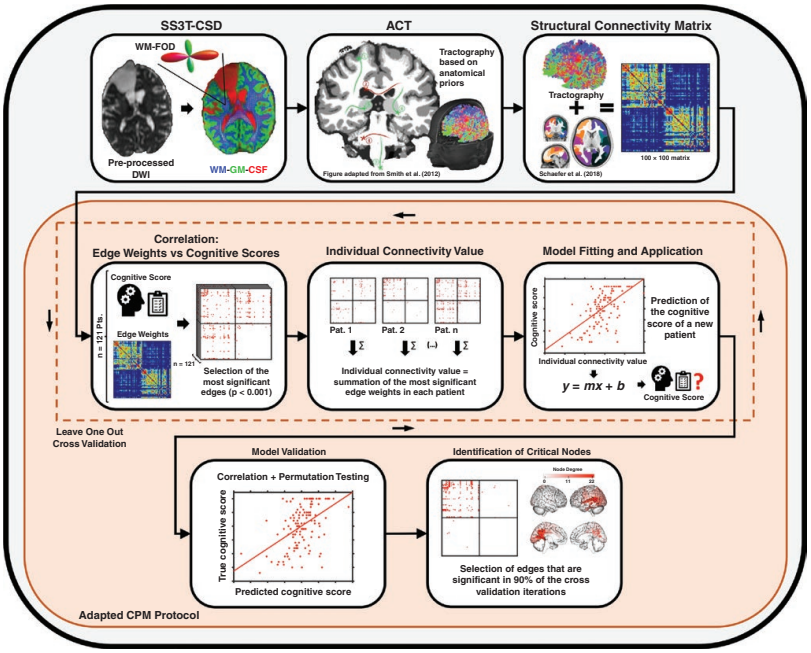

Figure 1. Overview of methods for determining the whole-brain structural connectome and generating and validating a connectome-based predictive model (CPM) for cognitive functioning in glioma patients following multimodality treatment. SS3T-CSD, single-shell 3-tissue constrained spherical deconvolution; WM, white matter; FOD, fiber orientation distribution function; DWI, diffusion-weighted magnetic resonance imaging; GM, gray matter; CSF, cerebrospinal fluid; ACT, Anatomically Constrained Tractography; Pts, patients; Pat, patient.

which comprises 100 nodes (50 in each hemisphere) at its lowest resolution, belonging to the following 7 networks: visual, somatomotor, dorsal attention, ventral attention, limbic, frontal control, and default mode network. The number of fibers connecting any 2 nodes was used to enter a 100 × 100 structural connectivity matrix, thus representing the edge weight between 2 nodes. Whole-brain tractography and structural connectivity matrices for 2 exemplary patients with left frontal and right temporal gliomas are shown in Figure 2.

Connectome-based Predictive Modeling

The relationship between structural brain connectivity and cognitive functions was analyzed using a well-established method (connectome-based predictive modeling [CPM]) initially described by Shen et al.[25] that uses machine-learning methods and cross-validation to predict behavioral outcomes from brain connectivity measures. CPM has been proven to perform equally or better compared to many existing approaches in brain-behavior prediction.[25] Also, compared to other machine-learning models, it has the advantages that it makes only use of linear operations, is purely data-driven, and can be clearly interpreted.

The CPM protocol comprises 4 steps which were performed in Matlab (Matlab R2022a, MathWorks, Natick, MA, USA). The structural connectivity matrices and corresponding cognitive test scores served as inputs. The main diagonal containing 100 meaningless entries was removed from the matrices for all further steps, leaving ([100 × 100]–100) = 9900 valid entries. For feature selection (i), each fiber count (edge weight) in the connectivity matrix was related to any of the cognitive test scores using Spearman's rank correlation, and only significant ($P < .001$) edges were selected. Next, summary connectivity values (ii) were calculated from the selected edges by separately summing the fiber counts of edges with negative or positive associations with the cognitive scores. For model construction (iii), linear regressions between the cognitive scores and the summary connectivity scores were computed. Furthermore, the relation between demographic, clinical, histomolecular and other tumor-related variates and cognitive performance was evaluated at this

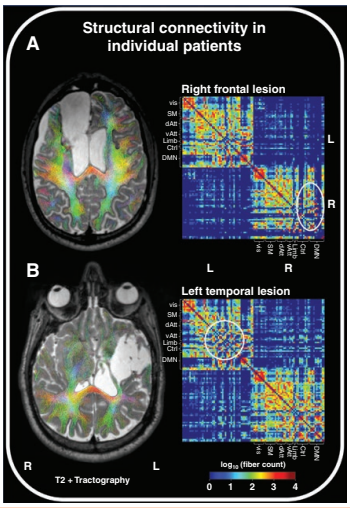

Figure 2. Whole-brain tractography and structural connectivity matrices in 2 exemplary patients with right frontal or left temporal gliomas. In the matrices, the log(10) of the fiber count connecting the respective cortical nodes belonging to 7 well-defined networks is color-coded as edge weight. White circles indicate sets of reduced connectivity. Vis, visual; SM, somatomotor; dAtt, dorsal attention; vAtt, ventral attention; Limb, limbic; Ctrl, frontal control; DMN, default mode network; L, left; R, right.

step by nonparametric statistical methods: age, education, time since treatment initiation, number of surgical interventions, number of radiotherapy series, number of chemotherapy courses, lesion volumes (Spearman rank correlation); sex, IDH mutation status (wildtype vs mutant), glioma Grade 3 versus Grade 4, presence of a recurrent tumor (Mann–Whitney *U*-Test); tumor location (Kruskal–Wallis analysis of variance). Univariate and multivariate models were constructed where the significant variables from this analysis were included in the CPM model as confounding covariates. Finally, the model's generalizability and predictive power (iv) were evaluated by leave-one-out cross-validation. The cognitive scores for each single patient were predicted using the described feature (edge) selection method and linear regression from the data of the remaining patients. The predicted scores were then compared to the patient's actual scores using both Pearson correlation and a permutation test with 100 iterations.

Brain Mapping of Edges and Nodes

As an additional step, binary matrices were constructed such that only those edges that correlated significantly with the cognitive scores in at least 90% of the cross-validation iterations (validated predictive edges) and had been included in the models with significant predictive power ($P < .05$) were labeled. For descriptive purposes, critically involved nodes of each network were identified from their degree, that is, the number of adjacent validated edges. The nonzero-degree-nodes' degree distribution was used for setting thresholds for critically involved nodes (degree ≥ mean + 1× standard deviation) and highly critical nodes (degree ≥ mean + 2× standard deviation). In addition, all validated edges were classified according to their belonging to within- or between network connections. The nodes and their degrees were then visualized in their anatomic location using the Connectivity Viewer of the BioImage Suite Web 1.2.0 (https://bioimagesuiteweb.github.io/webapp/connviewer.html?species=human).

Results

Cognitive Performance

The detailed cognitive test scores in glioma patients and healthy individuals are shown in Supplementary Table 3. Glioma patients performed significantly lower than healthy individuals in all tests except for the Number Transcoding test. The highest deviation from the control group was observed in trail-making tests (TMT-A, time needed: +53.1%; TMT-B, time needed: +72.4%), followed by the semantic word fluency test (Imagined Shopping Tour, number of items: −24.6%). The lowest deviation was observed in a test on verbal working memory (Digit Span Forward, items: −7.5%). Depending on the test applied, 10%–47% of the patients were prone to a clinically relevant deficit.

Connectome-based Predictive Modeling

As shown in Figure 2, the edge values (fiber counts) were clustered within the ipsilateral nodes of the different networks such that intra-hemispheric connectivity was more pronounced than inter-hemispheric connectivity. The number of connecting fibers of each node to any ipsi- or contralateral nodes spanned a wide range but was nearly equally distributed in the right (median fiber number, 48; range, 0–4462 fibers) compared to the left (median fiber number, 43; range, 0–4604 fibers) hemisphere. In lesions of both sides, the median nodal fiber count for intra-hemispheric connections was lower in the affected than in the contralateral hemisphere: median fiber number in left-sided lesions, 41 (range, 0–4035 fibers) versus 52 (range, 0–4849 fibers); median fiber number in right-sided lesions, 40 (range, 0–4013 fibers) versus 47 (range, 0–5265 fibers), representing an average fiber loss of 15%–20% per node in the affected hemisphere.

In the first step of the CPM analysis, 2770 node-to-node fiber counts with a significant correlation to any of the 10 cognitive test scores (predictive edges) were identified. In the vast majority (2704/2770 = 98%) of node-to-node fiber counts, the sign of the correlation indicated a positive association between fiber counts and cognitive scores (negative sign for the TMT-A and TMT-B, positive sign for all other tests, see Supplementary Table 4). A median number of 254 of the positively associated predictive edges per

cognitive test (range, 32–542) was selected for linear regression modeling between the connectivity values and the corresponding cognitive performance scores of all 121 patients. All linear relationships were significant ($P <$ .001), and most of them had a coefficient of determination (R^2) in the range between 0.35 and 0.45, examples shown in Supplementary Figure 1. Conversely, models built from the negatively associated edges had R^2-values in the range of 0.02 to 0.16 (Supplementary Table 4). The analysis of the demographic, clinical, or tumor-related variables showed significant ($P <$ .01) relations with cognitive scores for age (9 of 10 scores), education (8 of 10 scores), tumor location (3 of 10 scores), lesion volumes (1–5 of 10 scores depending on lesion type) and tumor recurrence (1 of 10 scores), but no significant associations for sex, tumor grade, IDH-status, interval, surgical procedures, radiotherapy series, or chemotherapy courses (Supplementary Table 5).

The predictive abilities of different models including the above-mentioned variates alone or in combination with the positively associated summary connectivity values are shown in Figure 3 and Supplementary Table 6. The pure connectivity models had a significantly higher mean coefficient of determination (0.330 ± 0.083) than the combined models from either age and education (0.141 ± 0.037) or recurrence and lesion volumes and tumor location (0.208 ± 0.071; both $P <$ .001, *t*-test). The coefficient of determination of the latter models increased significantly by including the connectivity values (mean increase by 0.190 and 0.225, respectively; both $P <$ .001), and all connectivity values proved their independent relation with the cognitive scores (all $P <$ .001) in the combined multiple regression models.

Therefore, the edges with a positive association to cognitive scores were exclusively used for the final, cross-validated model. The results for the correlation and permutation analyses between the predicted scores from the leave-one-out cross-validation and the actual scores are shown in Table 1 and Figure 4. The models predicted 7 out of 10 scores (median correlation coefficient, 0.47; range, 0.39–0.57) from 64 to 530 of 9900 (0.6%–5.4%) of the possible edges, underpinning the predictive value and potential generalizability of the developed model; illustrative examples are shown in Figure 4. However, the final model did not accurately predict the scores for the digit span tests evaluating the verbal working memory.

Brain Mapping of Validated Edges and Critical Nodes

The binary matrices of the cross-validated edges for some cognitive tests are shown in Figure 5A–C and Supplementary Figure 2 together with an anatomical representation of the validated edges and their adjacent nodes. The validated edges followed a pattern of mainly left intra-hemispheric as well as inter-hemispherical connections. Of note, the majority (overall 1660/1982 = 84%; Table 1) of the validated edges were between nodes of different networks (inter-network connections, median 208, range 38–386) rather than between nodes of the same network (median 19, range 5–41). This observation is also evident from the binary matrices (Figure 5A–C, Supplementary Figure 2) where all potential intra-network

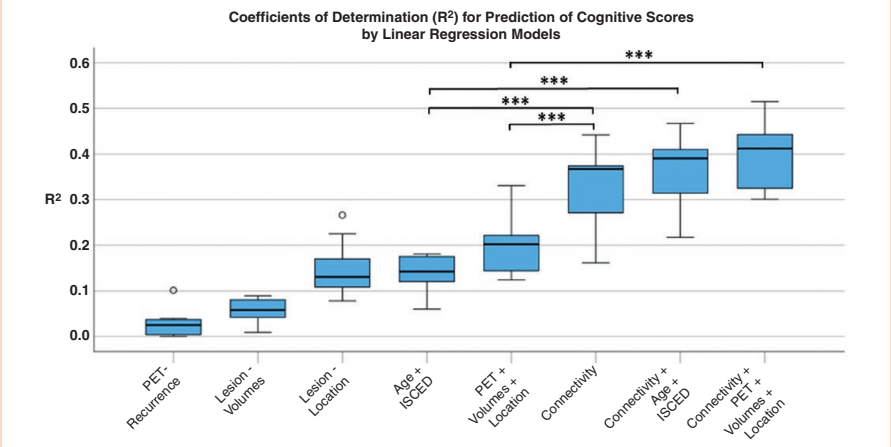

Figure 3. Performance of different linear regression models used for prediction of cognitive scores. The distributions of the coefficients of determination achieved in 10 cognitive tests are depicted as boxplots. The CPM-model using only the connectivity values outperformed the models using demographic and tumor-related variates, and the connectivity values significantly improved the performance of the latter models when additionally included. ISCED, International Standard Classification of Education; ***$P <$ .001.

Table 1. Results of Model Cross-validation (CV)

	Model cross-validation (CV)*				Identification of validated edges†		
Test (cognitive domains)	Average edge number included (%)‡	RMSE	Correlation coefficient (*r*)	*P*-value permutation	Validated intra-network edges	Validated inter-network edges	Total validated edges (%)‡
Trail-making Test A (s) (Attention, processing speed)	514 (5.2%)	31.61	0.388***	0.01*	82	344	426 (4.3%)
Trail-making Test B (s) (Executive function, concept shifting)	530 (5.4%)	71.66	0.470***	0.01*	74	386	460 (4.6%)
Imagined shopping tour [items] (Language, semantic word fluency)	205 (2.1%)	6.82	0.481***	0.01*	26	148	174 (1.8%)
Number transcoding [items] (Language processing)	64 (0.6%)	0.99	0.411***	0.01*	10	38	48 (0.5%)
Digit span Fw [weighted items] (Verbal working memory)	30 (0.3%)	2.43	0.123	0.13	CV not passed	CV not passed	CV not passed
Digit span Bw [weighted items] (Verbal working memory)	56 (0.6%)	2.58	0.132	0.16	CV not passed	CV not passed	CV not passed
Corsi block tapping Fw [weighted items] (Visuospatial working memory)	224 (2.3%)	2.32	0.202*	0.11	CV not passed	CV not passed	CV not passed
Corsi block tapping Bw [weighted items] (Visuospatial working memory)	319 (3.2%)	1.99	0.433***	0.01*	56	208	264 (2.7%)
Word list, immediate recall [items] (Verbal episodic memory)	440 (4.4%)	3.08	0.570***	0.01*	38	336	374 (3.8%)
Word list, delayed recall [items] (Verbal episodic memory)	272 (2.7%)	2.38	0.525***	0.01*	36	200	236 (2.4%)

Notes: Fw = Forward; Bw = Backward; RSME = Root (of) Mean Squared Error.
*Models based on edges positively associated with cognitive performance.
†Edges significant in 90% of cross-validation iterations.
‡No edges from the nodes to themselves, $n = ([100 \times 100]–100) = 9900$ possible edges.
*$P < .05$. ***$P < .001$.

connections are displayed in gray. The few negatively associated edges (identified in Step 1) were sparsely distributed with a tendency to be situated between nodes of the right hemisphere (Supplementary Figure 3).

A detailed heatmap of the network nodes and their degrees of adjacent validated edges concerning the raised cognitive scores are shown in Figure 5D. The nodes adjacent to a nonzero number of validated edges had a degree of 5.4 ± 5.2; therefore, nodes with a degree ≥10 validated edges were regarded as critical for descriptive purposes here. The distribution of these critically involved nodes varied considerably between domains. Critical nodes for attention/processing speed (TMT-A) and executive function/concept shifting (TMT-B) were mainly located in the left visual and somatomotor networks but also included nodes from the bilateral dorsal attention and default mode networks. For performance in visual working memory (Corsi Block Tapping), mainly nodes of the right dorsal attention and bilateral default mode networks proved critical and were predominantly connected by inter-hemispherical

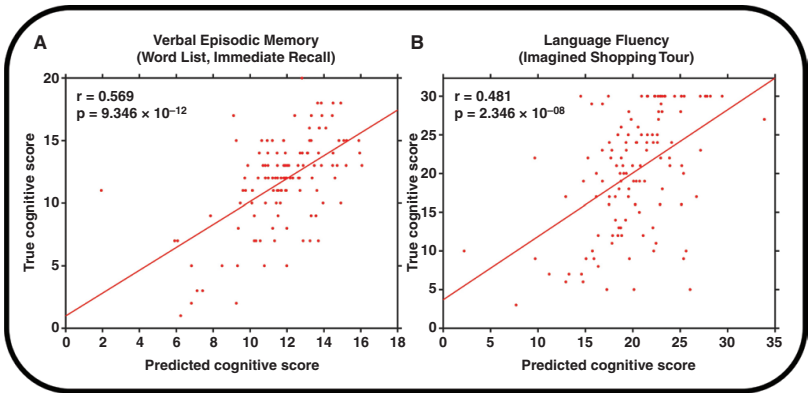

Figure 4. Correlation analysis between the predicted and actual scores of cognitive tests for verbal episodic memory (immediate recall) and language fluency in 121 glioma patients. *r*, correlation coefficient.

fibers. Nodes and connections critically involved in verbal semantic memory (Word List, immediate and delayed recall) were almost exclusively left-sided and included nodes from the visual, somatomotor, and default mode networks (Figure 5A–C; Supplementary Figure 2). Interestingly, highly critical nodes (degree ≥15 adjacent validated edges) included the default mode network nodes in the left temporal/parietal or bilateral posterior cingulate cortex in 4 to 5 of the 7 predictive models.

Discussion

As demonstrated in recent randomized trials and the present study, glioma patients are at high risk of developing cognitive decline during their course of disease.[3] Although the relationship between brain damage and neurological function is generally well established for the eloquent primary cortical areas and their associated fiber tracts,[35] the underlying causes of cognitive deterioration in brain tumor patients remain poorly understood.[36–38] Nevertheless, initial studies in glioma patients suggested that evaluating brain networks may help further elucidate the cognitive decline of various domains.[13–15,39,40] In the present study, we hypothesized that decreased structural connectivity in whole-brain networks is associated with cognitive deterioration in glioma patients. Therefore, we applied an innovative tractography algorithm[4,23] in combination with a network-based parcellation that allowed the construction of a whole-brain connectome of the structurally altered brain of pretreated glioma patients in conjunction with a well-developed method for predicting traits and symptoms from connectivity data.[25] Thus, we could show that reduced fiber numbers in subsets of connections mainly connecting different brain networks were significantly related to performance deficits in different cognitive domains. Critical cortical regions (nodes) having cross-validated connections to a high number of other nodes included mainly left-hemispheric cortical regions nodes and several cortical regions known as hubs, such as the bilateral precuneus or posterior cingulate cortex.[41]

As expected, lesion location concerning the major cerebral lobes was significantly associated with reduced scores in a subset of cognitive tests. Of note, this only gives a rough orientation and does not allow for a fine-grained characterization of the cortical regions and fiber tracts involved in the performance of specific cognitive domains. In principle, the relation between lesion location and symptom severity could have been brought down to the voxel level, resulting in the widely used method of voxel-based lesion-symptom mapping which has also been applied in brain tumors.[42] However, despite the high spatial resolution, this method has the disadvantage that it arbitrarily maps gray and white matter and can only be applied in brain locations with a representative number of lesions. This may result in diverging results depending on the pathology under investigation, for example, for tumors versus stroke.[43]

Whole-brain Connectome: The Importance of Networks and Hubs

Although the integrity of single fiber tracts appears to have a measurable impact on different aspects of cognitive functioning, most higher brain functions are probably supported by more general organizational principles governing the information flow in the brain. Regarding structural connectivity, several highly connected cortical regions have been identified and termed the "rich club."[41] Most of these are also present in functional resting-state networks (RSN)[44,45] and are predominantly located in the posterior part of the default mode network.[45,46] Functionally,

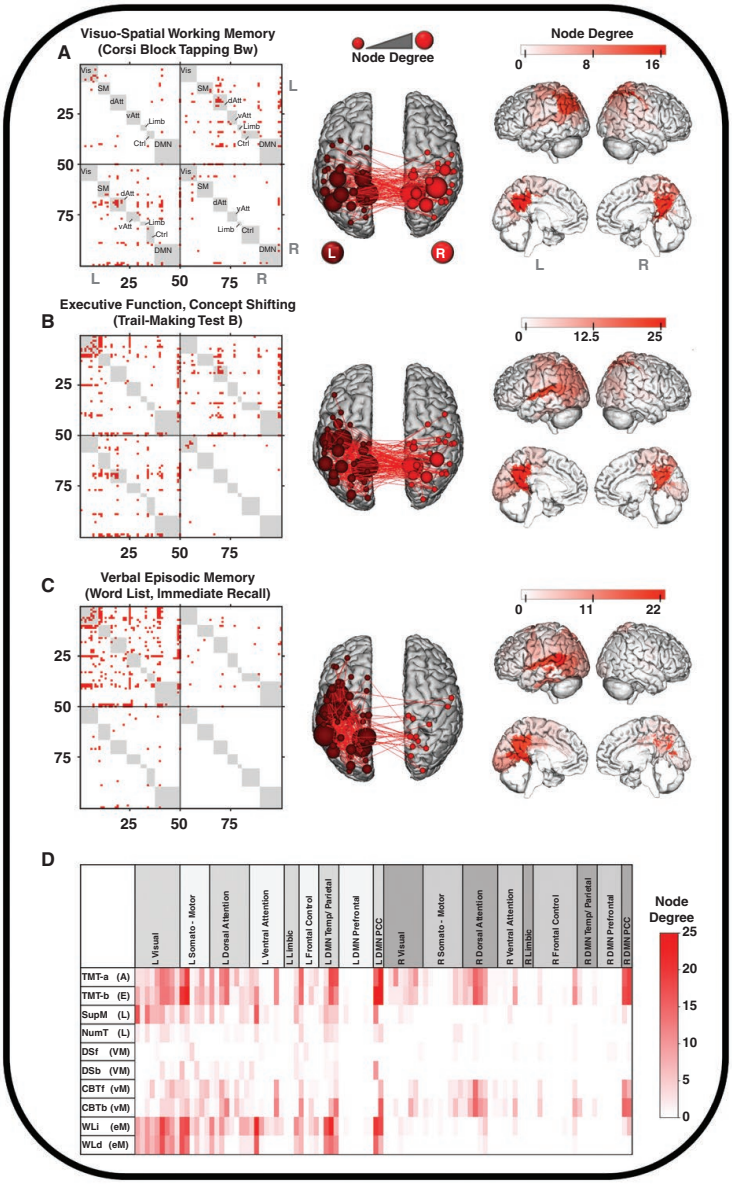

Figure 5. Left: Binary connectivity matrices labeling cross-validated predictive edges; membership of nodes to networks marked in gray. Middle/Right: Anatomical representation of the critical nodes by visualization of node degree and connecting edges. Results are shown for 3 representative cognitive tests. (**A**) Corsi Block Tapping (visual working memory), (**B**) Trail-making Test B (processing speed), (**C**) Word List,

immediate recall (verbal semantic memory). (**D**) Heatmap of the networks and nodes and their degrees of adjacent cross-validated predictive edges concerning the raised cognitive scores. Bw, Backward; L, left; R, right; Vis, visual; SM, somatomotor; dAtt, dorsal attention; vAtt, ventral attention; Limb, limbic; Ctrl, frontal control; DMN, default mode network; Temp, temporal; TMT-A (A), Trail-Making Test A (attention); TMT-B (E), Trail-Making Test B (executive function); SupM (L), Imagined Shopping Tour (language); DSf (VM), Digit Span Forward (verbal working memory); DSb (VM), Digit Span Backward (verbal working memory); CBTf (vM), Corsi Block Tapping Forward (visuospatial working memory); CBTb (vM), Corsi Block Tapping Backward (visuospatial working memory); WLi (eM), Word List, immediate recall (verbal episodic memory); WLd (eM), Word List, delayed recall (verbal episodic memory); PCC, posterior cingulate cortex.

they seem to serve primarily for connectivity between the RSNs, especially between the default mode, attention, and control networks.[45]

These findings and the availability of advanced MR imaging techniques in the clinic have led to more network-oriented approaches for investigating the dependence of cognitive performance on structural connectivity in perioperative glioma patients. In patients with low-grade gliomas, Cocherau et al.[17] studied a more extensive set of tracts using tract-wise lesion-symptom mapping and found the integrity of the left superior longitudinal fascicle and left frontal aslant/frontostriatal tracts to be most predictive for the development of postoperative disturbances in executive functioning and phonologic fluency. Liu et al.[18] constructed a whole-brain structural connectome from deterministic tractography in preoperative glioma patients. They observed that local (node) efficiency, a measure for communication strength among the first neighbors of a node, was generally reduced in tumor patients and particularly related to memory function in temporal tumors and to information processing speed in frontal tumors. Zhang et al.[16] applied navigated transcranial magnetic stimulation (nTMS) and whole-brain deterministic tractography in left-sided tumors and observed a correlation between the average node degree (and other connectome properties) of the left-hemispheric/nTMS-positive networks and the degree of aphasia. A network-level approach was also adopted by Mrah et al.,[19] who computed lesion overlap and white matter dysconnectivity scores for several atlas-based functional networks in low-grade glioma. Through a machine-learning algorithm, lesions or disconnections of the frontoparietal (control) network proved to be most predictive for postoperative deterioration in cognitive set-shifting.

In the present study, we used a network and node definition scheme encompassing the entire cerebral cortex and considered all potential structural connections between cortical nodes, including those lying outside anatomically designated tracts. Despite significant variation between cognitive domains, most predictive connections were those between different RSNs rather than within single RSNs. The distribution of critically involved nodes also varied considerably between domains but included nodes of the left visual and somatomotor networks and bilateral nodes of the dorsal attentional and default mode networks in several domains. Particularly critical nodes included the default mode network's left temporal and bilateral posterior cingulate cortex. These findings fit well with the view that structural connections between RSNs form the backbone of functional connectivity, enabling higher cognitive processes. From a more general point of view, these results may imply that cognitive decline in treated brain tumor patients shares a common mechanism with other major psychiatric and neurological disorders where the rich club nodes were also found to be predominantly involved,[47] such as the precuneus/posterior cingulate cortex in Alzheimer's disease.[48]

As cognitive performance depends on several nodes of different networks, the present models could be used to predict cognitive decline in individual glioma patients especially when local treatments such as surgery and radiotherapy are planned. In these situations, post-therapeutic cognitive deficits could arise unforeseen by clinical judgment or standard neuro-navigation, but may be anticipated or avoided by pre-therapeutic whole-brain tractography and critical node definitions as provided here.

Limitations

This study included patients with substantial variability in treatment intensity and time between treatment initiation and imaging/neurocognitive assessment. In addition, each patient was observed only once, such that longitudinal observations were not available. On the other hand, while group analyses are usually challenging to perform in this constellation, a rich, diverse pattern of structural damage may have facilitated the construction of a predictive model for cognition performance. From a methodological point of view, applying an atlas-based parcellation created from healthy subjects may be questionable because a functional restructuring of the brain, including shifts and deformations of cortical nodes, may have occurred in the patients. Finally, fiber tractography always approximates the actual white matter structure because even the most advanced methods may fail, especially in structurally altered brain tissue.

Conclusion

In summary, the present results suggest that the cognitive performance of pretreated glioma patients is strongly related to the structural connectivity between multiple brain networks and the integrity of known network hubs. This mirrors a pattern observed for other major neurological disorders. Whole-brain tractography in conjunction with the definition of critical cortical nodes should be further evaluated for improving local treatment planning in glioma patients.

Supplementary Material

Supplementary material is available online at *Neuro-Oncology* (https://academic.oup.com/neuro-oncology).

Keywords

brain networks | cognitive functions | diffusion-weighted imaging | glioma | structural connectivity

Funding

Open-access publication is funded by the Deutsche Forschungsgemeinschaft (DFG, German Research Foundation, contract number 491111487).

Acknowledgments

The technical assistance of N. Judov, T. Plum, S. Schaden, and L. Tellmann is gratefully acknowledged.

Conflict of Interest Statement

N.G. has received honoraria from Telix Pharmaceuticals and Blue Earth Diagnostics. The other authors report no conflict of interest.

Authorship Statement

M.F. and M.K. analyzed and interpreted most of the data. P.L., K.-J.L., and N.J.S. developed the MR and PET imaging techniques. S.C. provided the control group data. G.S. and C.P.F. performed the patient examinations. F.M.M., C.W.S., M.I.R., K.-J.L., G.R.F., N.G., and M.K. recruited the patients and conceptualized the study. All authors contributed to the article and approved the submitted version.

Data Availability

Anonymized and aggregated data are available upon reasonable request.

References

1. Lapointe S, Perry A, Butowski NA. Primary brain tumours in adults. *Lancet*. 2018;392(10145):432–446.
2. Louis DN, Perry A, Wesseling P, et al. The 2021 WHO classification of tumors of the central nervous system: a summary. *Neuro Oncol*. 2021;23(8):1231–1251.
3. De Roeck L, Gillebert CR, van Aert RCM, et al. Cognitive outcomes after multimodal treatment in adult glioma patients: a meta-analysis. *Neuro Oncol*. 2023;25(8):1395–1414.
4. Friedrich M, Farrher E, Caspers S, et al. Alterations in white matter fiber density associated with structural MRI and metabolic PET lesions following multimodal therapy in glioma patients. *Front Oncol*. 2022;12:998069; doi:10.3389/fonc.2022.998069
5. Le Fevre C, Cheng X, Loit MP, et al. Role of hippocampal location and radiation dose in glioblastoma patients with hippocampal atrophy. *Radiat Oncol*. 2021;16(1):112.
6. Landers MJF, Meesters SPL, van Zandvoort M, de Baene W, Rutten GM. The frontal aslant tract and its role in executive functions: a quantitative tractography study in glioma patients. *Brain Imag Behav*. 2022;16(3):1026–1039.
7. Liu D, Liu Y, Hu X, et al. Alterations of white matter integrity associated with cognitive deficits in patients with glioma. *Brain Behav*. 2020;10:e01639.
8. Nakajima R, Kinoshita M, Miyashita K, et al. Damage of the right dorsal superior longitudinal fascicle by awake surgery for glioma causes persistent visuospatial dysfunction. *Sci Rep*. 2017;7(1):17158.
9. Nakajima R, Kinoshita M, Okita H, et al. Neural networks mediating high-level mentalizing in patients with right cerebral hemispheric gliomas. *Front Behav Neurosci*. 2018;12:33.
10. Nakajima R, Yordanova YN, Duffau H, Herbet G. Neuropsychological evidence for the crucial role of the right arcuate fasciculus in the face-based mentalizing network: a disconnection analysis. *Neuropsychologia*. 2018;115:179–187.
11. Puglisi G, Howells H, Sciortino T, et al. Frontal pathways in cognitive control: direct evidence from intraoperative stimulation and diffusion tractography. *Brain*. 2019;142(8):2451–2465.
12. Chapman CH, Zhu T, Nazem-Zadeh M, et al. Diffusion tensor imaging predicts cognitive function change following partial brain radiotherapy for low-grade and benign tumors. *Radiother Oncol*. 2016;120(2):234–240.
13. Dadario NB, Brahimaj B, Yeung J, Sughrue ME. Reducing the cognitive footprint of brain tumor surgery. *Front Neurol*. 2021;12:711646.
14. Duffau H. Why brain radiation therapy should take account of the individual structural and functional connectivity: toward an irradiation "a la carte". *Crit Rev Oncol Hematol*. 2020;154:103073.
15. Herbet G, Duffau H. Revisiting the functional anatomy of the human brain: toward a meta-networking theory of cerebral functions. *Physiol Rev*. 2020;100(3):1181–1228.
16. Zhang H, Ille S, Sogerer L, et al. Elucidating the structural-functional connectome of language in glioma-induced aphasia using nTMS and DTI. *Hum Brain Mapp*. 2022;43(6):1836–1849.
17. Cochereau J, Lemaitre AL, Wager M, et al. Network-behavior mapping of lasting executive impairments after low-grade glioma surgery. *Brain Struct Funct*. 2020;225(8):2415–2429.
18. Liu Y, Yang K, Hu X, et al. Altered rich-club organization and regional topology are associated with cognitive decline in patients with frontal and temporal gliomas. *Front Hum Neurosci*. 2020;14:23.
19. Mrah S, Descoteaux M, Wager M, et al. Network-level prediction of set-shifting deterioration after lower-grade glioma resection. *J Neurosurg*. 2022;137:1329–1337.
20. Caspers S, Moebus S, Lux S, et al. Studying variability in human brain aging in a population-based German cohort-rationale and design of 1000BRAINS. *Front Aging Neurosci*. 2014;6:149.
21. Langen KJ, Galldiks N, Hattingen E, Shah NJ. Advances in neuro-oncology imaging. *Nat Rev Neurol*. 2017;13(5):279–289.
22. Schaefer A, Kong R, Gordon EM, et al. Local-global parcellation of the human cerebral cortex from intrinsic functional connectivity MRI. *Cereb Cortex*. 2018;28(9):3095–3114.
23. Aerts H, Dhollander T, Marinazzo D. Evaluating the performance of 3-tissue constrained spherical deconvolution pipelines for within-tumor tractography. *bioRxiv*. preprint. 2019; doi:10.1101/629873

24. Smith RE, Tournier JD, Calamante F, Connelly A. Anatomically-constrained tractography: improved diffusion MRI streamlines tractography through effective use of anatomical information. *Neuroimage*. 2012;62(3):1924–1938.
25. Shen X, Finn ES, Scheinost D, et al. Using connectome-based predictive modeling to predict individual behavior from brain connectivity. *Nat Protoc*. 2017;12(3):506–518.
26. Langen KJ, Stoffels G, Filss C, et al. Imaging of amino acid transport in brain tumours: positron emission tomography with O-(2-[(18)F]fluoroethyl)-L-tyrosine (FET). *Methods*. 2017;130:124–134.
27. Oken MM, Creech RH, Tormey DC, et al. Toxicity and response criteria of the Eastern Cooperative Oncology Group. *Am J Clin Oncol*. 1982;5(6):649–655.
28. Herzog H, Langen KJ, Weirich C, et al. High resolution BrainPET combined with simultaneous MRI. *Nuklearmedizin*. 2011;50(2):74–82.
29. Baek S, Park SH, Won E, Park YR, Kim HJ. Propensity score matching: a conceptual review for radiology researchers. *Korean J Radiol*. 2015;16(2):286–296.
30. Dhollander T, Connelly A. A novel iterative approach to reap the benefits of multi-tissue CSD from just single-shell (+b=0) diffusion MRI data. *Proc. Intl. Soc. Mag. Reson. Med*. 2016;24:3010.
31. Dhollander T, Raffelt D, Connelly A. Unsupervised 3-tissue response function estimation from single-shell or multi-shell diffusion MR data without a co-registered T1 image. *ISMRM Workshop on Breaking the Barriers of Diffusion MRI*. 2016:5.
32. Tournier JD, Calamante F, Connelly A. Robust determination of the fibre orientation distribution in diffusion MRI: non-negativity constrained super-resolved spherical deconvolution. *Neuroimage*. 2007;35(4):1459–1472.
33. Dhollander T, Tabbara R, Rosnarho-Tornstrand J, et al. Multi-tissue log-domain intensity and inhomogeneity normalisation for quantitative apparent fibre density. *Proc. Intl. Soc. Mag. Reson. Med*. 2021;29:2472.
34. Pauleit D, Floeth F, Hamacher K, et al. O-(2-[18F]fluoroethyl)-L-tyrosine PET combined with MRI improves the diagnostic assessment of cerebral gliomas. *Brain*. 2005;128(Pt 3):678–687.
35. Henderson F, Abdullah KG, Verma R, Brem S. Tractography and the connectome in neurosurgical treatment of gliomas: the premise, the progress, and the potential. *Neurosurg Focus*. 2020;48(2):E6.
36. Dallabona M, Sarubbo S, Merler S, et al. Impact of mass effect, tumor location, age, and surgery on the cognitive outcome of patients with high-grade gliomas: a longitudinal study. *Neuro-Oncol Pract*. 2017;4(4):229–240.
37. Habets EJJ, Hendriks EJ, Taphoorn MJB, et al. Association between tumor location and neurocognitive functioning using tumor localization maps. *J Neuro-Oncol*. 2019;144(3):573–582.
38. Hendriks EJ, Habets EJJ, Taphoorn MJB, et al. Linking late cognitive outcome with glioma surgery location using resection cavity maps. *Hum Brain Mapp*. 2018;39(5):2064–2074.
39. Nieberlein L, Rampp S, Gussew A, Prell J, Hartwigsen G. Reorganization and plasticity of the language network in patients with cerebral gliomas. *Neuroimage Clin*. 2023;37:103326.
40. Samuel N, Vetkas A, Pancholi A, et al. A network-based approach to glioma surgery: insights from functional neurosurgery. *Cancers*. 2021;13(23):6127.
41. van den Heuvel MP, Sporns O. Network hubs in the human brain. *Trends Cogn Sci*. 2013;17(12):683–696.
42. Fekonja LS, Wang Z, Doppelbauer L, et al. Lesion-symptom mapping of language impairments in patients suffering from left perisylvian gliomas. *Cortex*. 2021;144:1–14.
43. van Grinsven EE, Smits AR, van Kessel E, et al. The impact of etiology in lesion-symptom mapping - a direct comparison between tumor and stroke. *Neuroimage Clin*. 2023;37:103305.
44. Grayson DS, Ray S, Carpenter S, et al. Structural and functional rich club organization of the brain in children and adults. *PLoS One*. 2014;9(2):e88297.
45. van den Heuvel MP, Sporns O. An anatomical substrate for integration among functional networks in human cortex. *J Neurosci*. 2013;33(36):14489–14500.
46. Horn A, Ostwald D, Reisert M, Blankenburg F. The structural-functional connectome and the default mode network of the human brain. *Neuroimage*. 2014;102(Pt 1):142–151.
47. de Lange SC, Scholtens LH, Alzheimer's Disease Neuroimaging I, et al. Shared vulnerability for connectome alterations across psychiatric and neurological brain disorders. *Nat Hum Behav*. 2019;3(9):988–998.
48. Koch G, Casula EP, Bonni S, et al. Precuneus magnetic stimulation for Alzheimer's disease: a randomized, sham-controlled trial. *Brain*. 2022;145(11):3776–3786.

2.2.1 Supplementary data

Supplementary Material

Structural connectome-based predictive modeling of cognitive deficits in treated glioma patients

Michel Friedrich[1], Christian P. Filss[1], Philipp Lohmann[1], Felix M. Mottaghy[2], Gabriele Stoffels[1], Carolin Weiss Lucas[3,4], Maximilian I. Ruge[4,5], N. Jon Shah[1,6,7], Svenja Caspers[1,8], Karl-Josef Langen[1,2,4], Gereon R. Fink[1,9], Norbert Galldiks[1,4,9†], Martin Kocher[1,4,5†]

[†]**These authors contributed equally to senior authorship.**

Author affiliations

[1]Institute of Neuroscience and Medicine (INM-1, -3, -4, -11), Forschungszentrum Juelich, Juelich, Germany (MF, CPF, PL, GS, NJS, SC, KJL, GRF, NG, MK)

[2]Department of Nuclear Medicine, RWTH University Hospital Aachen, RWTH University Aachen, Aachen, Germany (FMM, KJL)

[3]Department of General Neurosurgery, Center for Neurosurgery, Faculty of Medicine and University Hospital Cologne, University of Cologne, Cologne, Germany (CWL)

[4]Center of Integrated Oncology (CIO), Universities of Aachen, Bonn, Cologne, and Duesseldorf, Germany (CWL, MIR, KJL, NG, MK)

[5]Department of Stereotaxy and Functional Neurosurgery, Center for Neurosurgery, Faculty of Medicine and University Hospital Cologne, Cologne, Germany (MIR, MK)

[6]Juelich-Aachen Research Alliance (JARA), Section JARA-Brain, Juelich, Germany (NJS)

[7]Department of Neurology, RWTH University Hospital Aachen, RWTH University Aachen, Aachen, Germany (NJS)

[8]Institute for Anatomy I, Medical Faculty and University Hospital Duesseldorf, Heinrich Heine University Duesseldorf, Duesseldorf, Germany (SC)

[9]Department of Neurology, Faculty of Medicine and University Hospital Cologne, University of Cologne, Cologne, Germany (GRF, NG)

Table S1 Patient characteristics

Sex (male/female)		73/48	
Age (years)		52	(28-74)
ECOG-PS (0/1/2/3)		58/56/6/1	
Education (ISCED-Score)		8	(3-10)
Employment (no/yes)		45/76	
Follow-up Interval (months)		14.4	(0.6-213.7)
Presenting Symptoms			
Aphasia		17	(14%)
Paresis		29	(24%)
Fatigue		19	(16%)
Vision disturbance		12	(10%)
Vertigo, Confusion		4	(3%)
WHO CNS 2021 Tumor Type			
GBM, IDH wildtype		72	(60%)
GBM, NOS		4	(3%)
Astrocytoma, IDH-mutated Grade 4		8	(7%)
Astrocytoma, IDH-mutated Grade 3		15	(12%)
Astrocytoma, NOS Grade 3		6	(5%)
Oligodendroglioma, IDH-mutated, 1p19q codeleted G3		13	(11%)
Oligodendroglioma NOS/NEC Grade 3		3	(2%)
Tumor Location[a]			
Frontal Left/Right		31/28	(26%/23%)
Parietal Left/Right		7/8	(6%/7%)
Temporal Left/Right		22/16	(18%/13%)
Occipital Left/Right		5/4	(4%/3%)
Lesion Volumes (mL)			
Resection cavity	(n= 90)	20.9	(0.3-172.5)
FLAIR hyperintense	(n=121)	53.4	(3.4-252.9)
T1 contrast-enhancing	(n= 99)	8.3	(0.01-122.9)
^{18}F-FET PET (TBR > 1.6)	(n= 79)	30.3	(2.6-227.8)
Treatment (Number of Procedures)			
Surgery[b]	(1/2/3/4)	101/17/2/1	
Radiotherapy	(0/1/2)	7/100/14	
Chemotherapy	(0/1/2/3)	10/91/16/4	
Corticosteroids (no/yes)		91/30	(75%/25%)
Anticonvulsants (no/yes)		49/72	(40%/60%)
^{18}F-FET PET diagnosed recurrence (no/yes)		63/58	(52%/48%)

Median (Range) unless otherwise stated; ECOG-PS, Eastern Cooperative Oncology Group Performance Score; ISCED, International Standard Classification of Education (1997); GBM, glioblastoma; IDH, Isocitrate-Dehydrogenase; NOS, not otherwise specified; NEC, not elsewhere classified; AA, anaplastic astrocytoma; AOD, anaplastic oligodendroglioma; 1p19q codel, 1p19q co-deleted; [a]main lobe involved; FLAIR, fluid-attenuated inversion recovery; ^{18}F-FET, O-(2-[^{18}F]fluoroethyl)-L-tyrosine; TBR, tumor-to-brain ratio; [b]including biopsy

Table S2 Description of Neurocognitive Tests

All tests were done with paper and pencil. The tests are shown here in the order in which they were presented to the patient.

- **Trail-Making Test A**: This widely used test assesses processing speed and attention. Small circles enclosing the numbers 1-25 are randomly distributed on a sheet of paper, and the patient is instructed to draw a connecting line in ascending order as quickly as possible without lifting the pencil. The time for completion is measured and given in seconds.[1,2]

- **Trail Making Test B**: This is a variant of the Trail-Making Test A, which measures executive function and concept shifting. Small circles with the numbers 1-13 and the letters A-L are randomly distributed on a sheet of paper, and the patient has to connect them in ascending, alternating order as quickly as possible, measured in seconds.[1,2]

- **Digit Span forward**: This is a common test for verbal working memory.[3] Increasingly long lists of number words are read to the patient, who is asked to recall each list immediately from memory. Two points are awarded for success on the first attempt. In the event of a failed attempt, another list of the same length is read to the patient, for which she receives one point if recalled correctly. After two failed attempts, the test is stopped, and the total score is counted.

- **Word List, immediate recall**: This test is part of the DemTect[4] battery widely used for dementia screening. A list of 10 items is read to the patient, who is instructed to recall as many items as possible immediately after presentation. The same list is then presented a second time, and the total number of correctly recalled items from these two runs (up to 20) is counted. No instruction is given to remember the items for later recall.

- **Imagined Shopping Tour**: This test is also part of the DemTect and is used to assess semantic word fluency. The patient is instructed to imagine a shopping trip in a supermarket, imagining and pronouncing as many products as possible within 60 seconds. The total number of items is counted (up to 30).

- **Number Transcoding**: This test is also part of the DemTect battery and tests aspects of language processing. Two numbers presented in numerical notation have to be transformed into whole words, and two numbers written in whole words have to be transformed to numerical notation. The number of successes (out of four) is counted.

- **Digit Span backward**: Same as Digit Span forward, but with the instruction to recall the list of numbers in reverse sequence.

- **Word List, delayed recall**: The patient is asked to recall the list of 10 items from the word list presented before (typical interval of 5-10 minutes), maximum score of 10 items.

- Corsi Block Tapping Test: This is a test for visual-spatial working memory.[5] The examiner taps increasingly long sequences of 10 small blocks mounted on a board, and the patient is asked to reproduce the sequence forward/backward by tapping the blocks himself. The same scoring scheme as for the digit span tests is applied.

Table S3 Cognitive test scores in glioma patients and healthy subjects

Test (Cognitive Domains)	**Glioma Patients**	**Healthy Subjects**	**Difference (%)**	**Patients (%) with Clinically Relevant Deficit[a]**
Trail-Making Test A [seconds] (Attention, processing speed)	47.3 ± 33.9 ***	30.9 ± 12.1	+53.1	39 (32%)
Trail-Making Test B [seconds] (Executive function, concept shifting)	117.6 ± 80.2 ***	68.2 ± 40.1	+72.4	34 (28%)
Imagined Shopping Tour [items] (Language, semantic word fluency)	20.2 ± 7.7 ***	26.8 ± 4.4	-24.6	57 (47%)
Number Transcoding [items] (Language processing)	3.3 ± 1.1 n.s.	3.6 ± 0.6	-8.3	21 (17%)
Digit Span Forward [weighted items] (Verbal working memory)	7.4 ± 2.3 **	8.0 ± 2.3	-7.5	12 (10%)
Digit Span Backward [weighted items] (Verbal working memory)	6.5 ± 2.5 ***	8.3 ± 2.3	-21.7	20 (17%)
Corsi Block Tapping Fw [weighted items] (Visuo-spatial working memory)	6.6 ± 2.3 *	7.4 ± 1.9	-10.8	27 (22%)
Corsi Block Tapping Bw [weighted items] (Visuo-spatial working memory)	4.8 ± 2.2 ***	6.0 ± 2.0	-20.0	28 (23%)
Word List, Immediate Recall [items] (Verbal episodic memory)	11.7 ± 3.7 ***	14.1 ± 2.6	-17.0	34 (28%)
Word List, Delayed Recall [items] (Verbal episodic memory)	4.5 ± 2.8 *	5.4 ± 2.4	-16.7	22 (18%)

Fw, Forward; Bw, Backward; [a]below the mean - 1.5 x the standard deviation of healthy subjects.
* $p < 0.05$, ** $p < 0.01$, *** $p < 0.001$, two-sided Mann–Whitney U-test

Table S4 Coefficients of determination (R^2) of univariate linear regression analysis for cognitive scores of the entire patient group. Summary connectivity values served as predictors and were calculated separately for edges positively and negatively associated with cognitive performance.

	Edges positively associated with cognitive performance		**Edges negatively associated with cognitive performance**	
Test (Cognitive Domains)	**Edge Number**	**Coefficient of Determination (R^2)**	**Edge Number**	**Coefficient of Determination (R^2)**
Trail-Making Test A (Attention, processing speed)	524	0.255 ***	16	0.070 **
Trail-Making Test B (Executive function, concept shifting)	542	0.365 ***	8	0.086 **
Imagined Shopping Tour (Language, semantic word fluency)	206	0.374 ***	6	0.093 **
Number Transcoding (Language processing)	66	0.369 ***	6	0.154 ***
Digit Span Forward (Verbal working memory)	32	0.161 ***	0	-------
Digit Span Backward (Verbal working memory)	56	0.271 ***	4	0.024
Corsi Block Tapping Forward (Visuo-spatial working memory)	226	0.294 ***	0	-------
Corsi Block Tapping Backward (Visuo-spatial working memory)	316	0.370 ***	12	0.158 ***
Word List, Immediate Recall (Verbal episodic memory)	454	0.442 ***	2	0.128 ***
Word List, Delayed Recall (Verbal episodic memory)	282	0.398 ***	12	0.107 ***

** $p < 0.01$, *** $p < 0.001$

Table S5 Clinical factors mainly unrelated to cognitive test scores in treated glioma patients

Test (Cognitive Domains)	**Sex (MWU p)**	**Tumor Grade (MWU p)**	**IDH-status (MWU p)**	**Interval (Spearman rho)**	**Pretreatment Surgery (Spearman rho)**	**Pretreatment Radiotherapy (Spearman rho)**	**Pretreatment Chemotherapy (Spearman rho)**
Trail-Making Test A (Attention, processing speed)	0.167	0.045	0.014 *	- 0.175	- 0.107	- 0.001	- 0.043
Trail-Making Test B (Executive. function, concept shifting)	0.159	0.223	0.101	- 0.134	- 0.090	- 0.036	- 0.003
Imagined Shopping Tour (Language, semantic word fluency)	0.361	0.464	0.969	- 0.024	- 0.038	- 0.015	- 0.088
Number Transcoding (Language processing)	0.482	0.426	0.765	- 0.051	- 0.074	- 0.047	- 0.075
Digit Span Forward (Verbal working memory)	0.685	0.107	0.129	- 0.031	- 0.066	- 0.083	- 0.026
Digit Span Backward (Verbal working memory)	0.564	0.153	0.190	0.214 *	0.143	0.082	0.136
Corsi Block Tapping Forward (Visuo-spatial working memory)	0.288	0.055	0.086	- 0.005	- 0.031	- 0.163	- 0.114
Corsi Block Tapping Backward (Visuo-spatial working memory)	0.726	0.099	0.049 *	0.041	0.042	0.044	0.015
Word List, Immediate Recall (Verbal episodic memory)	0.477	0.574	0.518	- 0.064	0.003	- 0.018	- 0.079
Word List, Delayed Recall (Verbal episodic memory)	0.911	0.610	0.078	- 0.014	0.054	0.034	- 0.094
Number of tests with p < 0.01	**0/10**	**0/10**	**0/10**	**0/10**	**0/10**	**0/10**	**0/10**

* p < 0.05, ** p < 0.01, *** p < 0.001; MWU, two-sided Mann–Whitney U-test; ISCED, International Standard Classification of Education

Table S6 Coefficients of determination (R^2) of multiple linear regression models of cognitive scores for the entire patient group, using different combinations of predictors.

Test (Cognitive Domains)	**PET-Recurrence**	**Lesion Volumes**	**Lesion Location**	**Age + ISCED**	**Recurrence + Volumes + Location**	**Summary Connectivity Values**	**Age + ISCED + Connectivity**	**PET-Recurrence + Volumes + Location + Connectivity**
Trail-Making Test A (Attention, processing speed)	0.039 *	0.060	0.130 *	0.131 ***	0.201 *	0.255***	0.291 ***	0.331 ***
Trail-Making Test B (Executive function, concept shifting)	0.036 *	0.052	0.080	0.179 ***	0.144	0.365***	0.392 ***	0.415 ***
Imagined Shopping Tour (Language, semantic word fluency)	0.003	0.080*	0.155 **	0.118 **	0.222 **	0.374***	0.389 ***	0.430 ***
Number Transcoding (Language processing)	0.009	0.009	0.131 *	0.141 ***	0.143	0.369 ***	0.401 ***	0.443 ***
Digit Span Forward (Verbal working memory)	0.000	0.032	0.170 **	0.060 *	0.212 **	0.161 ***	0.217 ***	0.301 ***
Digit Span Backward (Verbal working memory)	0.004	0.042	0.078	0.144 ***	0.124	0.271 ***	0.314 ***	0.315 ***
Corsi Block Tapping Forward (Visuo-spatial working memory)	0.018	0.084*	0.110	0.181 **	0.179 *	0.294 ***	0.343 ***	0.325 ***
Corsi Block Tapping Backward (Visuo-spatial working memory)	0.101 ***	0.056	0.108	0.175 ***	0.203 *	0.370 ***	0.410 ***	0.409 ***
Word List, Immediate Recall (Verbal episodic memory)	0.032 *	0.089*	0.225 ***	0.120 **	0.325 ***	0.442 ***	0.467 ***	0.515 ***
Word List, Delayed Recall (Verbal episodic memory)	0.037	0.073	0.266 ***	0.165 **	0.331 ***	0.398 ***	0.436 ***	0.493 ***
Mean (Standard Deviation) of R^2 p(Connectivity) in Combined Models	0.028 (0.030)	0.058 (0.025)	0.145 (0.061)	0.141 (0.037)	0.208 (0.071)	0.330 (0.083)	0.366 (0.075) all < 0.001***	0.398 (0.076) all < 0.001***

* $p < 0.05$, ** $p < 0.01$, *** $p < 0.001$; ISCED, International Standard Classification of Education (1997)

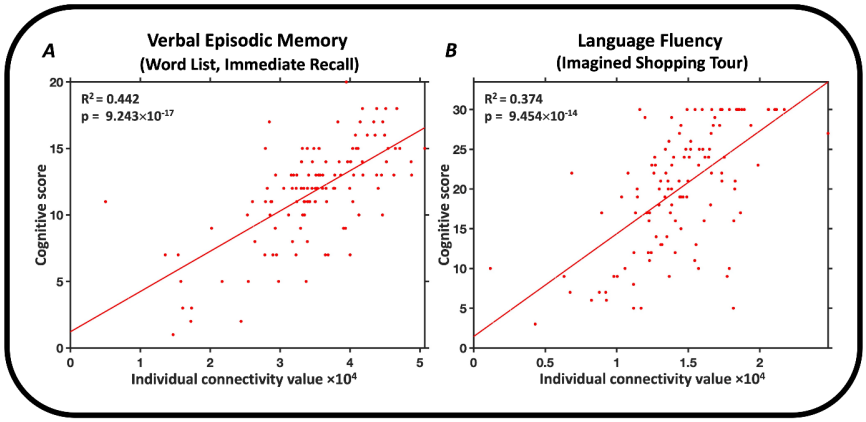

Figure S1 Linear regression analysis for the dependency of cognitive test scores for verbal episodic memory (immediate recall) and language fluency on the individual connectivity scores (summed fiber counts) in 121 glioma patients. R^2, coefficient of determination.

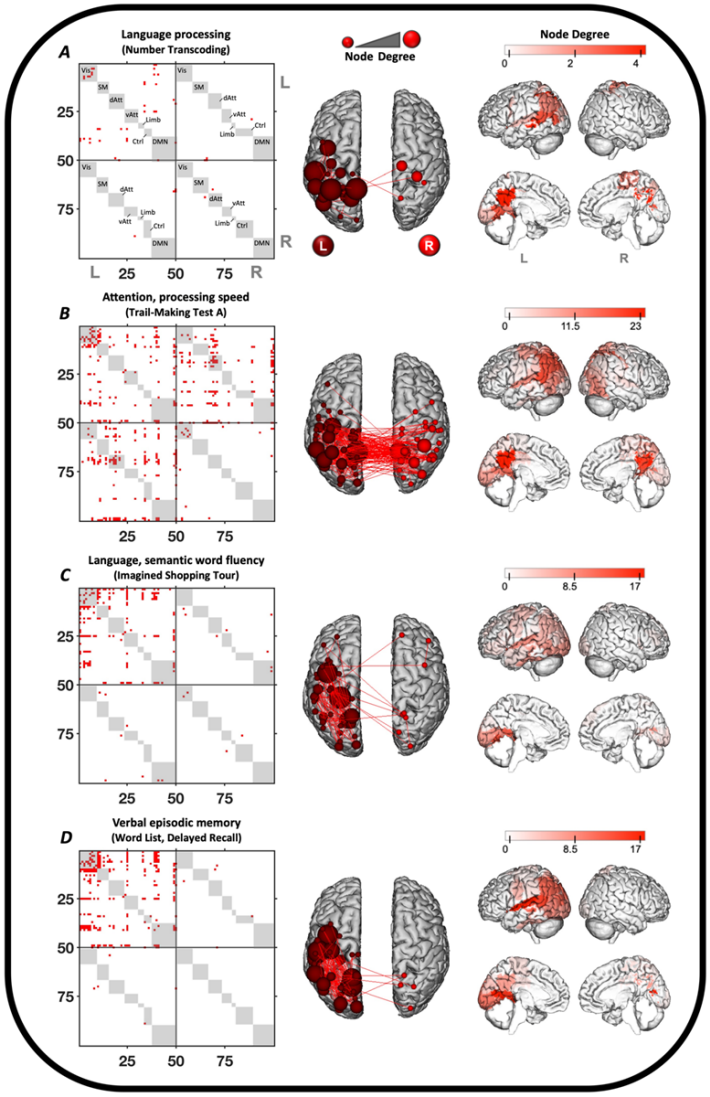

Figure S2 Left: Binary connectivity matrix labeling cross-validated predictive edges; node membership to networks marked in gray. Middle/Right: Anatomical representation of the critical nodes by visualization of node degree and connecting edges. Results are shown for four representative cognitive tests. **A:** Number transcoding (language processing), **B:** Trail-Making Test A (attention/processing speed), **C:** Imagined Shopping Tour (semantic word fluency), **D:** Word List, delayed recall (verbal episodic memory). Vis, visual; SM, somatomotor; dAtt, dorsal attention; vAtt, ventral attention; Limb, limbic; Ctr, frontal control; DMN, default mode network

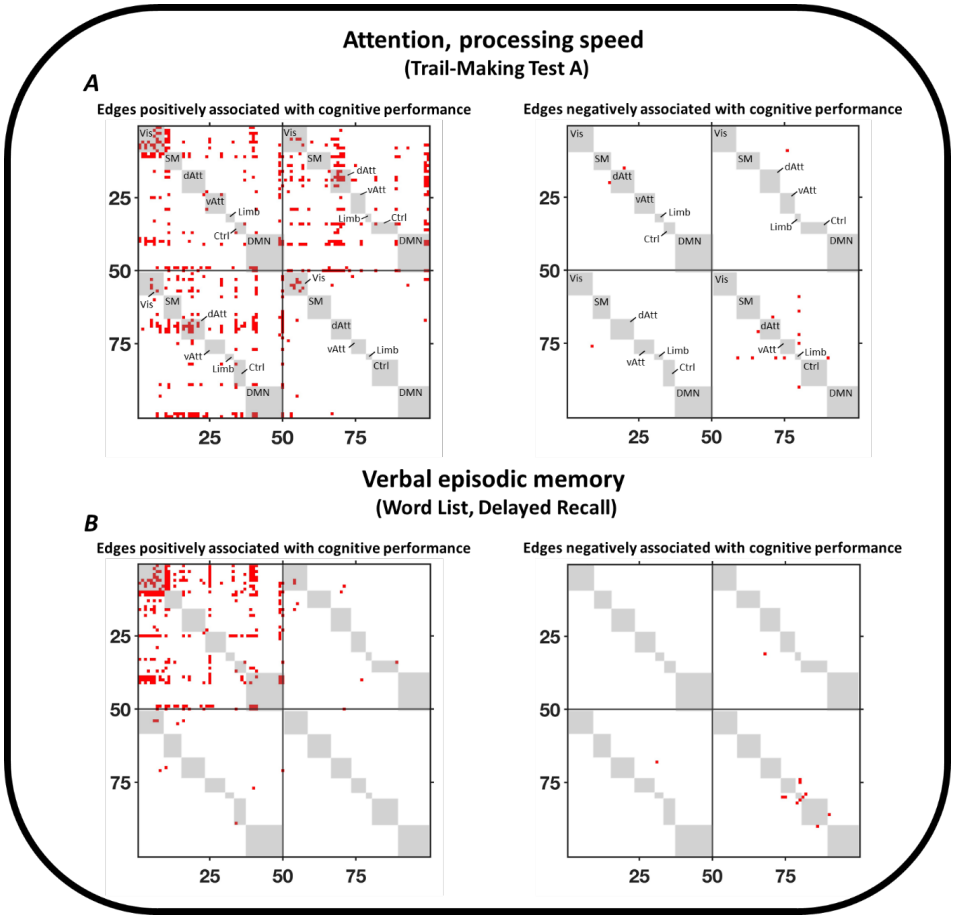

Figure S3 Binary connectivity matrices labeling predictive edges for two exemplary tests of **A**) Attention/processing speed (Trail-Making Test A) and **B**) Verbal episodic memory (delayed recall of word list). Node membership to networks marked in gray. Left: Edges positively associated with cognitive performance. Right: Edges negatively associated with cognitive performance. Vis, visual; SM, somatomotor; dAtt, dorsal attention; vAtt, ventral attention; Limb, limbic; Ctr, frontal control; DMN, default mode network

References to Supplement

1. Morris JC, Heyman A, Mohs RC, et al. The Consortium to Establish a Registry for Alzheimer's Disease (CERAD). Part I. Clinical and neuropsychological assessment of Alzheimer's disease. *Neurology.* 1989; 39(9):1159-1165.

2. Tombaugh TN. Trail Making Test A and B: normative data stratified by age and education. *Arch Clin Neuropsychol.* 2004; 19(2):203-214.

3. Oswald WD, Fleischmann UM. *Das Nürnberger-Alters-Inventar (NAI)*. Göttingen: Hogrefe; 1997.

4. Kalbe E, Kessler J, Calabrese P, et al. DemTect: a new, sensitive cognitive screening test to support the diagnosis of mild cognitive impairment and early dementia. *Int J Geriatr Psychiatry.* 2004; 19(2):136-143.

5. Berch DB, Krikorian R, Huha EM. The Corsi block-tapping task: methodological and theoretical considerations. *Brain Cogn.* 1998; 38(3):317-338.

2.3 Functional connectivity between tumor region and resting-state networks as imaging biomarker for overall survival in recurrent gliomas diagnosed by FET PET

Attribution and license information for the following PDFs:

Included publication with supplementary data: *Functional connectivity between tumor region and resting-state networks as imaging biomarker for overall survival in recurrent gliomas diagnosed by O-(2-[^{18}F]fluoroethyl)-L-tyrosine PET*

Michel Friedrich, Jan-Michael Werner, Joachim P Steinbach, Michael Sabel, Ulrich Herrlinger, Marc Piroth, Gabriele Stoffels, Christian P Filss, Philipp Lohmann, Nadim J Shah, Maximilian I Ruge, Felix M Mottaghy, Roland Goldbrunner, Karl-Josef Langen, Gereon R Fink, Martin Kocher, Norbert Galldiks

Originally published in Neuro-Oncology Advances, Volume 7, Issue 1, January-December 2025, vdaf023.

Available at: https://doi.org/10.1093/noajnl/vdaf023

Neuro-Oncology Advances

1

7(1), vdaf023, 2025 | https://doi.org/10.1093/noajnl/vdaf023 | Advance Access date 29 January 2025

Functional connectivity between tumor region and resting-state networks as imaging biomarker for overall survival in recurrent gliomas diagnosed by *O*-(2-[^{18}F] fluoroethyl)-L-tyrosine PET

Michel Friedrich, Jan-Michael Werner, Joachim P. Steinbach, Michael Sabel, Ulrich Herrlinger, Marc Piroth, Gabriele Stoffels, Christian P. Filss, Philipp Lohmann, Nadim J. Shah, Maximilian I. Ruge, Felix M. Mottaghy, Roland Goldbrunner, Karl-Josef Langen, Gereon R. Fink, Martin Kocher[‡], and Norbert Galldiks[‡]

All author affiliations are listed at the end of the article
[‡]Equal contribution to senior authorship.

Corresponding Author: Martin Kocher, MD, Institute of Neuroscience and Medicine, Forschungszentrum Juelich, Wilhelm-Johnen-Str., 52428 Juelich, Germany (m.kocher@fz-juelich.de).

Abstract

Background. Amino acid PET using the tracer *O*-(2-[^{18}F]fluoroethyl)-L-tyrosine (FET) is one of the most reliable imaging methods for detecting glioma recurrence. Here, we hypothesized that functional MR connectivity between the metabolic active recurrent tumor region and resting-state networks of the brain could serve as a prognostic imaging biomarker for overall survival (OS).

Methods. The study included 82 patients (26–81 years; median Eastern Cooperative Oncology Group performance score, 0) with recurrent gliomas following therapy (WHO-CNS 2021 grade 4 glioblastoma, $n = 57$; grade 3 or 4 astrocytoma, $n = 12$; grade 2 or 3 oligodendroglioma, $n = 13$) diagnosed by FET PET simultaneously acquired with functional resting-state MR. Functional connectivity (FC) was assessed between tumor regions and 7 canonical resting-state networks.

Results. WHO tumor grade and IDH mutation status were strong predictors of OS after recurrence ($P < .001$). Overall FC between tumor regions and networks was highest in oligodendrogliomas and was inversely related to tumor grade ($P = .031$). FC between the tumor region and the dorsal attention network was associated with longer OS (HR, 0.88; 95%CI, 0.80–0.97; $P = .007$), and showed an independent association with OS (HR, 0.90; 95%CI, 0.81–0.99; $P = .033$) in a model including clinical factors, tumor volume and MGMT. In the glioblastoma subgroup, tumor volume and FC between the tumor and the visual network (HR, 0.90; 95%CI, 0.82–0.99, $P = .031$) were independent predictors of survival.

Conclusions. Recurrent gliomas exhibit significant FC to resting-state networks of the brain. Besides tumor type and grade, high FC between the tumor and distinct networks could serve as independent prognostic factors for improved OS in these patients.

Key Points

- Recurrent gliomas exhibit functional connectivity to resting-state networks.
- Functional connectivity is higher in IDH-mutant gliomas than in glioblastomas.
- Tumor connectivity to visual/attention networks is a factor for survival.

Graphical Abstract

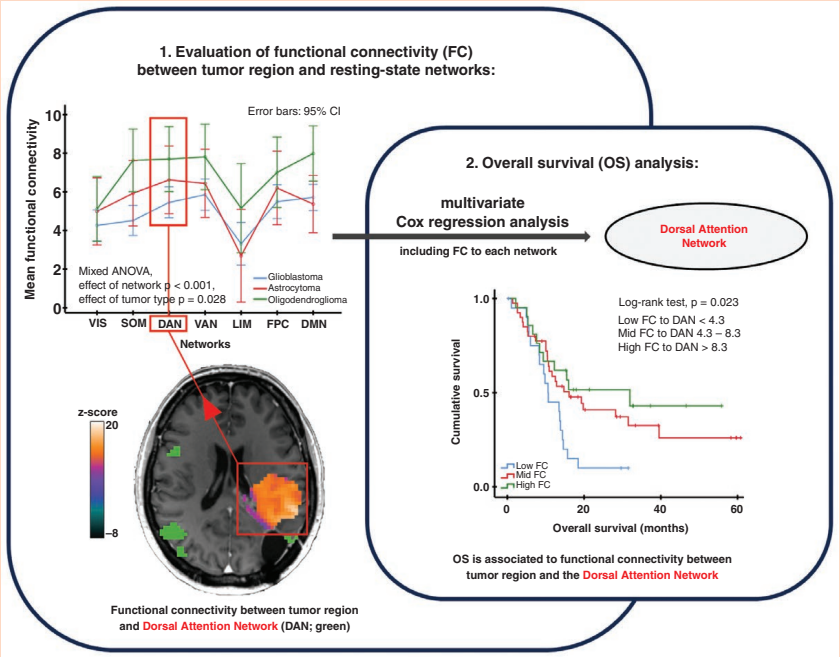

Importance of the Study

There is increasing evidence in oncological neuroscience that preserved functional connectivity (FC) between tumor-infiltrated brain regions and resting-state networks of the brain influence overall survival in primary gliomas. Here, we found that FC between the brain region infiltrated by metabolically active tumors and different resting-state networks also prevails in recurrent gliomas of different types and grades and is associated with overall survival. These results suggest that FC can be used as a novel prognostic biomarker for imaging in patients with recurrent glioma.

Gliomas are primary brain tumors with a strong tendency to infiltrate the normal brain tissue diffusely.[1] This growth pattern leads to a close interaction between tumor cells and the local microenvironment that comprises neurons, normal glia, and immunogenic and inflammatory cells.[2] In particular, the interaction between neuronal elements and glioma cells has recently attracted considerable attention and is now considered a critical aspect in the emerging field of *Cancer Neuroscience*.[3,4]

From a neurooncological perspective, the impact of neuronal activity on glial cells is an important issue, and there is clear evidence that neuronal activity induces and promotes glioma growth through paracrine signaling and the formation of excitatory glutaminergic synapses between neurons and glioma cells.[5–8] Conversely, developing a macroscopic glioma may affect neuronal activity and signal conduction locally and at distant sites. The functional impact of local glioma infiltration into the adjacent cortex has mainly been studied in the context of presurgical mapping before tumor resection. Typical task-evoked patterns of neuronal activity, assessed using electrophysiological methods[9–13] or magnetencephalography,[13,14] may be preserved in the glioma-infiltrated cortex.

Besides local effects, glioma growth and invasion may affect the integrity of whole-brain neural networks. Resting-state functional magnetic resonance imaging (rs-fMRI) has

been used to characterize alterations in whole-brain connectivity in patients with glioma, with consistent evidence of disturbed functional connectivity (FC) extending to the contralateral hemisphere.[15,16] Moreover, global network connectivity changes may serve as imaging biomarkers predicting survival predominantly in glioblastomas.[17–20] In addition, FC between tumor-infiltrated regions and networks of the brain has been investigated in newly diagnosed glioblastoma[21] and mixed cohorts of patients with primary and recurrent CNS WHO grade 2–4 gliomas.[22] In these studies, tumor voxels were frequently functionally connected to resting-state networks[21] or otherwise identified cortical areas,[22] and preserved FC was associated with better overall survival in certain subgroups.

In recurrent gliomas, the interactions of different therapeutic interventions comprising tumor resection, radiotherapy, and chemotherapy using alkylating drugs with glioma cells, neurons, and immunogenic/inflammatory cells may further complicate the situation, rendering outcome and survival less predictable[23–25]

In the present study, we investigated the FC between brain regions infiltrated by metabolic active tumors and resting-state networks using rs-fMRI in patients with recurrent glioma, including its prognostic value. In addition to anatomical MRI, diagnosis, localization, and extent of recurrent gliomas were assessed using amino acid PET with the tracer *O*-(2-[^{18}F]fluoroethyl)-L-tyrosine (FET), one of the most reliable noninvasive imaging methods for detecting glioma recurrence.[26]

Patients and Methods

Patient Characteristics

Patients were recruited as part of a prospective study that included glioma patients with a suspected recurrence/progression who were in good general condition (ECOG performance score, 0–1 at screening), had no major depression, were free of seizures (with or without anticonvulsive medication), and were able to undergo anatomical MRI, functional rs-fMRI and FET PET acquired simultaneously on a hybrid MR/PET scanner (for imaging protocols, see Supplementary Material). The Ethics Committee of the University of Cologne approved the study protocol (protocol number 17-365), and written informed consent was obtained from all patients per the Declaration of Helsinki.

Eighty-two adults ($n = 36$ women; $n = 46$ men; median age, 53 years; range, 26–81 years) with gliomas at recurrence were included. All tumors were histomolecularly characterized according to the 2021 classification of the WHO for Tumors of the CNS.[27] Patients were referred to the imaging facility of the Forschungszentrum Juelich (Research Center Juelich), Germany, by 5 university hospitals between February 2018 and August 2022. All patients had *Progressive Disease* on anatomical MRI according to the RANO 1.0 criteria[28] and a metabolically active tumor with pathologically increased tracer uptake as assessed by FET PET. The criteria for the additional FET PET-based diagnosis of glioma recurrence have been described previously.[29]

Fifty-seven patients (70%) had a CNS WHO grade 4 glioblastoma, 12 patients (14%) had a CNS WHO grade 3 or 4 astrocytoma, and 13 patients (16%) had a CNS WHO grade 2 or 3 oligodendroglioma (Table 1). Overall, 57 (70%) patients had IDH-wild-type tumors, and 25 (30%) patients had IDH-mutant tumors. First-line therapy had been applied according to respective guidelines at the initial diagnosis. For instance, most of the glioblastomas (83%) had undergone first-line therapy comprising surgery or biopsy, postoperative radiotherapy with concomitant and maintenance temozolomide chemotherapy,[30] or temozolomide plus lomustine chemoradiation according to the CeTeG/NOA-09 trial.[31] In patients with astrocytomas, a combination of surgery or biopsy, radiotherapy with concomitant and maintenance temozolomide chemotherapy was the most common first-line therapy (83%). At initial diagnosis, patients with oligodendroglioma had undergone either surgery alone or surgery followed by radiotherapy and adjuvant nitrosourea-based chemotherapy.

The median time interval between initial diagnosis and recurrence depended on tumor type (glioblastoma, 9.4 months; astrocytoma, 44.6 months; oligodendroglioma, 59.3 months). Table 1 shows the number of therapy lines (eg, surgical interventions including stereotactic biopsy, radiotherapy series, and chemotherapies) applied until the time of diagnosis of recurrence.

Image Preprocessing and Generation of Lesion Masks

The functional imaging data passed the standard SPM12/CONN toolbox preprocessing steps.[32] These include motion correction, removal of outliers, regressing out noise signals from the cerebrospinal fluid and white matter, slice-timing correction, smoothing with 5 mm FWHM, and bandpass filtering to 0.008–0.09 Hz. Afterward, functional and structural images were non-rigidly co-registered to the MNI-152 standard brain template using the SPM12/CONN unified segmentation and registration algorithm. From the structural MR and PET images, 4 binary lesion masks were generated for the subsequent analysis of FC. These included lesions with pathologically increased FET uptake, T1 contrast-enhancing lesions, T2/FLAIR hyperintensities, and resection cavities. Segmentation of tumor regions with pathologically increased FET PET uptake at a tumor-to-brain ratio of 1.6 or more[33] was performed using an FSL script (FSL toolbox, https://fsl.fmrib.ox.ac.uk). For this purpose, the PET images were converted into standardized tumor-to-brain ratio images whereby the average tracer activity in the unaffected brain served as the reference. T1 contrast-enhancing lesions and T2/FLAIR hyperintensities were automatically segmented using the deep learning software HD-GLIO (https://github.com/NeuroAI-HD/HD-GLIO), while resection cavities were manually contoured by an experienced radiation oncologist (MK). All segmentations were visually inspected, manually corrected, and finally merged into a composite lesion mask. The location of the metabolic active, FET-avid recurrent tumors with respect to the 4 major lobes of each hemisphere was calculated from the maximal volumetric overlap of the PET mask with the lobe definitions from the MNI-152 standard brain template.

Table 1. Patient Characteristics

	N	% or range
Sex (male/female)	46/36	56/44%
Median age and range (years)	53	26 - 81
ECOG score (0/1/2/3)	48/28/5/1	59/34/6/1%
Main symptom		
None	34	41%
Aphasia	10	12%
Paresis	17	21%
Fatigue, Dizziness	12	15%
Vision Impairment	9	11%
Tumor type and WHO CNS tumor grade		
Glioblastoma, IDH-wild-type, CNS WHO grade 4	57	69%
Astrocytoma, IDH-mutant, CNS WHO grade 3/4	9/3	11/4%
Oligodendroglioma, IDH-mutant, CNS WHO grade 2/3	10/3	12/4%
IDH mutational status		
Wild-type/mutant	57/25	69/31%
MGMT promoter methylation status		
Methylated/non-methylated/unknown	47/26/9	57/32/11%
FET PET tumor location[a]		
Frontal left/right	16/15	20/18%
Parietal left/right	6/13	7/16%
Temporal left/right	13/14	16/17%
Occipital left/right	2/2	2/2%
Basal ganglia left	1	1%
Lesion volumes (mL)		
Resection cavity	3.2	0.0 - 124.0
FLAIR hyperintensity	59.4	8.0 - 250.9
T1 contrast-enhancing lesions	5.6	0.0 - 80.5
FET PET (TBR > 1.6)	36.8	2.4 - 226.3
Interval between initial diagnosis and recurrence (months)		
Glioblastoma	9.4	0.4 - 97.5
Astrocytoma	44.6	0.9 - 80.8
Oligodendroglioma	59.3	1.3 - 145.4
Pretreatment (number of procedures)		
Surgery[b] (1/2/3/4)	69/10/2/1	84/12/3/1%
Radiotherapy (0/1/2)	9/65/8	11/79/10%
Chemotherapy (0/1/2/3/4)	14/51/12/3/2	17/62/15/4/2%
Extent of resection at initial diagnosis		
None/biopsy/partial/complete	3/18/9/52	4/22/11/63%
Corticosteroids (no/yes)	63/19	77/23%
Anticonvulsants (no/yes)	27/55	33/67%

Abbreviations: ECOG, Eastern Cooperative Oncology Group performance score; IDH, isocitrate dehydrogenase; MGMT, O^6-methylguanine-DNA methyltransferase; FLAIR, fluid-attenuated inversion recovery; FET, O-(2-[^{18}F]fluoroethyl)-L-tyrosine; TBR, tumor-to-brain ratio; [a]main lobe involved; [b]including biopsy.

Determination of FC Between Tumor Region and Networks

FC between the metabolically active tumor region and a set of specified resting-state networks was determined by a variant of the FSL dual regression method[34–36] where atlas-based network masks served as seeds. We analyzed 7 resting-state networks defined in the Yeo atlas,[37] ie, the visual, somatomotor, dorsal attention, ventral attention, limbic, fronto-parietal control, and default mode networks. The corresponding binary atlas network masks were cropped by the individual pathological areas (composite lesion masks) and served as seed regions. The average blood-oxygen-level-dependent (BOLD) time series from the voxels in the cropped network masks was calculated and used as a regressor. Network-specific regression coefficients were then calculated for all voxels, normalized to z-scores, and stored as connectivity maps describing the strength of FC between each voxel and the analyzed network. Finally, we computed the average normalized regression coefficient of the voxels within the segmented PET lesion to obtain the FC between the tumor region and each of the 7 networks. The average of the individual network connectivity values was used as a measure of whole-brain connectivity. In addition, the spatial proximity of the tumor to the resting-state networks was determined where we used the center of gravity of the PET lesion and the centroids of the network nodes to calculate the mean distance (proximity) between the PET lesion and each network.

Statistical Analysis

Statistical analysis was performed using the SPSS statistical software package (version 25, IBM Corporation). Independent-sample two-sided *t*-tests or one-way ANOVA were performed to determine group differences for continuous variates. A mixed, repeated-measures ANOVA with Greenhouse-Geisser correction for non-sphericity was used to analyze differences in FC between individual networks and as a function of tumor type, IDH mutational status, and CNS WHO tumor grade. For analysis of overall survival, the duration between the date of imaging and the date of death was recorded, or data were censored at the time of the last available follow-up. The association of FC between brain regions infiltrated by metabolic active tumor and networks alone as well as along with tumor-related (tumor type, CNS WHO tumor grade, IDH mutational status) and other common prognostic factors (ie, age, the extent of resection, Eastern Cooperative Oncology Group (ECOG) performance score, O^6-methylguanine-DNA methyltransferase (MGMT) promotor methylation status, metabolic active tumor volume) on overall survival was estimated using Kaplan–Maier analysis with log-rank tests or Cox regression analysis. For Kaplan–Maier analysis of FC, patients were grouped into quartiles or with respect to the median. For the multivariate survival analysis, either a Cox regression analysis with simultaneous or stepwise-forward inclusion of variables was used (detailed in *Results*). Forward inclusion was additionally validated by stepwise backward exclusion. Unless otherwise stated, *P*-values less than .05 were considered statistically significant. Survival

analysis was also performed in the subgroup of IDH-wild-type glioblastoma patients.

Results

Most recurrent tumors were in the frontal ($n = 31$; 39%) or temporal ($n = 27$; 33%) lobes. The median volume of the FET PET-avid lesions was 36.8 mL (range, 2.4–226.3 mL), and the median average tumor-to-brain ratio (TBR_{mean}) was 2.17 (range, 1.88–2.94). Metabolic active tumor volume did not depend on the tumor type, CNS WHO tumor grade, or IDH mutational status (ANOVA and two-sided *t*-test, $P > .05$). In contrast, tumor-to-brain ratios depended on the CNS WHO tumor grade (ANOVA, $P = .031$) but not on the tumor type or IDH mutational status (ANOVA and two-sided *t*-test, $P > .05$). Figure 1 shows FET PET images of two exemplary patients.

FC Between Tumor Region and Resting-State Networks

Overall FC between brain regions infiltrated by metabolic active tumor and resting-state networks (mean of all 7 canonical networks) was significantly higher in IDH-mutant gliomas than in IDH-wild-type gliomas (two-sided *t*-test, $P = .028$; Figure 2A). Also, it depended significantly on the WHO CNS tumor type (ANOVA, $P = .028$; Figure 2B). In IDH-mutant gliomas, oligodendrogliomas had the highest FC (z-score, 6.9 ± 1.9), while in astrocytomas the FC was closer to that of the glioblastomas (z-score, 5.5 ± 1.3 vs. 4.9 ± 2.6; Figure 2B). In addition, connectivity was inversely related to the CNS WHO tumor grade (ANOVA, $P = .031$; Figure 2C). FC of the PET-avid tumor regions differed significantly concerning the 7 resting-state networks (mixed repeated-measures ANOVA, within subjects' effect, $P < .001$; Figure 2D-F). Overall, the highest connectivity was observed between the tumor regions and the ventral attention (z-score, 6.2 ± 3.1), dorsal attention (z-score, 6.0 ± 3.1), default mode (z-score, 6.0 ± 2.7) and frontoparietal control (z-score, 5.8 ± 3.3) networks, while the lowest connectivity was to the limbic network (z-score, 3.5 ± 4.2). Furthermore, the observed association between tumor type, CNS WHO tumor grade, IDH mutational status, and whole-brain connectivity was well preserved throughout all networks (mixed ANOVA, between subjects' effect, range of *P*-values, .028–.031; Figure 2D-F). Of note, the connectivity between the tumor region and networks was not associated with the tumor location regarding the cerebral lobes (ANOVA, $P = .96$). In addition, the FC was inversely related to the proximity of the tumor to the resting-state networks ($P < .05$ for most networks, see Supplementary Table S1 and Figure S1).

Association of FC Between Tumor Region and Resting-State Networks and Overall Survival

The overall survival after diagnosis of tumor recurrence diagnosed by FET PET was significantly associated with the tumor type, CNS WHO grade, and IDH mutational status (Kaplan–Meier analysis, all $P < .001$; Figure 3A, 3B). Univariate Cox regression analysis revealed a significant association between improved overall survival and the connectivity of brain regions infiltrated by metabolic active tumor with the visual, somatomotor, and DAN (range of *P*-values, .041–.007; Table 2). Subsequent stepwise forward and confirmatory backward multivariate Cox regression analysis including all 7 networks refined this association to the dorsal attention network (DAN) alone (HR, 0.88; 95% CI, 0.80–0.97; $P = .007$, Table 2). Figure 1 shows the DAN and two exemplary patients with high and low FC between the tumor region and the DAN. The connectivity between the tumor region and the DAN was almost normally distributed (z-score, 5.98 ± 3.13; Figure 3C). Patients with the highest FC between tumor and DAN (upper quartile, z-score > 8.3, $n = 21$) had a median overall survival of 31.9 months. In contrast, patients with intermediate (middle quartiles, z-score 4.3–8.3, $n = 40$) or low FC (lower quartile, z-score < 4.3, $n = 21$) had a median overall survival of 16.1 months and 10.6 months, respectively (log-rank test, $P = .023$; Figure 3D).

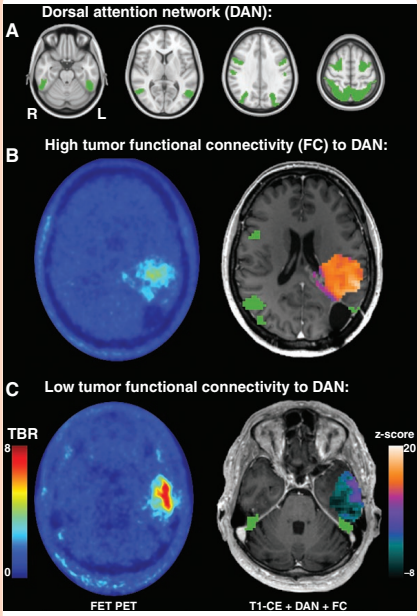

Figure 1. (A) Location of the dorsal attention network (DAN) in the MNI-152 standard space. (B) and (C), exemplary patients with high or low functional connectivity between brain regions infiltrated by metabolic active tumor and the DAN (right) and the corresponding *O*-(2-[^{18}F]fluoroethyl)-L-tyrosine (FET) PET images (left). Functional connectivity (FC) of the tumor region was superimposed on the T1-weighted contrast-enhanced (T1-CE) image together with the DAN mask from (A). Abbreviation: TBR, tumor-to-brain-ratio.

Furthermore, FC between the metabolic active tumor regions and the DAN had an independent association with overall survival (HR, 0.90; 95% CI, 0.81–0.99; $P = .033$) in a multivariate model (Table 3) that excluded features correlated with connectivity (IDH, tumor type, tumor grade) but included other tumor-related variables such as the metabolically active tumor volume ($P = .023$) and MGMT promoter methylation status ($P = .057$), as well as common prognostic factors such as age ($P = .215$), extent of resection at initial diagnosis ($P = .162$), and ECOG score ($P = .172$).

In the survival analysis of the subgroup of IDH-wild-type glioblastoma patients, univariate and subsequent stepwise forward and confirmatory backward multivariate Cox regression analysis comprising all 7 networks indicated a significant association between improved overall survival and the connectivity of the metabolic active tumor regions with the visual network (*P*-values, univariate and multivariate .023; Table 2). The connectivity with the visual network was almost normally distributed (z-score, 4.26 ± 3.34; Figure 3E). Overall survival of the glioblastoma patients differed significantly depending on the level of FC between tumor region and visual network (Kaplan–Maier analysis, log-rank test, $P = .007$; Figure 3F), where patients with high FC (z-score > 4.6 [median], $n = 29$) had a median overall survival of 12.5 months and patients with low FC (z-score < 4.6 [median], $n = 28$) one of 9.5 months. A final multivariate model including metabolically active tumor volume ($P = .011$), MGMT promoter methylation status ($P = .314$), age ($P = .232$), extent of resection at initial diagnosis ($P = .824$) and ECOG score ($P = .865$) confirmed the independent association of FC between tumor region and the visual network with overall survival (HR, 0.90; 95% CI, 0.82–0.99; $P = .031$; Table 3). The mean distances (proximities) of the PET lesions to the DAN (all patients, $P = .34$) and to the visual network (IDH-wild-type patients, $P = .47$) were not significantly associated with overall survival in the univariate analyses and were therefore not included in the multivariate models.

Discussion

Main Findings

The present study evaluated FC between the brain region infiltrated by metabolic active tumor and a set of canonical resting-state networks using the BOLD signal of the metabolic active tumor region in a cohort of patients with recurrent gliomas of varying histomorphologic and molecular characteristics. Tumor regions were diagnosed by a combination of anatomical MRI and FET PET, and FC of the metabolic active tumor differed between the networks and was highest with the 4 large associative networks (ie, the dorsal attention, ventral attention, frontoparietal control, and default mode network). Overall and network-specific connectivity of tumor regions was highest in oligodendroglioma and was significantly higher in IDH-mutant than in IDH-wild-type tumors. In the overall cohort, CNS WHO tumor grade and IDH mutational status were the most significant prognostic factors for longer overall survival but preserved FC between recurrent glioma and the DAN was also a prognostic factor. Importantly, in the subgroup of recurrent IDH-wild-type glioblastoma, connectivity between the tumor region and the visual network was an independent predictor of overall survival. The present investigation differs from similar recent reports[11,13,21,22] in that FET PET was used for tumor definition, that FC of gliomas of different WHO CNS types and grades was systematically analyzed, and that only patients with recurrent gliomas were included. FET PET was used because it is a highly reliable measure of glioma infiltration. Several biopsy-controlled studies have shown that FET PET in conjunction with an empirical threshold for tumor-to-brain ratio outperformed MRI-based methods in terms of accuracy.[38–40]

Glioma Interaction Within Directly Infiltrated Cortex

From a clinical point of view, glioma infiltration of normal brain tissue raises the question of whether the tumor-infiltrated cortex is still functional and can be safely resected. Classical electrophysiological mapping techniques comprising direct cortical stimulation and somatosensory evoked potentials have proven the presence of functional cortex within grossly abnormal tumor tissue.[9,10] These findings were confirmed using advanced electrophysiological methods, such as task-related spectral power perturbations in the high-gamma range[11–13] and magnetoencephalography.[14] While these clinical studies do not allow for unraveling details and directions of interactions between glioma cells and neurons, ample experimental evidence shows that neurons connect to glioma cells via electrically active gap junctions and glutaminergic synapses.[8] In turn, as Krishna et al. outlined,[13] preclinical studies suggest that glioma cells induce neuronal hyperexcitability in the tumor-infiltrated cortex by glutamate release[41,42] and reduction of GABAergic inhibitory interneurons.[43] In patients, neuronal hyperexcitability has also been observed in the form of increased task-induced high-gamma power during intraoperative electrocorticography.[13] Of note, the interaction between glioma and neurons went far beyond the directly infiltrated cortex, as tasks recruited neighboring cortical areas that were not normally involved.[13]

Connectivity Between Tumor Region and Brain-Wide Networks

Apart from close local structural and functional connections between glioma tissue and neural elements as characterized above, glioma-infiltrated cortical regions maintain long-range functional connections to other brain regions and networks. For example, Krishna et al. investigated 19 patients with glioblastoma using magnetoencephalography and observed that up to 50% of the intratumoral voxels included in the contrast-enhanced or FLAIR-hyperintense tumor regions were strongly connected to the rest of the brain.[13] Furthermore, Mandal and co-workers[11] used rs-fMRI in 17 low-grade gliomas to evaluate the participation of tumor-infiltrated cortex in large-scale cognitive circuits, using the same network definition

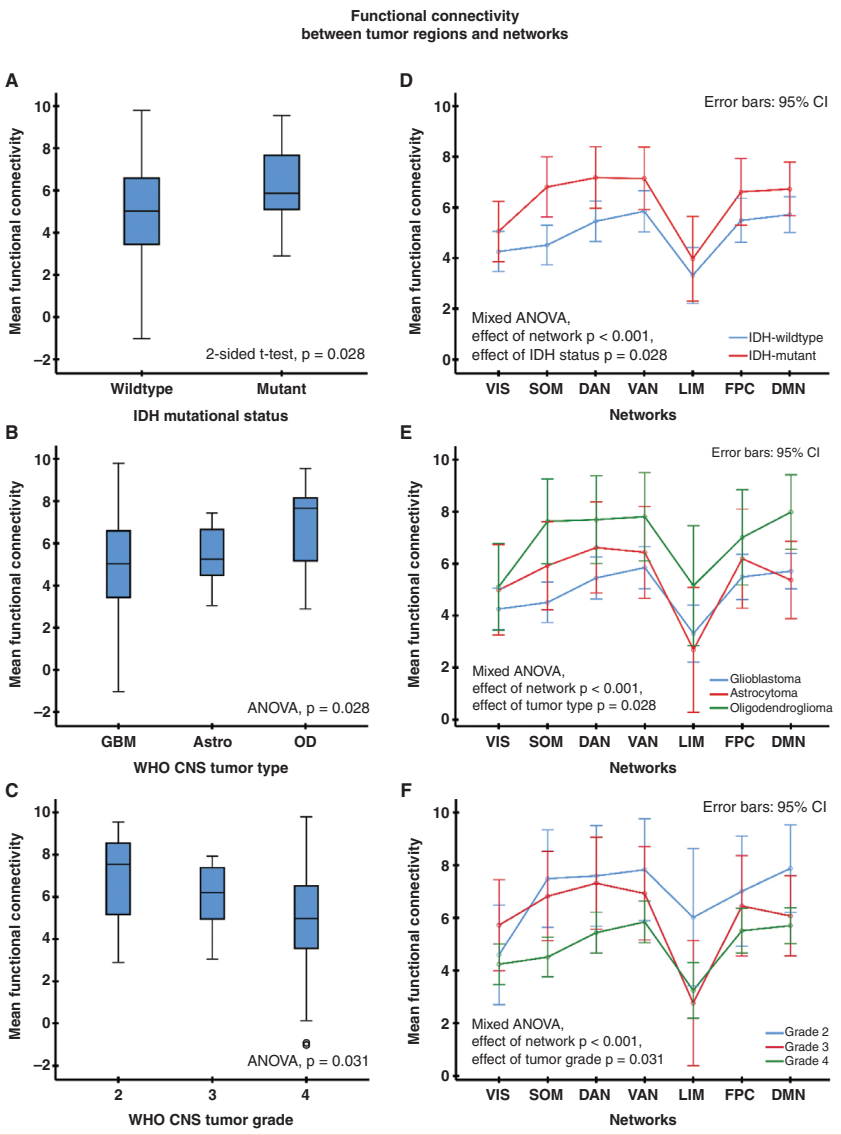

Figure 2. Mean overall functional connectivity between brain regions infiltrated by metabolic active tumor and 7 canonical resting-state networks (A-C) as well as network-specific connectivity (D-F) in patients with recurrent glioma related to the IDH mutational status (top row), tumor type (middle row), and CNS WHO tumor grade (bottom row). Abbreviations: IDH, isocitrate dehydrogenase; ANOVA, analysis of variance; CI, confidence interval; VIS, visual; SOM, somatomotor network; DAN, dorsal attention network; VAN, ventral attention network; LIM, limbic network; FPC, frontal-parietal control network; DMN, default mode network; GBM, glioblastoma; Astro, astrocytoma; OD, oligodendroglioma

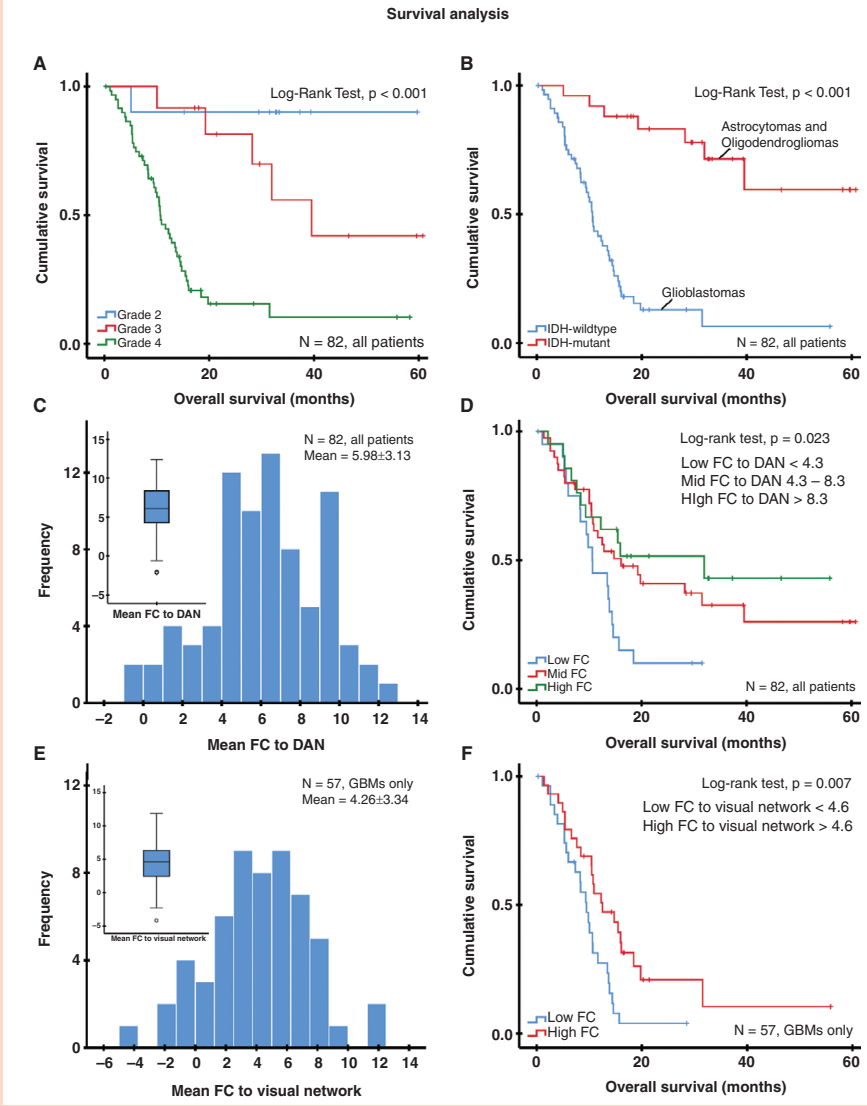

Figure 3. Kaplan–Meier survival curves in patients with recurrent gliomas of different CNS WHO tumor grades (A), different IDH mutational status (B), and various levels of functional connectivity (low, middle, and upper quartile) between brain regions infiltrated by metabolic active tumor and the dorsal attention network (D). The distribution of network connectivity between the tumor regions and the dorsal attention network is visualized as a histogram and boxplot (C). Results for the IDH wild-type glioblastoma subgroup regarding the distribution of network connectivity between tumor and visual network are shown in (E), as well as Kaplan–Meier survival curves with a median (4.6) classification of connectivity into high and low in (F). Abbreviations: IDH, isocitrate dehydrogenase; FC, functional connectivity; DAN, dorsal attention network; N, number of patients.

Table 2. Univariate and Multivariate[#] Cox Regression Analysis for Association Between Tumor-to-Network Resting-State Functional Connectivity and Overall Survival in Recurrent Gliomas

	Entire patient cohort		Glioblastoma patients	
Resting-state network	*P*-value (univariate)	*P*-value (multivariate)[#]	*P*-value (univariate)	*P*-value (multivariate)[#]
Visual	.036	.677	.023	.023
Somatomotor	.041	.720	.794	.329
Dorsal Attention	.007	.007	.107	.936
Ventral Attention	.246	.101	.875	.222
Limbic	.997	.900	.759	.838
Frontoparietal	.309	.159	.704	.370
Default Mode	.453	.133	.946	.102

[#]forward stepwise inclusion.

Table 3. Univariate and Multivariate Cox Regression Analysis to Evaluate Tumor-Related and Common Prognostic Factors on Overall Survival in Recurrent Gliomas Diagnosed With FET PET

	Entire patient cohort, FC between tumor and dorsal attention network		GBM patients, FC between tumor and visual network	
Factor	*P*-value (univariate)	*P*-value (multivariate)	*P*-value (univariate)	*P*-value (multivariate)
Connectivity between tumor and network	.007	.033	.023	.031
Metabolic active tumor volume	.012	.023	.003	.011
Age	.237	.215	.887	.232
MGMT promoter methylation status	.003	.057	.319	.314
Extent of resection at initial diagnosis	.008	.162	.961	.824
ECOG score	.001	.172	.051	.865

as in the present study.[37] Of note, the tumor locations that were active during a task that probed executive functions were found to exhibit significant FC with the DAN. More recently, Daniel and colleagues[21] evaluated 57 patients with newly diagnosed glioblastoma using rs-fMRI. By applying a heuristic threshold, up to 60% of intratumoral voxels were functionally connected to at least 1 of the 7 canonical networks, although this proportion largely varied between patients. In addition, tumor voxels did not connect specifically to any resting-state network. Another study evaluated FC between tumor and brain in 54 patients with CNS WHO grade 2–4 gliomas in the newly diagnosed or recurrent setting.[22] Again, significant resting-state FC between the tumors and the unaffected brain was observed in that study. In the newly diagnosed tumors, the set of brain voxels functionally connected with the tumor resembled the frontoparietal control network, while in the recurrent tumors, the location of the connected brain voxels resembled the DAN.[22]

Regarding glioma grade and IDH mutational status, it can be expected that the lower the tumor grade and the less aggressive the tumor growth, the higher the preserved neuronal population and the less disturbed the local and distant functional organization of the infiltrated cortex, as observed here in recurrent gliomas. Taken together, these results, including the present study's findings, suggest that in both newly diagnosed and recurrent gliomas, a substantial proportion of cortical tissue infiltrated by the glioma is locally functional and remains remotely connected. FC between the brain region infiltrated by metabolic active tumor and other parts of the brain is present to varying degrees in all canonical networks and does depend on the location but rather on the tumor's invasiveness.

Association Between Tumor Region and Brain Connectivity and Survival

In the present study, we observed a significant association of FC between the region infiltrated by metabolic active tumor and the brain and overall survival. In this sense, a higher FC between the tumor region and the visual, somatomotor, and DAN was associated with a lower risk for death. Similarly, Daniel et al.[21] found that higher tumor intra-network connectivity was associated with longer overall survival in patients with newly diagnosed glioblastoma. Interestingly, reduced or absent FC was observed in the necrotic tumor regions compared to the solid, contrast-enhancing regions. The authors hypothesized that tumors with better-preserved physiology have a more favorable prognosis, which is supported by the observation in the present study that FC between tumor regions and networks was higher in CNS WHO grade 2 or 3 and IDH-mutant gliomas than in IDH-wild-type gliomas. Nevertheless, these results are only partly in line with those from Sprugnoli et al.[22] in newly diagnosed gliomas, where the connectivity of the solid tumor with various contiguous brain regions correlated either positively (right parieto-temporal) or negatively (right or left frontal) with the duration of survival. However,

in recurrent malignant gliomas, only one positively correlated cluster (i.e. right frontal) was identified.[22] These partly discrepant findings may result from the varying methods of defining the solid parts in tumors of different tumor grades, which we here attempted to overcome by adding amino acid PET with the tracer FET to anatomical MRI in all examined patients.

The present observation that the connectivity between brain regions infiltrated by metabolic active tumor and the DAN (whole cohort) and the visual network (IDH-wild-type glioblastoma) was associated with a significant improvement in overall survival could be related to the specific function of this networks for cognitive performance. The DAN is mainly involved in goal-directed, voluntary control of visuospatial attention,[44,45] a cognitive domain that plays an important role for executive functioning and is naturally also depending on the visual network. In addition, the visual network is an important resource not only for object recognition but also for spatial orientation and goal-directed actions with objects[46] and for posture[47] and thus has a major influence on daily physical functioning. As mentioned, Mandal and colleagues[11] observed that tumor-infiltrated cortical regions that were active during an executive task may have significant FC with the DAN. Although not specifically addressing the DAN, Krishna, and colleagues[13] also observed that gliomas may remodel FC such that task-relevant neural responses activate tumor-infiltrated cortex well beyond the cortical regions that are normally recruited in the healthy brain. Thus, the improved survival of IDH-mutant or wild-type gliomas could in part be related to the ability of the affected brain to recruit tumor-infiltrated, distant regions to serve vision, visual attention, and executive functions which are closely associated with prognosis.[48]

Limitations

Only a limited number of patients were available for the present study, and these showed some heterogeneity in treatment. Therefore, important relationships between FC and overall survival may have been overlooked in the analysis, especially in the group of IDH-mutant gliomas.

Conclusion

The present results indicate that recurrent gliomas, as defined by pathologically increased FET uptake, maintain functionally connected to most of the major known resting-state networks. FC between brain regions infiltrated by metabolic active tumors and networks was generally higher in low-grade and IDH-mutant recurrent gliomas, and connectivity with the dorsal attention and visual networks proved to be an additional prognostic factor for improved overall survival. Thus, the close glioma-neural relationships observed in primary gliomas appear also to play a prognostic role in recurrent gliomas, suggesting that FC may be used as a novel prognostic imaging biomarker in patients with recurrent gliomas.

Supplementary Material

Supplementary material is available online at *Neuro-Oncology Advances* (https://academic.oup.com/noa).

Keywords

amino acid PET | BOLD signal | cancer neuroscience | functional MRI | prognostic biomarker

Lay Summary

Brain tumors not only affect the connections between different parts of the brain, but they can also connect themselves functionally with the healthy brain. The authors of this study wanted to see whether the strength of these tumor-to-brain connections could be used to see how long patients with a specific brain tumor called gliomas would live. To do this, they obtained advanced brain imaging on 82 patients who had gliomas that came back after initial treatment. Their results showed that patients with stronger connections between the tumor and certain brain networks, like those involved in vision or attention, tended to live longer.

Funding

This open-access publication is funded by the Deutsche Forschungsgemeinschaft (DFG, German Research Foundation, contract number 491111487).

Acknowledgments

The technical assistance of N. Judov, T. Plum, S. Schaden, and L. Tellmann is gratefully acknowledged.

Conflict of interest statement

M. Friedrich: None; J.M. Werner: None; J.P. Steinbach: Honoraria for presentations, educational events, and advisory board participation from Boehringer Ingelheim, Med-Update, Roche, Novocure, Seagen, GSK, Servier; M. Sabel: None; U. Herrlinger: Consulting fees and speaker honoraria from Medac; M. Piroth: None; G. Stoffels: None; C.P. Filss: None; P. Lohmann: Speaker honoraria from Blue Earth Diagnostics; advisory board participation for Servier; N.J. Shah: None; M.I. Ruge: None; F.M. Mottaghy: None; R. Goldbrunner: None; K.-J. Langen: Honoraria from Telix Pharmaceuticals for consultancy services; G.R. Fink: None; M. Kocher: None; N. Galldiks: Honoraria from Blue Earth Diagnostics for lectures and from Telix Pharmaceuticals and Servier for advisory board participation.

Authorship statement

Study design: M.F., K.J.F., M.K., and N.G.. Data acquisition: M.F., J.M.W., J.P.S., M.S., U.H., M.P., G.S., C.P.F., N.J.S., F.M.M., M.K., and N.G.. Data analysis, writing of manuscript drafts: M.F., J.M.W., J.P.S., M.S., U.H., M.P., P.L., K.J.L., M.K., and N.G.. Interpretation of data: M.F., J.M.W., J.P.S., M.S., U.H., C.P.F., P.L., M.I.R., F.M.M., R.G., K.J.L., G.R.F., M.K., and N.G.. Revising manuscript, approving final content of manuscript: all.

Data availability

Anonymized and aggregated data are available on reasonable request.

Affiliations

Institute of Neuroscience and Medicine (INM-3, INM-4, INM-11), Forschungszentrum Juelich, Juelich, Germany (M.F., G.S., C.P.F., P.L., N.J.S., K.J.L, G.R.F., M.K, N.G.); Department of Neurology, Faculty of Medicine and University Hospital Cologne, University of Cologne, Cologne, Germany (J.M.W., G.R.F., N.G.); Center of Integrated Oncology Aachen Bonn Cologne Duesseldorf (CIO ABCD), Cologne, Germany (M.S., U.H., M.I.R., R.G., M.K, N.G.); Department of Neuro-Oncology, University Hospital Frankfurt - Goethe-University, Frankfurt, Germany (J.P.S.); Department of Neurosurgery, Heinrich Heine University Medical Faculty and University Hospital Düsseldorf, Düsseldorf, Germany (M.S.); Department of Neurooncology, Center for Neurology, University Hospital Bonn, Bonn, Germany (U.H.); Department of Radiation Oncology, Helios University Hospital Wuppertal, Faculty of Health, Witten/Herdecke University, Wuppertal, Germany (M.P.); Juelich-Aachen Research Alliance (JARA), Section JARA-Brain, Juelich, Germany (N.J.S.); Department of Neurology, RWTH University Hospital Aachen, RWTH University Aachen, Aachen, Germany (N.J.S.); Department for Stereotaxy and Functional Neurosurgery, Center for Neurosurgery, Faculty of Medicine and University Hospital Cologne, Cologne, Germany (M.I.R., M.K.); Department of Nuclear Medicine, RWTH University Hospital Aachen, RWTH University Aachen, Aachen, Germany (C.P.F., P.L., F.M.M., K.J.L.); Department of Radiology and Nuclear Medicine, Maastricht University Medical Center, Maastricht, The Netherlands (F.M.M.); Center for Neurosurgery, Department of General Neurosurgery, Faculty of Medicine and University Hospital Cologne, University of Cologne, Cologne, Germany (R.G.)

References

1. Cuddapah VA, Robel S, Watkins S, Sontheimer H. A neurocentric perspective on glioma invasion. *Nat Rev Neurosci*. 2014;15(7):455–465.
2. Sharma P, Aaroe A, Liang J, Puduvalli VK. Tumor microenvironment in glioblastoma: Current and emerging concepts. *Neurooncol. Adv.*. 2023;5(1):vdad009.
3. Monje M, Borniger JC, D'Silva NJ, et al. Roadmap for the emerging field of cancer neuroscience. *Cell*. 2020;181(2):219–222.
4. Winkler F, Venkatesh HS, Amit M, et al. Cancer neuroscience: State of the field, emerging directions. *Cell*. 2023;186(8):1689–1707.
5. Mandal AS, Romero-Garcia R, Hart MG, Suckling J. Genetic, cellular, and connectomic characterization of the brain regions commonly plagued by glioma. *Brain*. 2020;143(11):3294–3307.
6. Venkataramani V, Tanev DI, Strahle C, et al. Glutamatergic synaptic input to glioma cells drives brain tumour progression. *Nature*. 2019;573(7775):532–538.
7. Venkatesh HS, Johung TB, Caretti V, et al. Neuronal activity promotes glioma growth through neuroligin-3 secretion. *Cell*. 2015;161(4):803–816.
8. Venkatesh HS, Morishita W, Geraghty AC, et al. Electrical and synaptic integration of glioma into neural circuits. *Nature*. 2019;573(7775):539–545.
9. Ojemann JG, Miller JW, Silbergeld DL. Preserved function in brain invaded by tumor. *Neurosurgery*. 1996;39(2):253–258; discussion 258–259.
10. Skirboll SS, Ojemann GA, Berger MS, Lettich E, Winn HR. Functional cortex and subcortical white matter located within gliomas. *Neurosurgery*. 1996;38(4):678–684; discussion 684–675.
11. Mandal AS, Wiener C, Assem M, et al. Tumour-infiltrated cortex participates in large-scale cognitive circuits. *Cortex*. 2024;173:1–15.
12. Aabedi AA, Lipkin B, Kaur J, et al. Functional alterations in cortical processing of speech in glioma-infiltrated cortex. *Proc Natl Acad Sci U S A*. 2021;118(46):e2108959118.
13. Krishna S, Choudhury A, Keough MB, et al. Glioblastoma remodelling of human neural circuits decreases survival. *Nature*. 2023;617(7961):599–607.
14. Schiffbauer H, Ferrari P, Rowley HA, Berger MS, Roberts TP. Functional activity within brain tumors: A magnetic source imaging study. *Neurosurgery*. 2001;49(6):1313–1320; discussion 1320–1311.
15. Ghinda DC, Wu JS, Duncan NW, Northoff G. How much is enough-Can resting state fMRI provide a demarcation for neurosurgical resection in glioma? *Neurosci Biobehav Rev*. 2018;84:245–261.
16. Stoecklein VM, Stoecklein S, Galie F, et al. Resting-state fMRI detects alterations in whole brain connectivity related to tumor biology in glioma patients. *Neuro Oncol*. 2020;22(9):1388–1398.
17. Liu L, Zhang H, Wu J, et al. Overall survival time prediction for high-grade glioma patients based on large-scale brain functional networks. *Brain Imaging Behav*. 2019;13(5):1333–1351.
18. Daniel AGS, Hacker CD, Lee JJ, et al. Homotopic functional connectivity disruptions in glioma patients are associated with tumor malignancy and overall survival. *Neurooncol Adv.*. 2021;3(1):vdab176.
19. Lamichhane B, Daniel AGS, Lee JJ, et al. Machine learning analytics of resting-state functional connectivity predicts survival outcomes of glioblastoma multiforme patients. *Front Neurol*. 2021;12:642241.
20. Luckett PH, Olufawo M, Lamichhane B, et al. Predicting survival in glioblastoma with multimodal neuroimaging and machine learning. *J Neurooncol*. 2023;164(2):309–320.
21. Daniel AGS, Park KY, Roland JL, et al. Functional connectivity within glioblastoma impacts overall survival. *Neuro Oncol*. 2021;23(3):412–421.
22. Sprugnoli G, Rigolo L, Faria M, et al. Tumor BOLD connectivity profile correlates with glioma patients' survival. *Neurooncol. Adv.*. 2022;4(1):vdac153.
23. Park JK, Hodges T, Arko L, et al. Scale to predict survival after surgery for recurrent glioblastoma multiforme. *J Clin Oncol*. 2010;28(24):3838–3843.
24. Pineda E, Domenech M, Hernandez A, Comas S, Balana C. Recurrent glioblastoma: Ongoing clinical challenges and future prospects. *Onco Targets Ther*. 2023;16:71–86.
25. Vaz-Salgado MA, Villamayor M, Albarran V, et al. Recurrent glioblastoma: A review of the treatment options. *Cancers (Basel)*. 2023;15(17):4279.

26. Langen KJ, Stoffels G, Filss C, et al. Imaging of amino acid transport in brain tumours: Positron emission tomography with O-(2-[(18)F]fluoroethyl)-L-tyrosine (FET). *Methods*. 2017;130:124–134.
27. Louis DN, Perry A, Wesseling P, et al. The 2021 WHO classification of tumors of the central nervous system: A summary. *Neuro Oncol*. 2021;23(8):1231–1251.
28. Wen PY, Macdonald DR, Reardon DA, et al. Updated response assessment criteria for high-grade gliomas: Response assessment in neuro-oncology working group. *J Clin Oncol*. 2010;28(11):1963–1972.
29. Galldiks N, Stoffels G, Filss C, et al. The use of dynamic O-(2-18F-fluoroethyl)-l-tyrosine PET in the diagnosis of patients with progressive and recurrent glioma. *Neuro Oncol*. 2015;17(9):1293–1300.
30. Stupp R, Hegi ME, Mason WP, et al; European Organisation for Research and Treatment of Cancer Brain Tumour and Radiation Oncology Groups. Effects of radiotherapy with concomitant and adjuvant temozolomide versus radiotherapy alone on survival in glioblastoma in a randomised phase III study: 5-year analysis of the EORTC-NCIC trial. *Lancet Oncol*. 2009;10(5):459–466.
31. Herrlinger U, Tzaridis T, Mack F, et al; Neurooncology Working Group of the German Cancer Society. Lomustine-temozolomide combination therapy versus standard temozolomide therapy in patients with newly diagnosed glioblastoma with methylated MGMT promoter (CeTeG/NOA-09): A randomised, open-label, phase 3 trial. *Lancet*. 2019;393(10172):678–688.
32. Whitfield-Gabrieli S, Nieto-Castanon A. Conn: A functional connectivity toolbox for correlated and anticorrelated brain networks. *Brain Connect*. 2012;2(3):125–141.
33. Pauleit D, Floeth F, Tellmann L, et al. Comparison of O-(2-18F-fluoroethyl)-L-tyrosine PET and 3-123I-iodo-alpha-methyl-L-tyrosine SPECT in brain tumors. *J Nucl Med*. 2004;45(3):374–381.
34. Beckmann CF, Mackay CE, Filippini N, Smith SM. Group comparison of resting-state FMRI data using multi-subject ICA and dual regression. *Neuroimage*. 2009;47(Suppl 1):S148.
35. Kelly RE, Jr, Hoptman MJ, Lee S, et al. Seed-based dual regression: An illustration of the impact of dual regression's inherent filtering of global signal. *J Neurosci Methods*. 2022;366:109410.
36. Nickerson LD, Smith SM, Ongur D, Beckmann CF. Using dual regression to investigate network shape and amplitude in functional connectivity analyses. *Front Neurosci*. 2017;11:115.
37. Yeo BT, Krienen FM, Sepulcre J, et al. The organization of the human cerebral cortex estimated by intrinsic functional connectivity. *J Neurophysiol*. 2011;106(3):1125–1165.
38. Mauler J, Lohmann P, Maudsley AA, et al. Diagnostic accuracy of MR spectroscopic imaging and (18)F-FET PET for identifying glioma: A biopsy-controlled hybrid PET/MRI study. *J Nucl Med*. 2024;65(1):16–21.
39. Pauleit D, Floeth F, Hamacher K, et al. O-(2-[18F]fluoroethyl)-L-tyrosine PET combined with MRI improves the diagnostic assessment of cerebral gliomas. *Brain*. 2005;128(Pt 3):678–687.
40. Song S, Cheng Y, Ma J, et al. Simultaneous FET-PET and contrast-enhanced MRI based on hybrid PET/MR improves delineation of tumor spatial biodistribution in gliomas: A biopsy validation study. *Eur J Nucl Med Mol Imaging*. 2020;47(6):1458–1467.
41. Buckingham SC, Campbell SL, Haas BR, et al. Glutamate release by primary brain tumors induces epileptic activity. *Nat Med*. 2011;17(10):1269–1274.
42. Campbell SL, Buckingham SC, Sontheimer H. Human glioma cells induce hyperexcitability in cortical networks. *Epilepsia*. 2012;53(8):1360–1370.
43. Campbell SL, Robel S, Cuddapah VA, et al. GABAergic disinhibition and impaired KCC2 cotransporter activity underlie tumor-associated epilepsy. *Glia*. 2015;63(1):23–36.
44. Corbetta M, Shulman GL. Control of goal-directed and stimulus-driven attention in the brain. *Nat Rev Neurosci*. 2002;3(3):201–215.
45. Kincade JM, Abrams RA, Astafiev SV, Shulman GL, Corbetta M. An event-related functional magnetic resonance imaging study of voluntary and stimulus-driven orienting of attention. *J Neurosci*. 2005;25(18):4593–4604.
46. Erlikhman G, Caplovitz GP, Gurariy G, Medina J, Snow JC. Towards a unified perspective of object shape and motion processing in human dorsal cortex. *Conscious Cogn*. 2018;64:106–120.
47. Wade MG, Jones G. The role of vision and spatial orientation in the maintenance of posture. *Phys Ther*. 1997;77(6):619–628.
48. Johnson DR, Sawyer AM, Meyers CA, O'Neill BP, Wefel JS. Early measures of cognitive function predict survival in patients with newly diagnosed glioblastoma. *Neuro Oncol*. 2012;14(6):808–816.

2.3.1 Supplementary data

Supplemental Material

Functional connectivity between tumor region and resting-state networks as imaging biomarker for overall survival in recurrent gliomas diagnosed by FET PET

Michel Friedrich, Jan-Michael Werner, Joachim P. Steinbach, Michael Sabel, Ulrich Herrlinger, Marc Piroth, Gabriele Stoffels, Christian P. Filss, Philipp Lohmann, Nadim J. Shah, Maximilian I. Ruge, Felix M. Mottaghy, Roland Goldbrunner, Karl-Josef Langen, Gereon R. Fink, Martin Kocher*, and Norbert Galldiks*

***equal contribution to senior authorship**

Institute of Neuroscience and Medicine (INM-3, INM-4, INM-11), Forschungszentrum Juelich, Juelich, Germany (MF, GS, CPF, PL, NJS, KJL, GRF, MK and NG)

Department of Neurology, Faculty of Medicine and University Hospital Cologne, University of Cologne, Cologne, Germany (JMW, GRF and NG)

Center of Integrated Oncology Aachen Bonn Cologne Duesseldorf (CIO ABCD), Germany (MS, UH, MIR, RG, MK and NG)

Department of Neuro-Oncology, University Hospital Frankfurt - Goethe-University, Frankfurt, Germany (JPS)

Department of Neurosurgery, Heinrich Heine University Medical Faculty and University Hospital Düsseldorf, Düsseldorf, Germany (MS)

Department of Neurooncology, Center for Neurology, University Hospital Bonn, Bonn, Germany (UH)

Department of Radiation Oncology, Helios University Hospital Wuppertal, Faculty of Health, Witten/Herdecke University, Wuppertal, Germany (MP)

Juelich-Aachen Research Alliance (JARA), Section JARA-Brain, Juelich, Germany (NJS)

Department of Neurology, RWTH University Hospital Aachen, RWTH University Aachen, Aachen, Germany (NJS)

Department for Stereotaxy and Functional Neurosurgery, Center for Neurosurgery, Faculty of Medicine and University Hospital Cologne, Cologne, Germany (MIR and MK)

Department of Nuclear Medicine, RWTH University Hospital Aachen, RWTH University Aachen, Aachen, Germany (CPF, PL, FMM, KJL)

Department of Radiology and Nuclear Medicine, Maastricht University Medical Center, Maastricht, Netherlands (FMM)

Center for Neurosurgery, Department of General Neurosurgery, Faculty of Medicine and University Hospital Cologne, University of Cologne, Cologne, Germany (RG)

Imaging protocols

O-(2-[^{18}F]-fluoroethyl)-L-tyrosine (FET) PET, structural MR, and resting-state functional magnetic resonance imaging (rs-fMR) images were acquired simultaneously using a 3T hybrid scanner (Siemens Tim-Trio/BrainPET, Siemens Medical Systems, Erlangen, Germany). For this purpose, the scanner was equipped with a birdcage-like quadrature transmitter head coil mounted on the couch, an 8-channel receiver coil, and a PET insert consisting of 72 rings (axial field-of-view, 19.2 cm; center spatial resolution, 3 mm FWHM). FET PET images were obtained following Herzog et al.[1].

The structural MRI protocol comprised a 3D high-resolution T1-weighted magnetization-prepared rapid acquisition gradient echo (MPRAGE) native scan (176 slices; repetition time TR = 2250 ms; echo time TE = 3.03 ms; field of view (FoV) = 256 × 256 mm^2; flip angle = 9°; voxel size = 1 × 1 × 1 mm^3), a contrast-enhanced MPRAGE scan recorded after injection of gadolinium-based contrast agent, a T2-weighted sampling perfection with application-optimized contrasts using different flip angle evolution scan (176 slices; repetition time TR = 3.2 ms; echo time TE = 417 ms; FoV = 256 × 256 mm^2; voxel size = 1 × 1 × 1 mm^3), and a T2-weighted fluid-attenuated inversion recovery (T2/FLAIR) scan (25 slices; TR = 9000 ms; TE = 3.86 ms; FoV = 220 × 220 mm^2; flip angle = 150°; voxel size = 0.9 × 0.9 × 4 mm^3). To acquire rs-fMRI data, patients were instructed to relax and let their minds wander, but not fall asleep. Within 11 minutes, a total of 300 functional volumes were acquired with a gradient-echo echo-planar imaging pulse sequence (36 axial slices; slice thickness, 3.1 mm; TR = 2200 ms; TE = 30 ms; flip angle = 90°; FoV = 200 × 200 mm^2; in-plane voxel-size, 3.1 × 3.1 mm^2).

Table S1: Regression analyses for the entire patient cohort between the mean functional connectivity (z-score) of the metabolically active tumor region and its proximity (mm) to the networks.

Resting-State Network	**Coefficient of Determination (R^2)**	**p-value**	**Slope of the regression model**
Visual	0.063	0.023	-0.040
Somatomotor	0.115	0.002	-0.097
Dorsal Attention	0.103	0.003	-0.071
Ventral Attention	0.069	0.017	-0.080
Limbic	0.195	0.001	-0.103
Frontoparietal	0.040	0.072	-0.059
Default Mode	0.023	0.174	-0.052

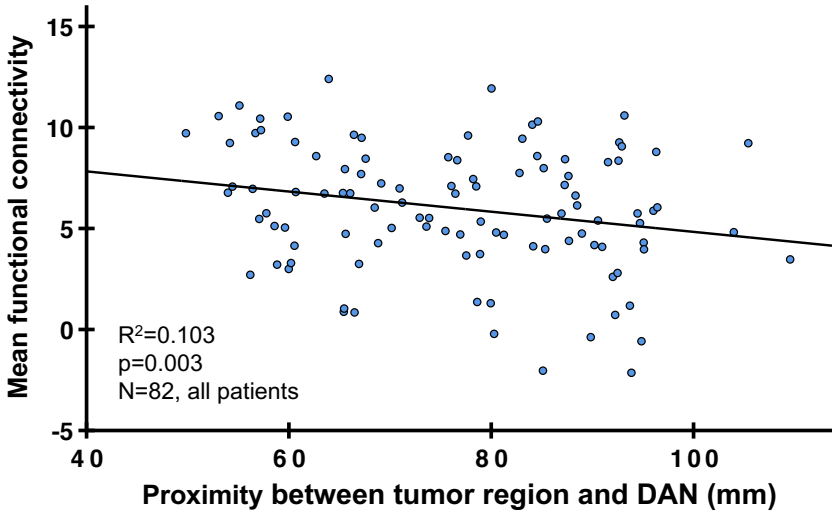

Figure S1: Regression analyses for the entire patient cohort between the mean functional connectivity (z-score) of the metabolically active tumor region and its proximity (mm) to the dorsal attention network. Abbreviations: R^2, coefficient of determination; N, number of patients

References

1. Herzog H, Langen KJ, Weirich C, et al. High resolution BrainPET combined with simultaneous MRI. *Nuklearmedizin.* 2011; 50(2):74-82.

3 Discussion

This thesis addresses three neuro-oncologically relevant aspects of tumor- and treatment-related changes in brain connectivity observed in patients with recurrent glioma. Each aspect was investigated in a separate study. The first two studies examined the same cohort of 121 patients, while the third study focused on a specific subset of 82 patients with metabolically active recurrent gliomas.

Initially, the local white matter integrity of structural brain lesions indicated by pathologic MRI and FET PET findings as well as their overall impact on the patients' performance status was investigated. The effect of altered integrity of local structural connectivity in four different lesion types - resection cavity, FET-avid tumor, contrast-enhanced lesions and FLAIR hyperintense signal alterations - on the Eastern Cooperative Oncology Group (ECOG) performance score of the patients was assed and compared with a matched cohort of 121 healthy controls. For this purpose, fiber density images were used that originate from a self-established state-of-the-art tractography pipeline, which enables the adequately resolution of the white matter fiber architecture even within tumor affected areas (see Section 3.2).

The second aspect involved a more specific breakdown of the impairment of structural connectivity within 100 different brain areas, organized into seven resting-state networks of the Schaefer-Yeo brain atlas[132], to assess the impact on several cognitive functions. For this purpose, an analysis method based on machine learning with integrated cross-validation was used. The underlying CPM method was originally developed for functional data and successfully adapted for the analysis of structural connectomes in the course of this work. Based on the tractographies of the first study in combination with a network-based parcellation, whole-brain connectomes were generated, which were then related to the patients' cognitive performance scores using the adapted CPM method. The approach was used to identify vulnerable edges, nodes and networks that are relevant for specific cognitive functions in treated patients with glioma at recurrence.

Given that structural organization of brain forms the backbone of functional connectivity, the third and final aspect analyzed was the impact on patients' functional connectivity. Particular attention was paid to the emerging field of *Cancer Neuroscience*, which is becoming increasingly important in neuro-oncology. Here, the interactions between tumor and the normal brain are investigated. With this in mind, the functional connectivity between brain regions infiltrated by a metabolic active glioma and set of the seven canonical resting-state networks of Schaefer-Yeo brain atlas[132] was investigated using

seed-based dual regression analysis, a modification of seed-based correlation analysis. In addition, the results were linked to the overall survival of the patients.

Overall, this work deals with the question of how our brain is able to generate adequate behavior when the underlying brain connectivity is disrupted at different levels by gliomas and their treatment. In this context, a clearer understanding of the pathology of altered brain connectivity could additionally provide a more reliable prediction of disease progression and side effects and support the choice of tailored therapies, leading to an improved quality of life for the patient.

3.1 Main findings

The methodological challenges and clinical implications of the following results will be elucidated in the course of the discussion. The first study confirmed the hypothesis that the various glioma- and treatment-induced structural brain lesions, as indicated by pathological MRI and FET PET findings, have a differential impact on white matter fiber density[2]. Local fiber density was significantly reduced in all lesion types examined, although to a different extent. The comparison with a matched cohort of healthy controls revealed, as expected, an almost complete reduction within the resection cavities. The reduction remained strong in contrast-enhanced and FET-avid lesions and was less pronounced, but still significant, in regions with FLAIR hyperintense signal alterations. It turned out that only the total fiber loss (1 – [patient fiber density / reference fiber density] * lesion volume) in contrast-enhanced lesions and FLAIR hyperintense signal alterations was associated with a significantly reduced ECOG performance score. Moreover, the reduction of fiber density within the metabolically active glioma was inversely related to its FET uptake.

The second study further specified the effects of glioma growth and treatments on the structural connectivity of individual network nodes and their associated cognitive functions[133]. It has been shown that a reduced fiber count across subsets of specific edges that predominantly interconnect different brain networks was significantly associated with impairments in different cognitive domains. In general, the nodes that turned out to be critical for cognitive critical function showed a high degree of connectivity with other nodes, and comprised mainly left hemispheric nodes and cortical hubs such as the bilateral precuneus or the posterior cingulate cortex.

In a specific subset of patients evaluated in the third study where metabolic active recurrent gliomas were diagnosed by a combination of anatomical MRI and FET PET, results indicated a preserved functional connectivity between brain regions infiltrated by

the metabolic active tumor and various canonical resting-state networks[134]. The functional connectivity differed significantly between networks and was mostly expressed to the four major associative networks (i.e., the dorsal attention network, the ventral attention network, the frontoparietal control network and the default mode network). In terms of tumor type, mean functional connectivity to all networks and individual connectivity to each network was highest in oligodendrogliomas, compared to glioblastomas and astrocytomas. This relation also applied to the *IDH*-mutant in contrast to *IDH*-wildtype gliomas. In addition to the most significant prognostic factors, i.e., the WHO tumor grade and *IDH* mutational status, the preserved functional connectivity between tumor region and the dorsal attention network appeared to be a potential additional prognostic factor for longer overall survival. In the subgroup of *IDH* wild-type glioblastomas, the functional connectivity of the tumor with the visual network even proved to be an independent prognostic factor for overall survival.

3.2 Methods for assessing structural connectivity in patients with glioma

The accurate determination and the subsequent analysis of the white matter fiber architecture is of fundamental importance in the context of the present work. The entire analysis of the first two studies is based on the same fiber mapping framework. Both the fiber density images of the patients and the connectomes were derived from the resulting tractographies. The establishment of a reliable tractography pipeline that is applicable to patients with treated brain tumor required extensive preparatory work before the actual analysis on structural connectivity could be started. Although tractography is already used routinely for preoperative planning, it is anything but trivial to perform whole-brain fiber mapping in a brain distorted by tumor growth and treatment effects. Tractography for treatment planning is usually based on DTI[103,123,124], but its ability to resolve complex fiber architectures is a priori limited[104], resulting in anatomically implausible or erroneously missing fiber tracts[103,104]. However, especially in the local treatment of brain tumors, e.g., by surgery and radiotherapy, it is essential to precisely localize the white matter tracts in order to spare them. For this reason, we decided to go beyond classical DTI and adopt a tractography approach based on an advanced diffusion model that avoids the usual limitations that have so far prevented broad clinical application. These include, for instance, the need for a large or wide range of b-values, which are difficult to achieve on clinical scanners and also lead to impractically long scan times[106]. A promising approach that could be considered are modern diffusion models based on CSD, which have improved significantly in recent years in terms of their acquisition

requirements and reliability in pathologically disturbed brain regions[126]. Especially these disturbed regions complicate the fiber mapping considerably.

3.2.1 Potential confounding factors in treated glioma

White matter fibers may be spatially impaired by brain tumors and treatment effects. They can be widened, displaced, infiltrated and/or interrupted by the tumor[73]. There is also the risk of vasogenic cerebral edema in gliomas due to a damaged blood-brain barrier. Defective tight junctions can cause plasma components to leak from the blood into the extracellular space, leading to cerebral edema and increased intracranial pressure, which can damage neuronal fibers. Another trigger for the formation of acute cerebral edema is an inflammatory reaction of the surrounding tissue caused by radiotherapy. As edema is associated with the increase of intra-tissue water compartments characterized by isotropic diffusion, it hampers the determination of anisotropic diffusion of the white mater fiber orientations[135,136]. Radiotherapy can also induce necrosis or gliosis in the irradiated brain tissue. The latter leads to hypertrophy of the glial cells or to their proliferation, which can result in the formation of scar tissue also affecting fiber tracts. However, resection has the most obvious influence on the brain structure, as there is no brain tissue left in the resulting resection cavities. All of the above factors caused by the tumor or its treatment led to deviations from normal brain tissue, which makes correct fiber mapping difficult. How this has presently been taken into account by the application of a modified tractography pipeline as discussed in the following sections.

3.2.2 Constrained spherical deconvolution models

The key requirement for diffusion models that allow the measured non-isotropic diffusion-weighted MRI signal to be related to the assumed local fiber architecture is a high angular resolution of the signal with low influence from other sources, such as freely diffusing water[135,136] or other tissue types in the brain. In this context, the novel Single-Shell 3-Tissue CSD (SS3T-CSD)[137,138] proved to be the preferred method, which, along with the Single-Tissue CSD (ST-CSD)[106] and Multi-Shell Multi-Tissue CSD (MSMT-CSD)[139], was one of the three CSD models available at the time of our studies. The term shell here refers to a DWI image with a specific b-value. In the course of the establishment of the present tractography pipeline prior to the start of the analysis, all models were compared with each other and evaluated for their applicability in patients with glioma. Although MSMT-CSD was already well established for healthy brains, it failed to estimate fiber orientations in tumor-affected areas, resulting in immense underestimation and exclusion of FODs and subsequently calculated fibers[2,126]. MSMT-CSD is a refined version of the

original ST-CSD. Already the ST-CSD showed a significant improvement in tractography compared to DTI, even in the presence of tumors[103,140]. Its major drawback was that the estimated FODs suffered from strong distortions due to random noise caused by isotropic diffusion signal contributions from other tissue types in the brain[126]. The MSMT-CSD improved this by also taking into account the signal contribution of gray matter and cerebrospinal fluid based on b-value tissue dependencies[139]. This enabled a more accurate estimation of the FODs at the tissue interfaces and thus even more precise fiber tracking[139]. However, areas affected by the tumor are often misclassified as gray matter-like tissue[126], leading to underestimation or exclusion of the white matter-specific FODs. Another downside of MSMT-CSD is the requirement of a multi-shell imaging protocol to adequately account for the signal contributions of the other tissue types. In comparison, SS3T-CSD only requires a HARDI protocol with a single b-value and non-diffusion-weighted images (b-value=0) for superior results. This reduces the acquisition effort and computation time for the various pre-processing steps such as motion and distortion corrections that need to be performed for each b-value contrast[126]. But the main advantage of the novel SS3T-CSD model is its ability to estimate white matter FODs as bias-free as possible, even within the tumor area[126,137,138], by accounting for contamination of each brain voxel by freely diffusing water, as found in cerebrospinal fluid or edema[141], or by gray matter isotropic signal contribution. To ensure a high angular resolution in our studies and thus the best results of the SS3T-CSD model, a HARDI scheme with 120 directions at a b-value of 2700 s/mm^2 was applied, providing an optimal contrast-to-noise ratio within the shell and between the shell and the non-diffusion-weighted data[126]. Nevertheless, lower b-values are also feasible while maintaining the quality at a reduced level.

3.2.3 Anatomically-constrained tractography

In addition to the state-of-the-art SS3T-CSD diffusion model described above, the present tractography framework makes use of another advanced approach called anatomically-constrained tractography (ACT)[116]. It improves the biological plausibility of the computed fibers derived from the FODs of the diffusion model by making the tractography even more accurate based on prior anatomical information[116]. This information is obtained by segmenting the whole brain into tissue components of the white matter, the cerebrospinal fluid as well as the cortical and subcortical gray matter on the basis of a structural T1 image. In this way, cerebrospinal fluid filled structures such as the ventricles and gray matter are omitted for the fiber propagation. This segmentation is clearly to be distinguished from the tissue segmentation of advanced CSD models, which is used to correctly scale FOD amplitudes. Although ACT

segmentation is also intended to provide more reliable termination criteria, it leaves FODs untouched. In this way, fibers based on less accurately estimated FODs can be subsequently sorted out at the tractography level, since even the SS3T-CSD does not provide completely accurate results, so false positives fibers are still possible. Apart from guidance of fiber propagation and termination, the other features of ACT were also used to improve tractography. These included the removal of anatomically unrealistic fiber courses as well as very short fibers at the gray-white matter interface, which cannot be accurately resolved with the low resolution of DWI, and the backtracking option for probabilistic tractography[116]. This option will find a more suitable termination for fibers running in an endpoint that was poorly supported by the image data.

The disadvantage of ACT is that it was developed for use in healthy tissue and would otherwise lead to incorrect fiber calculations in brain structures that have been altered by tumors and treatment effects, for example. Compared to healthy brains, these regions may exhibit atypical fiber tracts that would be incorrectly removed by ACT. Therefore, the lesioned regions had to be released from the above-mentioned restrictions for fiber propagation. This was done using a composite lesion mask consisting of all types of lesions, including resection cavities, FET-avid tumor, contrast-enhanced lesions and FLAIR hyperintense signal alterations. In addition, the lesion area also interfered with advanced ACT seed point generation, which restricts the seeds to the interface between gray and white matter. Theoretically, this would improve the homogeneity of streamline density in the entire white matter and thus improve biological plausibility[116]. However, the seeding algorithm proved unable to correctly detect the interface between gray and white matter in the lesion area, resulting in an imbalance in the number of seeding points in favor of healthy tissue. As a result, the majority of the seeds were accepted as fibers, given the higher probability of acceptance in healthy tissue. Accordingly, the number of fibers was nearly equivalent or even higher than in healthy controls, despite pathological and treatment-related brain damage. Therefore, a random seed point generation was applied to ensure a homogeneous seed distribution throughout the brain, even in the lesion region. In this way, the propagation of fibers from a seed point depended only on the local tissue properties that actually determine the presence of fibers. Even if whole brain seeding means a lower homogeneity of the resulting fiber density, a quantitative comparison would not have been possible without it. Nonetheless, it should be emphasized that this is a common seeding variant offered by the applied tractography software.

3.2.4 Fiber tracking analysis

After the development of a tractography pipeline suitable for treated patients with glioma, there were also some aspects to consider when analyzing the resulting tractographies in order to obtain reliable results. For the initial analysis of integrity of local structural connectivity within different lesion types, the tractographies were first converted into fiber density images[118,119] in which each image voxel is indicative of the number of fibers passing through it. The fiber density within the lesions was then compared to a matched control group. In a similar study on fiber density in patients with glioblastoma, a paradoxical positive correlation was found between the degree of tumor infiltration and fiber density for different tumor regions[142]. This was probably due to a less sophisticated tractography pipeline, but also to the fact that a comparable reference fiber density is difficult to achieve due to the inhomogeneous distribution of fiber tracts in the brain. In order to obtain a solid and comparable estimate of the local and relative fiber density in our study, all steps up to the final fiber density images were performed almost identically for the patient and subject data, with the exception of the echo-planar imaging distortion correction during pre-processing of the DWI data that were not available for the healthy subjects. This could cause inward deformation, particularly of the frontal tracts. However, there was no evidence of this, presumably as a result of correct spatial normalization of the fiber density images to the Montreal Neurosciences Institute (MNI) template. To obtain a generally representative reference fiber density, the fiber density images of the healthy subjects were transformed into the MNI space for subsequent averaging. Despite efforts to obtain a reliable fiber density, it is evident from the results that the resection cavities still erroneously contain a minimal residual fiber density. This could be due to the difficulty of manually segmenting the boundaries of the resection cavity, which may have included individual voxels with tissue in the segmentation. It should also be noted that although the tractography framework used here provides a very good approximation of the actual fiber architecture, it is not free of false positive fibers, especially when considering that the influence of the ACT was omitted in the lesion region (see Section 3.2.3), which could have filtered out fibers outside of the white matter.

After analyzing the integrity of the local white matter architecture, the structural connectivity at the network level between different nodes was further investigated, focusing on the relationship between structural connectivity and cognitive functions. This is usually achieved by correlating measurements of individual structural connectivity with cognitive function, as was done here, where tractography data were converted into structural connectivity matrices and correlated with the results of cognitive performance tests. However, simple correlation or similar regression models tend to over-fit the data

and make it difficult to generalize the results[120]. For this reason, a machine learning approach, including cross-validation, based on CPM[120] was adapted for the analysis. In contrast to simple correlation, cross-validation provides a more conservative approach by validating the strength of a relationship in an independent sample that was not used to train the model[120]. This ensures independence between feature selection and prediction, eliminating confounding effects and false inferences at the population level[120,143]. More generally, the ability to generalize results facilitates the creation of new models that advance our understanding of the functional organization of the brain, as well as their translation into clinical applications, e.g., in the form of neuroimaging-based biomarkers. Other strengths of CPM are that it is purely data-driven and based on linear operations, which enables fast computation, simple software implementation and clearly interpretable results. In this way, it achieves the same or even better performance than comparable approaches[120].

3.3 Alterations of structural connectivity in patients with glioma

Structural connectivity describes the physical connections between cortical regions (nodes) via white matter tracts (edges) that form the basis of the functional organization of the brain. In patients with brain tumor, these neural fibers may be structural altered such as disrupted by the tumor or recurrent tumor growth[144]. In addition, structural tissue damage resulting from multimodal treatment, including tumor resection, radiation therapy, alkylating chemotherapy, or combinations thereof, may also cause further disruption[145-148]. Although standard anatomical MRI and amino acid PET, such as FET PET, can reveal these gross structural tissue changes, they do not yet provide any insight into the actual damage to the microstructural integrity of the white matter[149,150]. Therefore, modern DWI techniques[151-153] are needed and applied in this work. Brain tumor patients often develop deficits in general performance[154] and cognition that increase with survival time and intensity of therapy[155,156] as a result of cerebral tissue damage. This impairs not only direct fiber tracts of eloquent cortical regions, but also more extensive and far-reaching areas of white matter[156-158] along with the connections of multiple functional networks[159]. Individualized identification of vulnerable structures at risk for neurological or cognitive deficits is therefore of particular interest for local treatment planning, such as surgery and radiotherapy. Since damage to healthy brain tissue is usually unavoidable, it is important to determine which areas can be damaged without functional consequences and what intensity of treatment is acceptable. The field of neuro-oncology has already focused on defining selected structures at risk in neurosurgery or radiotherapy[103]. However, a better understanding of the effects of the tumor and its treatment on the white matter architecture could further elucidate the

pathological mechanisms and facilitate clinical application, e.g., to optimize treatment planning.

To get a first overview of how structural connectivity is impaired within in cohort of 121 treated patients with glioma at recurrence, local white matter integrity was analyzed in different lesion areas and related to the general performance (ECOG score) of the patients. Fiber density within the resection cavity, FET-avid and contrast-enhanced tumor, as well as FLAIR hyperintense signal alterations were examined and compared with a matched cohort of 121 healthy controls. To gain a more detailed understanding of how structural connectivity influences patients' behavior apart from their overall performance, we also investigated a finer structural organization of the brain together with a comprehensive cognitive test battery. As indicated by other studies, the long-term outcome of higher-order cognitive function in patients with glioma relies less on the integrity of individual nodes or edges than on the preservation of multiple distributed networks[124,127,128]. We therefore investigated the relationship between cognitive performance and structural connectivity in gliomas on a network basis. A total of 100 different brain areas organized into seven networks were examined to identify vulnerable nodes, edges and networks relevant to specific cognitive functions. The determination of the structural connectivity between the individual nodes as well as the initial determination of fiber density was based on the above-mentioned tractography pipeline, which has been shown to be able to adequately map neuronal fibers even in the structurally distorted brains of treated patients with glioma (see Section 3.2.2). Moreover, the network-based analysis that related individual behavior to structural connectivity was based on the robust and easy-to-implement machine learning method CPM (see Section 3.2.4). The integrated cross-validation increases the relevance of the results through their generalizability and thus facilitates the possible transfer to clinical applications[120].

3.3.1 Integrity of local structural connectivity

The local fiber density of the white matter was significantly reduced in all four lesion types examined in the patients with glioma. As expected, the reduction in the resection cavity was almost total. The residual fibers can be partly explained by inaccurate segmentation and fiber tracking (see Section 3.2.4). Apart from the resection cavity, the reduction was most pronounced in contrast-enhancing tumor parts, closely followed by the FET-avid tumor regions in PET, and was lowest in FLAIR hyperintense signal alterations. In comparison, Stadlbauer and colleagues previously found that the fiber density of non-enhancing WHO grade II or III gliomas decreased sharply from the periphery to the tumor center[160]. However, the fiber loss in the tumor center was most likely overestimated due to the inappropriate use of a DTI-based fiber density estimation (see Section 3.2). A

significant tumor-induced reduction in fiber density was also found in another study focusing on tumor infiltration of the corticospinal tract in motor-eloquent WHO grade III or IV gliomas, where fiber density was reduced in the peritumoral region as well as in the corticospinal tract itself[161].

Moreover, it seems that the fiber density within the tumor depends on its cell density. As shown in our study, the reduction of fiber density within the metabolically active glioma was inversely related to its FET uptake, which has been found to be correlated with tumor cell density in gliomas in previous studies[162,163]. This relation was further validated by another study that demonstrated an inverse correlation between fiber density and tissue choline levels, which is a measure of membrane turnover and cell density[164]. Thus, tumor cell density, which can be measured non-invasively with FET PET, could be a potential biomarker indicative of tumor aggressiveness with regard to the amount of destruction of the normal fiber architecture.

The analyzed hyperintense FLAIR signal alterations are mainly representative of vasogenic edema caused by tumor-induced disruption of the blood-brain barrier[165,166] or late side effects of radiotherapy within the white matter[167]. The latter include demyelination, axonal degeneration and astrogliosis[156]. Here, we attempted to distinguish between both lesion classes by visual inspection using morphological criteria. The differentiation between edema and radiation-induced gliosis proved to be difficult, so that the classification should be treated with caution. Especially in edematous tissue regions, the tractography pipeline used in this work should provide a much more reliable fiber assessment than the conventional DTI. Edema refers to the presence of extracellular water, which interferes with the determination of the anisotropic diffusion signal of the white matter fiber[135,136] due to the superposition of its isotropic diffusion signal. Therefore, in our tractography pipeline, we used the SS3T-CSD diffusion model, which also takes into account the contamination of each brain voxel by freely diffusing water, as occurs in edema, when calculating fiber orientation[126,137,138]. This allowed us to quantify for the first time the relative fiber loss due to edema, which was approximately 50%. Fiber loss can be explained by the increased interstitial pressure associated with vasogenic edema, which can displace, compress, or disrupt nerve fibers in the affected edematous region[72]. Notably, fiber loss in brain regions affected by radiation damage was similar to that induced by edema. In contrast, previous studies have used only surrogate markers of white matter integrity based on DTI [150,168-172].

3.3.2 Effects of structural connectivity changes on behavioral performance

The impact of structural connectivity changes on patient behavioral performance was first assessed by relating the total fiber loss induced by each of the four lesion types to patients' overall performance as expressed by their ECOG score. Surprisingly, only the contrast-enhancing glioma and FLAIR hyperintense signal alterations were associated with a significantly reduced ECOG score. The different effects of the individual lesion types could be due to their specific characteristics and partly to the cohort of patients studied. The well-planned neurosurgical interventions that relied on neuroanatomical and neurofunctional expertise likely ensured that most patients recovered without long-term neurological deficits, as reflected by their unaffected ECOG score. Furthermore, FET-avid glioma regions and most contrast-enhancing lesions predominantly reflect recurrent tumor growth, whereby the higher sensitivity of amino acid PET compared to MRI probably led to earlier detection of tumor infiltration. Therefore, the corresponding loss in fiber density was not severe enough to affect the patient's overall performance. Due to the constant risk of developing radiation-induced damage or a recurrent tumor, FET PET was performed regularly during the follow-up. This made early detection of asymptomatic, smaller tumors possible, in contrast to initial diagnosis where the tumors may already have progressed to advanced stages. Although the FLAIR hyperintense signal changes showed the least reduction in fiber density, they were the only ones, apart from the contrast-enhanced lesions with a strong reduction, that led to a reduced ECOG score. The recurrent glioma growth in contrast-enhanced lesions was most likely associated with severe disruption of the fiber tracts in certain locations, leading to the reduced ECOG score. The hyperintense FLAIR signal alterations, which were mainly associated with vasogenic edema and/or radiation-induced tissue damage, had a similar impact on the ECOG score, but probably because they tended to affect a large brain volume. In particular, in edema, axons are still present but may become dysfunctional due to compression.

The contrast enhancing lesions and FLAIR hyperintense signal alterations have been found to influence the general performance of patients with glioma at recurrence, at least in terms of ECOG score. However, it remains unclear how the apparent loss of fiber density was related to specific cognitive functions and their corresponding cortical nodes, edges, and networks. Therefore, a CPM-based analysis was used to establish relationships between their structural connectivity and individual cognitive functions. While the effects of brain lesions in eloquent primary cortical areas and their corresponding fiber tracts on neurological function are generally well known[173], the underlying mechanisms of cognitive decline in patients with gliomas have not been

clearly elucidated[174-176]. In this context, initial studies in patients with glioma indicated that the evaluation of brain networks could facilitate a deeper understanding of this decline[177-181]. Therefore, we analyzed the structural connectivity within and between seven networks defined of the Schaefer-Yeo brain atlas[132] that span the entire cerebral cortex, and comprise the visual, somatomotor, dorsal attention, ventral attention, limbic, frontal control, and default mode networks. This approach had the advantage of considering all potential structural connections between cortical nodes, even those outside the anatomically defined pathways. Our results show that reduced fiber count in specific subsets of edges was significantly associated with lower performance in several cognitive domains. This was particularly true for edges between different resting-state networks rather than within individual networks. The corresponding nodes were predominantly located in the left hemisphere, along with the bilateral precuneus or posterior cingulate cortex. Despite the different distribution of identified nodes within the investigated cognitive domains, several of the node sets contained the same nodes, e.g., within the left visual and somatomotor networks as well as bilateral nodes of the dorsal attention network and the default mode network. Critical nodes were defined by a high node degree, which here refers to the number of cross-validated critical edges connected to the node. Among the most critical nodes were the left temporal and the bilateral posterior cingulate cortex of the default mode network.

These results fit seamlessly into the general concept of the structural and functional organization of the human brain, according to which functionally similar nodes are grouped into modules (e.g., resting-state networks) that are globally integrated by certain critical nodes (connectivity between modules). These so-called connector hubs mediate neural information and are characterized by a high node degree. This global integration of modules is associated with perception, cognition and action[7]. Some of the connector hubs are also highly interconnected to further optimize intermodal exchange by regulating the global integration of modules and optimizing cognitive processes[11]. This phenomenon is called rich-club organization and is usually established by long-range structural connections. Rich-club nodes have been identified primarily in functional resting-state networks[26,182] and in the posterior part of the default mode network including the cingulate regions and the precuneus[26,183].

In terms of our results, this means that the edges that were significantly associated with reduced performance in different cognitive domains took part in global integration, as they were connected to different resting-state networks, with several nodes showing a very high degree of adjacent edges. These nodes especially comprised prominent network hubs known to be involved in the rich-club, such as the bilateral precuneus or

the posterior cingulate cortex. In particular, these two regions are also strongly linked to other neurological disorders, such as Alzheimer's disease[184]. This suggests that cognitive decline in patients with treated glioma may be driven by a mechanism similar to other major psychiatric and neurological disorders, where the rich-club nodes have also been found to be predominantly involved[185]. In general, the rich-club nodes are particularly important in psychiatric and neurological disorders and are usually affected by altered functional and structural connectivity[11]. In addition, pathological lesions occur more frequently in rich-club regions than in peripheral nodal regions, suggesting that brain disorders are more strongly associated with damage to central brain regions[11].

3.4 Functional connectivity in patients with glioma

Beyond the tumor- and treatment-related effects on structural connectivity and the resulting consequences for patient behavior, these effects should also be reflected in altered functional connectivity, since functional connectivity is based on the structural organization of the brain via the white matter fiber tracts. In contrast to structural connectivity, functionally connected areas do not necessarily have to be directly connected. Functional connectivity merely indicates whether the activity of two brain areas correlates with each other in time. However, different functional connectivity patterns can arise independent of the invariant structural architecture of the brain. Therefore, functionally correlated brain regions can be more accurately described as having a functional relationship along multiple or all anatomical edges that exist between the two nodes[28,32]. This means that functional connectivity provides a complementary perspective on connectivity changes in treated patients with glioma at recurrence.

Of particular interest in the field of neuro-oncology is the consideration of functional connectivity within glioma infiltrated tumor regions. The key question that arises from a clinical perspective during treatment planning is whether or to what extent the infiltrated tissue is still functional. Therefore, the functional evaluation of the local cortex infiltrated by gliomas has been mainly investigated in the context of preoperative mapping using electrophysiological methods[87,186-189] or magnetoencephalography[87,190]. It has been shown that typical task-evoked patterns of neuronal activity are preserved in glioma-infiltrated cortex. Nevertheless, the tumor affects the integrity of neuronal networks throughout the brain as shown by the observation that patients with gliomas showed changes in resting-state functional connectivity of the entire brain, even extending to the contralateral hemisphere[3,4]. Recently, research has increasingly focused on the effects of connectivity between tumor regions and the healthy brain at different scales. It turns out that the diffuse infiltration of gliomas into normal brain tissue[75] is accompanied by a

close interaction between tumor cells and the local microenvironment[191]. Especially the emerging field of *Cancer Neuroscience* is concerned with the microstructural interaction between neurons and glioma cells[192,193]. Current findings suggest that paracrine signaling and the formation of excitatory glutaminergic synapses between neurons and glioma cells induce and promote glioma growth through neuronal activity[91-93,194]. From a more macroscopic point of view, tumor-infiltrated brain regions also exhibit functional connectivity to resting-state networks. For example, studies in newly diagnosed glioblastomas[5] and patients with primary and recurrent CNS WHO grade 2-4 gliomas[6] revealed that tumor voxels were often functionally associated with resting-state networks[5] or other identified cortical areas[6]. Notably, preserved functional connectivity was even associated with better overall survival in certain subgroups, making the results particularly interesting for clinical application as a diagnostic biomarker[5,6].

Therefore, we hypothesized that functional connectivity between tumor-infiltrated brain regions and resting-state networks is also impaired in pretreated gliomas at recurrence and, furthermore, that preserved functional connectivity is associated with improved overall survival. This was investigated in a subset of 82 treated patients with metabolically active glioma at recurrence diagnosed using a combination of anatomical MRI and FET PET. As one of the most reliable non-invasive imaging modalities for the detection of glioma recurrence[195], FET PET was used to delineate the tumor region of interest. Based on this definition, functional connectivity between metabolically active glioma regions and seven resting-state networks was investigated using rs-fMRI in combination with seed-based correlation analysis. Here we again assessed the seven resting-state networks from the Schaefer-Yeo brain atlas[132] covering the visual, somatomotor, dorsal attention, ventral attention, limbic, frontal control, and default mode network. Finally, the functional connectivity was associated with patients' overall survival. New insights from this approach may contribute to a new prognostic biomarker specifically for treated patients with glioma at recurrence. This is important because, compared to patients with newly diagnosed gliomas, current therapeutic interventions such as resection, radiotherapy, and alkylating chemotherapy may lead to interactions with glioma cells, neurons, and immunogenic/inflammatory cells that further complicate prognosis[129-131].

3.4.1 Functional connectivity between glioma region and brain networks

In the present work, the metabolically active glioma region showed significantly varying degrees of functional connectivity to each of the seven canonical resting-state networks, with the highest connectivity to the four major associative networks dorsal attention, ventral attention, frontoparietal control, and default mode network. Our analysis of fiber

density already suggested that brain connectivity is preserved within the tumor, as residual fiber density was measured in both the contrast-enhanced and metabolically active glioma regions (see Section 3.3.1). Several recent studies using rs-fMRI have also shown that cortical regions infiltrated by gliomas are functionally connected to other cortical areas and networks[5,6,87,188]. For example, Sprugnoli and colleagues showed in 54 patients with newly diagnosed and recurrent CNS WHO grade 2-4 gliomas that there was significant resting-state functional connectivity between the tumors and the unaffected brain[6]. The functional connectivity of recurrent gliomas proved to be different from that of newly diagnosed ones, which underlines the need for a specific biomarker for recurrent patients (see Section 3.4). In the above mentioned work, the distribution of brain voxels functionally connected to recurrent gliomas resembled the dorsal attention network, whereas in newly diagnosed gliomas it resembled the frontoparietal control network[6].

The overall functional connectivity (i.e., the mean of all seven canonical networks) between metabolically active glioma regions and resting-state networks in our work was higher in *IDH*-mutant gliomas than in *IDH*-wildtype gliomas, with oligodendrogliomas showing the highest preserved connectivity. This was also true for each individual network. With regard to tumor type and *IDH* mutational status, the findings indicate that the less aggressively the tumor grows, the higher the residual functional connectivity in recurrent gliomas. It seems likely that this is due to a maintained neuron population preserving the functional local and remote architecture of the infiltrated brain regions. This is also consistent with our findings that the reduction in fiber density in the metabolically active glioma was inversely related to FET uptake (see Section 3.3.1), where FET uptake has been correlated with glioma cell density in previous studies[162,163]. Thus, the increased tumor cell density indicates higher tumor aggressiveness, which reduces local structural connectivity that serves as the basis for functional connectivity. This could be the underlying mechanism for the reduced functional connectivity depending on tumor aggressiveness.

3.4.2 Prognostic value of glioma-whole brain functional connectivity

Recent studies suggest that the connectivity between the glioma region and the rest of the brain may have some prognostic potential[5,6,87]. Most comparable to our work is the study by Daniel and colleagues, who also found that higher intra-network connectivity of the tumor was associated with longer overall survival[5]. However, these results focus only on patients with newly diagnosed glioblastoma and do not relate survival to individual resting-state networks. In contrast, we examined functional connectivity of the metabolically active tumor region in treated patients with recurrent gliomas, including

glioblastoma, astrocytoma, and oligodendroglioma. We observed that high functional connectivity between the recurrent glioma and specific networks, such as the visual, somatomotor, and dorsal attention networks, was associated with overall survival. In particular, functional connectivity to the dorsal attention network for the entire patient cohort and to the visual network for glioblastoma patients proved to be an independent prognostic factor for improved overall survival. This is of particular interest for glioblastoma patients, which is one of the most aggressive and lethal forms of glioma with a median survival time of 14-17 months[53-55] despite aggressive treatment. In terms of clinical application, we have shown that in glioblastoma patients, functional connectivity between the tumor and the visual network can be used to classify patients into better and worse prognosis groups. This may be particularly useful for treatment planning and patients' management. Daniel and colleagues also found reduced or absent functional connectivity in necrotic tumor regions, as opposed to solid, contrast-enhanced tumor parts, leading them to assume that brain tumors with better preserved physiology would also have a better prognosis[5]. This is consistent with our findings that functional connectivity with the rest of the brain was inversely related to WHO tumor grade and was higher in *IDH*-mutant than in *IDH*-wildtype gliomas. Sprugnoli and colleagues also examined functional connectivity between the tumor region and several adjacent brain regions in recurrent and newly diagnosed patients with glioma and the association between functional connectivity and survival[6]. Interestingly, the brain voxels functionally connected to the tumor resembled the dorsal attention network in the recurrent tumors. However, the functional connectivity correlated either positively or negatively with survival in newly diagnosed glioma. This may reflect the different way in which the solid brain tumor was delineated compared to our work. In addition to anatomical MRI, we used amino acid PET with the tracer FET, which allows for more accurate diagnoses and delineation of the solid tumor[196].

Due to actual lack of further research that deals with functional connectivity between tumor region and distinct brain networks it is difficult to find a convincing explanation why the functional connectivity to the dorsal attention and visual network was decisive for the prognosis. Given the current state of knowledge, it is tempting to speculate that the association with improved overall survival is related to specific preserved cognitive functions of these networks and their underlying connectivity. The dorsal attention network is primarily related to the goal-directed, voluntary control of visuospatial attention[197,198] which also depends on the visual network. This cognitive domain is particularly important for executive function. It has been shown that cognitive performance in various domains of executive functioning, but also attention, are of particular importance for the survival of patients with newly diagnosed glioblastoma[199].

Interestingly, in a recent study, functionally active cortical regions infiltrated by a glioma showed significant connectivity with the dorsal attention network during an executive function task[188]. In addition, gliomas may remodel functional neuronal circuits so that task-relevant neuronal responses activate the tumor-infiltrated cortex far beyond the cortical regions normally recruited in the healthy brain[87]. In this way, the preserved functional connectivity with the dorsal attention and visual networks could be partly explained by the ability of the affected brain to recruit tumor-infiltrated distant regions, possibly in an attempt to preserve important cognitive functions that affect survival[87,199].

3.5 Limitations

All three studies included in this thesis have the same limitations in terms of the patient cohort studied. We focused on treated patients with recurrent glioma, but repeated, regular radiological follow-up data was only available for a few patients. Due to the lack of longitudinal follow-up, the intensity of treatment as well as the time between treatment initiation and imaging along with the timing of neurocognitive assessment (on the day of imaging) varied widely between them. Nevertheless, it seems plausible that a representative cross-section of treated patients, who collectively display a wide range of structural damage patterns, may have contributed to the development of robust CPM prediction models for cognitive performance.

Furthermore, despite all efforts, boundaries of the individual segmented brain lesions were still difficult to determine, as they usually occurred simultaneously and even overlapped in contrast-enhanced and FET-avid glioma regions. However, in a sub-analysis of non-superimposed contrast-enhanced (n=24) and FET-avid gliomas (n=9), the fiber density obtained was within the range of the entire cohort. In addition, hyperintense FLAIR signal alterations may be a surrogate of tumor infiltration without contrast enhancement. Overall, the fiber densities observed in the four lesion areas appear to correctly reflect the intensity of the pathologic and therapeutic effects, as they differed significantly from each other and also fell within the expected intensity ranges. This indicates that the above limitations only apply to a minor extent and that the tractography framework used provides reliable results. However, it is striking that the resection cavity exhibited a minimal but obviously incorrect residual fiber density. As already discussed, (see Section 3.2.4), this can be partly explained by the difficulty in achieving precise segmentation of the resection cavity boundaries. In general, it should be noted that even the well adapted tractography framework for patients with gliomas used here, which is based on state-of-the-art techniques, is in the end only able to approximate the actual fiber architecture as closely as possible, without being completely

free of false positive fibers. In addition, the subclassification of hyperintense FLAIR signal alterations into edema and radiation-induced gliosis proved to be highly challenging and should be considered with appropriate caution (see Section 3.3.1). In the end, a considerable fraction of patients remained unclassified, nevertheless it was shown that there was no significant difference between the lesion types in their effect on fiber density.

Another aspect to consider is that shifts and deformations of cortical areas cannot be excluded in brains affected by pathology and treatment. Neither are the effects of neuroplasticity, which can take various forms, ranging from functional changes in existing structures to the formation and proliferation of new structures[35,36]. Of course, such changes cannot be taken into account in an atlas-based parcellation that originates from healthy subjects, as in the Schaefer-Yeo brain atlas[132] used here. However, this seems to play only a minor role in the patients we studied, as the results of the second study fit seamlessly into the general concept of the structural and functional organization of the human brain and also reflect features known in other neurological disorders.

The determination of functional connectivity between the glioma region and the rest of the brain was based on resting-state fMRI, which has the great advantage that it can also be used in patients who are unable to perform a task, e.g., patients with neurological deficits. Unfortunately, this does not identify the actual source of the measured connectivity. On the one hand, it is possible that functionally intact brain tissue was preserved within the tumor region[186,188,190], maybe to the diffuse infiltration of gliomas. On the other hand, the measured functional connectivity may also originate from the tumor itself. There is clear evidence that high-grade gliomas integrate into neuronal networks through bidirectional interactions[87]. In this way, gliomas promote tumor proliferation through neuron-glioma synapses and paracrine signiling[89-92], increase neuronal excitability[200-203] and even remodel functional neuronal circuits[87]. Contrary to our and other findings[5,204,205], Krishna and colleagues showed that an overall high functional connectivity as measured by MEG between glioblastomas and the rest of the brain shortens overall survival[87]. They assumed that reduced survival is driven by the connectivity of the tumor, which seems plausible since neuronal activity of the tumor promotes tumor proliferation. In the present analysis, however, it is possible that we measured both, the connectivity of functionally intact brain tissue and the connectivity of the glioma itself, whereby the connectivity of the remaining brain tissue to brain regions important for survival (see Section 3.4.2) predominates. This assumption is further supported by the fact that the diagnosis of recurrent glioma was based on amino acid PET using the tracer FET, in addition to anatomical MRI. It is likely the enhanced

sensitivity of amino acid PET in comparison to MRI have facilitated an earlier detection of glioma infiltration. As a result, the tissue damage caused by glioma growth may be less pronounced, while the functionality of the infiltrated brain tissue remains intact. Similar effects were already observed in our first study, where the associated loss of fiber density was less pronounced in the FET-avid gliomas region then in the contrast-enhanced lesion and did not affect overall performance (see Section 3.3.2). This suggests that functionally active tissue was largely preserved in our cohort and was the main source of connectivity that influenced overall survival.

4 Conclusion and Outlook

The present work constitutes a substantial contribution to a broader comprehension of tumor- and treatment-induced alterations in brain connectivity and their resulting impact on cognitive function and survival in patients with recurrent glioma. Our findings on the structural and functional organization of patients with glioma may promote the improvement of treatment efficiency in the future, especially with regard to the planning of local therapies such as surgery and radiotherapy.

In particular, it should be noted that FLAIR hyperintense signal alterations, which are mainly associated with vasogenic edema and/or treatment-induced tissue damage, have a similar impact on the overall performance (ECOG) of patients as contrast-enhanced lesions, which are mainly associated with glioma. In this regard, FLAIR hyperintense signal alterations showed the least reduction in fiber density, and it appears that radiation-induced damage was of the same magnitude as that caused by edema. In addition, fiber density was inversely related to glioma cell density, which can be measured non-invasively by FET PET uptake and may be a potential biomarker that provides an initial indication of tumor aggressiveness.

To further elucidate the impact of structural changes on the underlying cognitive functions, we have gathered a growing body of evidence suggesting that the outcome of higher-order cognitive function in patients with glioma depends on the preserved integrity of multiple distributed networks. These results perfectly complement and consolidate the current state of research in this area[124,127,128]. Moreover, they are clinically translatable. Despite clinical assessment or standard neuro-navigation, cognitive deficits still occur following treatment. These could be reduced or even eliminated if the definition of critical nodes presented here would be taken into account. Therefore, the long-term focus should no longer be on protecting single vulnerable structures, such as the motor and language pathways in neurosurgery or the hippocampus during radiotherapy, but rather on preserving the integrity of multiple interconnected brain networks, including known network hubs. Thus, our results suggest that efforts should be made to preserve edges between resting-state networks with corresponding nodes located primarily in the left hemisphere, as these are particularly important for maintaining cognitive function. Most affected nodes were concentrated in the left visual and somatomotor network and included bilateral nodes of the dorsal attention network and the default mode network. Especially the left temporal and bilateral posterior cingulate cortices of the default mode network are considered highly valuable for preservation.

In this context, it would be conceivable to further develop the machine-learning approaches like the CPM model of the present study in order to use it in the future for the prediction of cognitive decline in individual patients with glioma, in particular for the planning of local therapies. However, this only yields meaningful in conjunction with advanced tractography methods. It is time to move beyond the outdated DTI-based tractography techniques. Their inability to resolve complex fiber architectures[104] leads to anatomically implausible or erroneously missing tracts[103,104], which threaten survival[125] and may cause irreparable neurological deficits[126]. Consequently, advanced tractography techniques will be essential in the coming years and we have already demonstrated state-of-the-art tractography methods based on an advanced diffusion model with CSD[105,106] that would be easy to implement in clinical practice[106]. Given the high potential to improve local treatment planning in patients with glioma, further exploration of modern whole-brain tractography that goes beyond DTI in conjunction with the definition of critical cortical nodes is strongly recommended.

Our results on functional connectivity, including those of other present studies[5,6,87,188], suggest that gliomas generally exhibit varying degrees of functional connectivity with all canonical networks in a substantial portion of the cortical tissue infiltrated by the tumor, regardless of disease and treatment outcome. As a result, the inclusion of functional connectivity promises to add significant value to future clinical diagnosis and may open the door to a variety of therapeutic strategies aimed at improving cognitive outcomes and survival. Our findings indicate that functional connectivity between recurrent gliomas and diverse networks may serve as an additional prognostic factor for improved overall survival. This has the potential to provide a novel imaging-based prognostic biomarker for patients with recurrent gliomas. Especially glioblastomas can be classified into groups with better and worse prognosis based on their connectivity to the visual network. This is a very sensitive group of patients who have the lowest survival rates in tumor diseases, so treatment planning and patients' management could be better adapted accordingly.

In conclusion, the present work demonstrates the particular need to go beyond outdated DTI methods to improve brain tumor treatment. To maintain the overall performance of patients with gliomas and reduce cognitive decline, treatment planning must adopt a more network-based approach to preserve eloquent structures. In this context, the influence of edema and gliosis is a factor that should not be overlooked. Finally, the functional connectivity between the glioma region and the surrounding brain holds great clinical potential for prognostication.

References

1. Guye M, Bartolomei F, Ranjeva J-P. Imaging structural and functional connectivity: towards a unified definition of human brain organization? *Current Opinion in Neurology.* 2008; 21(4):393-403.

2. Friedrich M, Farrher E, Caspers S, et al. Alterations in white matter fiber density associated with structural MRI and metabolic PET lesions following multimodal therapy in glioma patients. *Frontiers in Oncology.* 2022; 12.

3. Ghinda DC, Wu J-S, Duncan NW, Northoff G. How much is enough—Can resting state fMRI provide a demarcation for neurosurgical resection in glioma? *Neuroscience & Biobehavioral Reviews.* 2018; 84:245-261.

4. Stoecklein VM, Stoecklein S, Galiè F, et al. Resting-state fMRI detects alterations in whole brain connectivity related to tumor biology in glioma patients. *Neuro-Oncology.* 2020; 22(9):1388-1398.

5. Daniel AGS, Park KY, Roland JL, et al. Functional connectivity within glioblastoma impacts overall survival. *Neuro-Oncology.* 2020; 23(3):412-421.

6. Sprugnoli G, Rigolo L, Faria M, et al. Tumor BOLD connectivity profile correlates with glioma patients' survival. *Neuro-Oncology Advances.* 2022; 4(1).

7. Park H-J, Friston K. Structural and Functional Brain Networks: From Connections to Cognition. *Science.* 2013; 342(6158):1238411.

8. Sporns O. Graph theory methods: applications in brain networks. *Dialogues in Clinical Neuroscience.* 2018; 20(2):111-121.

9. Sporns O, Betzel RF. Modular Brain Networks. *Annual Review of Psychology.* 2016; 67(Volume 67, 2016):613-640.

10. Sporns O, Zwi JD. The small world of the cerebral cortex. *Neuroinformatics.* 2004; 2(2):145-162.

11. Kim D-J, Min B-K. Rich-club in the brain’s macrostructure: Insights from graph theoretical analysis. *Computational and Structural Biotechnology Journal.* 2020; 18:1761-1773.

12. Sporns O. Network attributes for segregation and integration in the human brain. *Current Opinion in Neurobiology.* 2013; 23(2):162-171.

13. Sporns O. Contributions and challenges for network models in cognitive neuroscience. *Nature Neuroscience.* 2014; 17(5):652-660.

14. Kocher M, Gleichgerrcht E, Nesland T, et al. Individual variability in the anatomical distribution of nodes participating in rich club structural networks. *Frontiers in Neural Circuits.* 2015; 9(APR).

15. Buckner RL, Krienen FM, Yeo BTT. Opportunities and limitations of intrinsic functional connectivity MRI. *Nature Neuroscience.* 2013; 16(7):832-837.

16. Laird AR, Eickhoff SB, Rottschy C, Bzdok D, Ray KL, Fox PT. Networks of task co-activations. *NeuroImage.* 2013; 80:505-514.

17. Smith SM, Fox PT, Miller KL, et al. Correspondence of the brain's functional architecture during activation and rest. *Proceedings of the National Academy of Sciences.* 2009; 106(31):13040-13045.

18. Greicius MD, Supekar K, Menon V, Dougherty RF. Resting-State Functional Connectivity Reflects Structural Connectivity in the Default Mode Network. *Cerebral Cortex.* 2008; 19(1):72-78.

19. Hermundstad AM, Bassett DS, Brown KS, et al. Structural foundations of resting-state and task-based functional connectivity in the human brain. *Proceedings of the National Academy of Sciences.* 2013; 110(15):6169-6174.

20. van den Heuvel MP, Mandl RCW, Kahn RS, Hulshoff Pol HE. Functionally linked resting-state networks reflect the underlying structural connectivity architecture of the human brain. *Human Brain Mapping.* 2009; 30(10):3127-3141.

21. Honey CJ, Sporns O, Cammoun L, et al. Predicting human resting-state functional connectivity from structural connectivity. *Proceedings of the National Academy of Sciences.* 2009; 106(6):2035-2040.

22. Meunier D, Lambiotte R, Fornito A, Ersche K, Bullmore ET. Hierarchical modularity in human brain functional networks. *Frontiers in Neuroinformatics.* 2009; 3.

23. Allen EA, Damaraju E, Plis SM, Erhardt EB, Eichele T, Calhoun VD. Tracking Whole-Brain Connectivity Dynamics in the Resting State. *Cerebral Cortex.* 2012; 24(3):663-676.

24. Park B, Kim JI, Lee D, Jeong S-O, Lee JD, Park H-J. Are brain networks stable during a 24-hour period? *NeuroImage.* 2012; 59(1):456-466.

25. van den Heuvel MP, Sporns O. Rich-Club Organization of the Human Connectome. *The Journal of Neuroscience.* 2011; 31(44):15775-15786.

26. van den Heuvel MP, Sporns O. An Anatomical Substrate for Integration among Functional Networks in Human Cortex. *The Journal of Neuroscience.* 2013; 33(36):14489-14500.

27. Crossley NA, Mechelli A, Vértes PE, et al. Cognitive relevance of the community structure of the human brain functional coactivation network. *Proceedings of the National Academy of Sciences.* 2013; 110(28):11583-11588.

28. Petersen Steven E, Sporns O. Brain Networks and Cognitive Architectures. *Neuron.* 2015; 88(1):207-219.

29. Hutchison RM, Womelsdorf T, Allen EA, et al. Dynamic functional connectivity: Promise, issues, and interpretations. *NeuroImage.* 2013; 80:360-378.

30. Buckner RL, Krienen FM, Castellanos A, Diaz JC, Yeo BTT. The organization of the human cerebellum estimated by intrinsic functional connectivity. *Journal of Neurophysiology.* 2011; 106(5):2322-2345.

31. Fotiadis P, Parkes L, Davis KA, Satterthwaite TD, Shinohara RT, Bassett DS. Structure–function coupling in macroscale human brain networks. *Nature Reviews Neuroscience.* 2024; 25(10):688-704.

32. Power Jonathan D, Schlaggar Bradley L, Petersen Steven E. Studying Brain Organization via Spontaneous fMRI Signal. *Neuron.* 2014; 84(4):681-696.

33. Lewis CM, Baldassarre A, Committeri G, Romani GL, Corbetta M. Learning sculpts the spontaneous activity of the resting human brain. *Proceedings of the National Academy of Sciences.* 2009; 106(41):17558-17563.

34. Mackey AP, Hill SS, Stone SI, Bunge SA. Differential effects of reasoning and speed training in children. *Developmental Science.* 2011; 14(3):582-590.

35. Lubrini G, Martín-Montes A, Díez-Ascaso O, Díez-Tejedor E. Brain disease, connectivity, plasticity and cognitive therapy: A neurological view of mental disorders. *Neurología (English Edition).*

36. Hrvoj-Mihic B, Bienvenu T, Stefanacci L, Muotri AR, Semendeferi K. Evolution, development, and plasticity of the human brain: From molecules to bones. *Frontiers in Human Neuroscience.* 2013(OCT).

37. Watts DJ, Strogatz SH. Collective dynamics of 'small-world9 networks. *Nature.* 1998; 393(6684):440-442.

38. Schoonheim MM, Meijer KA, Geurts JJG. Network Collapse and Cognitive Impairment in Multiple Sclerosis. *Frontiers in Neurology.* 2015; 6.

39. Bonavita S, Gallo A, Sacco R, et al. Distributed changes in default-mode resting-state connectivity in multiple sclerosis. *Multiple Sclerosis Journal.* 2011; 17(4):411-422.

40. Cruz-Gómez ÁJ, Ventura-Campos N, Belenguer A, Ávila C, Forn C. The link between resting-state functional connectivity and cognition in MS patients. *Multiple Sclerosis Journal.* 2014; 20(3):338-348.

41. Hong YJ, Yoon B, Lim S-C, et al. Microstructural changes in the hippocampus and posterior cingulate in mild cognitive impairment and Alzheimer's disease: a diffusion tensor imaging study. *Neurological Sciences.* 2013; 34(7):1215-1221.

42. Chang YT, Huang CW, Chang YH, et al. Amyloid burden in the hippocampus and default mode network: Relationships with gray matter volume and cognitive performance in mild stage Alzheimer disease. *Medicine (United States).* 2015; 94(16).

43. Iorgulescu JB, Sun C, Neff C, et al. Molecular biomarker-defined brain tumors: Epidemiology, validity, and completeness in the United States. *Neuro-Oncology.* 2022; 24(11):1989-2000.

44. van den Bent MJ, Geurts M, French PJ, et al. Primary brain tumours in adults. *The Lancet.* 2023; 402(10412):1564-1579.

45. Lapointe S, Perry A, Butowski NA. Primary brain tumours in adults. *The Lancet.* 2018; 392(10145):432-446.

46. Braganza MZ, Kitahara CM, Berrington de González A, Inskip PD, Johnson KJ, Rajaraman P. Ionizing radiation and the risk of brain and central nervous system tumors: a systematic review. *Neuro-Oncology.* 2012; 14(11):1316-1324.

47. Wen PY, Schiff D, Quant E, Lee EQ. *Neurologic complications of cancer therapy*: Demos Medical Publishing; 2011.

48. Wrensch M, Minn Y, Chew T, Bondy M, Berger MS. Epidemiology of primary brain tumors: Current concepts and review of the literature. *Neuro-Oncology.* 2002; 4(4):278-299.

49. Schüz J, Pirie K, Reeves GK, Floud S, Beral V, Collaborators ftMWS. Cellular Telephone Use and the Risk of Brain Tumors: Update of the UK Million Women Study. *JNCI: Journal of the National Cancer Institute.* 2022; 114(5):704-711.

50. Melin BS, Barnholtz-Sloan JS, Wrensch MR, et al. Genome-wide association study of glioma subtypes identifies specific differences in genetic susceptibility to glioblastoma and non-glioblastoma tumors. *Nature Genetics.* 2017; 49(5):789-794.

51. Ijzerman-Korevaar M, Snijders TJ, de Graeff A, Teunissen SCCM, de Vos FYF. Prevalence of symptoms in glioma patients throughout the disease trajectory: a systematic review. *Journal of Neuro-Oncology.* 2018; 140(3):485-496.

52. Ostrom QT, Cioffi G, Waite K, Kruchko C, Barnholtz-Sloan JS. CBTRUS Statistical Report: Primary Brain and Other Central Nervous System Tumors Diagnosed in the United States in 2014–2018. *Neuro-Oncology.* 2021; 23(Supplement_3):iii1-iii105.

53. Lassman AB, Pugh SL, Wang TJC, et al. Depatuxizumab mafodotin in EGFR-amplified newly diagnosed glioblastoma: A phase III randomized clinical trial. *Neuro-Oncology.* 2022; 25(2):339-350.

54. Gilbert MR, Wang M, Aldape KD, et al. Dose-Dense Temozolomide for Newly Diagnosed Glioblastoma: A Randomized Phase III Clinical Trial. *Journal of Clinical Oncology.* 2013; 31(32):4085-4091.

55. Stupp R, Mason WP, Van Den Bent MJ, et al. Radiotherapy plus concomitant and adjuvant temozolomide for glioblastoma. *New England journal of medicine.* 2005; 352(10):987-996.

56. Dang L, White DW, Gross S, et al. Cancer-associated IDH1 mutations produce 2-hydroxyglutarate. *Nature.* 2009; 462(7274):739-744.

57. Engelhard HH, Stelea A, Mundt A. Oligodendroglioma and anaplastic oligodendroglioma:: Clinical features, treatment, and prognosis. *Surgical Neurology.* 2003; 60(5):443-456.

58. Network CGAR. Comprehensive, integrative genomic analysis of diffuse lower-grade gliomas. *New England Journal of Medicine.* 2015; 372(26):2481-2498.

59. Smits M. MRI biomarkers in neuro-oncology. *Nature Reviews Neurology.* 2021; 17(8):486-500.

60. Galldiks N, Lohmann P, Friedrich M, et al. PET imaging of gliomas: Status quo and quo vadis? *Neuro-Oncology.* 2024.

61. Hamacher K, Coenen HH. Efficient routine production of the 18F-labelled amino acid O-(2-[18F]fluoroethyl)-l-tyrosine. *Applied Radiation and Isotopes.* 2002; 57(6):853-856.

62. Stegmayr C, Stoffels G, Filß C, et al. Current trends in the use of O-(2-[18F]fluoroethyl)-L-tyrosine ([18F]FET) in neurooncology. *Nuclear Medicine and Biology.* 2021; 92:78-84.

63. Heinzel A, Dedic D, Galldiks N, et al. Two Decades of Brain Tumour Imaging with O-(2-[18F]fluoroethyl)-L-tyrosine PET: The Forschungszentrum Jülich Experience. *Cancers.* 2022; 14(14):3336.

64. Galldiks N, Wollring M, Werner J-M, et al. An updated review on the diagnosis and assessment of post-treatment relapse in brain metastases using PET. *Expert Review of Neurotherapeutics.* 2022; 22(11-12):915-921.

65. Hutterer M, Nowosielski M, Putzer D, et al. [18F]-fluoro-ethyl-l-tyrosine PET: a valuable diagnostic tool in neuro-oncology, but not all that glitters is glioma. *Neuro-Oncology.* 2013; 15(3):341-351.

66. Dunet V, Rossier C, Buck A, Stupp R, Prior JO. Performance of ¹⁸F-Fluoro-Ethyl-Tyrosine (¹⁸F-FET) PET for the Differential Diagnosis of Primary Brain Tumor: A Systematic Review and Metaanalysis. *Journal of Nuclear Medicine.* 2012; 53(2):207-214.

67. Louis DN, Perry A, Wesseling P, et al. The 2021 WHO Classification of Tumors of the Central Nervous System: a summary. *Neuro-Oncology.* 2021; 23(8):1231-1251.

68. Nafe R, Porto L, Samp P-F, You S-J, Hattingen E. Adult-type and Pediatric-type Diffuse Gliomas. *Clinical Neuroradiology.* 2023; 33(3):611-624.

69. Coburger J, Wirtz CR. Fluorescence guided surgery by 5-ALA and intraoperative MRI in high grade glioma: a systematic review. *Journal of Neuro-Oncology.* 2019; 141(3):533-546.

70. Eyüpoglu IY, Buchfelder M, Savaskan NE. Surgical resection of malignant gliomas—role in optimizing patient outcome. *Nature Reviews Neurology.* 2013; 9(3):141-151.

71. Flies CM, Friedrich M, Lohmann P, et al. Treatment-associated imaging changes in newly diagnosed MGMT promoter-methylated glioblastoma undergoing chemoradiation with or without cilengitide. *Neuro-Oncology.* 2024; 26(5):902-910.

72. Jellison BJ, Field AS, Medow J, Lazar M, Salamat MS, Alexander AL. Diffusion Tensor Imaging of Cerebral White Matter: A Pictorial Review of Physics, Fiber Tract Anatomy, and Tumor Imaging Patterns. *American Journal of Neuroradiology.* 2004; 25(3):356-369.

73. Itagiba VGA, Borges R, Cruz Jr LCHd, Furtado AD, Domingues RC, Gasparetto EL. Uso do tensor de difusão na avaliação dos padrões de acometimento da substância branca em pacientes com tumores cerebrais: é uma ferramenta útil para o diagnóstico diferencial? *Radiologia Brasileira.* 2010; 43.

74. Salvalaggio A, Pini L, Bertoldo A, Corbetta M. Glioblastoma and brain connectivity: the need for a paradigm shift. *The Lancet Neurology.* 2024; 23(7):740-748.

75. Cuddapah VA, Robel S, Watkins S, Sontheimer H. A neurocentric perspective on glioma invasion. *Nature Reviews Neuroscience.* 2014; 15(7):455-465.

76. Ferrer VP, Moura Neto V, Mentlein R. Glioma infiltration and extracellular matrix: key players and modulators. *Glia.* 2018; 66(8):1542-1565.

77. Huang-Hobbs E, Cheng Y-T, Ko Y, et al. Remote neuronal activity drives glioma progression through SEMA4F. *Nature.* 2023; 619(7971):844-850.

78. Wei Y, Li C, Cui Z, et al. Structural connectome quantifies tumour invasion and predicts survival in glioblastoma patients. *Brain.* 2022; 146(4):1714-1727.

79. Yuan B, Zhang N, Yan J, Cheng J, Lu J, Wu J. Tumor grade-related language and control network reorganization in patients with left cerebral glioma. *Cortex.* 2020; 129:141-157.

80. Jütten K, Mainz V, Delev D, et al. Asymmetric tumor-related alterations of network-specific intrinsic functional connectivity in glioma patients. *Human Brain Mapping.* 2020; 41(16):4549-4561.

81. Silvestri E, Moretto M, Facchini S, et al. Widespread cortical functional disconnection in gliomas: an individual network mapping approach. *Brain Communications.* 2022; 4(2).

82. De Baene W, Rutten G-JM, Sitskoorn MM. Cognitive functioning in glioma patients is related to functional connectivity measures of the non-tumoural hemisphere. *European Journal of Neuroscience.* 2019; 50(12):3921-3933.

83. Park KY, Snyder AZ, Olufawo M, et al. Glioblastoma induces whole-brain spectral change in resting state fMRI: Associations with clinical comorbidities and overall survival. *NeuroImage: Clinical.* 2023; 39:103476.

84. Hart MG, Romero-Garcia R, Price SJ, Suckling J. Global Effects of Focal Brain Tumors on Functional Complexity and Network Robustness: A Prospective Cohort Study. *Neurosurgery.* 2019; 84(6):1201-1213.

85. Daniel AGS, Park KY, Roland JL, et al. Functional connectivity within glioblastoma impacts overall survival. *Neuro Oncol.* 2021; 23(3):412-421.

86. Heinzel A, Mottaghy FM, Filss C, et al. The impact of brain lesions on health-related quality of life in patients with WHO CNS grade 3 or 4 glioma: a lesion-function and resting-state fMRI analysis. *Journal of Neuro-Oncology.* 2023; 161(3):643-654.

87. Krishna S, Choudhury A, Keough MB, et al. Glioblastoma remodelling of human neural circuits decreases survival. *Nature.* 2023; 617(7961):599-607.

88. Jung E, Alfonso J, Osswald M, Monyer H, Wick W, Winkler F. Emerging intersections between neuroscience and glioma biology. *Nature Neuroscience.* 2019; 22(12):1951-1960.

89. Venkatesh HS. The neural regulation of cancer. *Science.* 2019; 366(6468):965-965.

90. Taylor KR, Barron T, Hui A, et al. Glioma synapses recruit mechanisms of adaptive plasticity. *Nature.* 2023; 623(7986):366-374.

91. Venkataramani V, Tanev DI, Strahle C, et al. Glutamatergic synaptic input to glioma cells drives brain tumour progression. *Nature.* 2019; 573(7775):532-538.

92. Venkatesh HS, Morishita W, Geraghty AC, et al. Electrical and synaptic integration of glioma into neural circuits. *Nature.* 2019; 573(7775):539-545.

93. Mandal AS, Romero-Garcia R, Hart MG, Suckling J. Genetic, cellular, and connectomic characterization of the brain regions commonly plagued by glioma. *Brain.* 2020; 143(11):3294-3307.

94. Romero-Garcia R, Mandal AS, Bethlehem RAI, Crespo-Facorro B, Hart MG, Suckling J. Transcriptomic and connectomic correlates of differential spatial patterning among gliomas. *Brain.* 2022; 146(3):1200-1211.

95. Mandal AS, Romero-Garcia R, Seidlitz J, Hart MG, Alexander-Bloch AF, Suckling J. Lesion covariance networks reveal proposed origins and pathways of diffuse gliomas. *Brain Communications.* 2021; 3(4).

96. Sansone G, Pini L, Salvalaggio A, et al. Patterns of gray and white matter functional networks involvement in glioblastoma patients: indirect mapping from clinical MRI scans. *Frontiers in Neurology.* 2023; 14.

97. Mukherjee P, Berman JI, Chung SW, Hess CP, Henry RG. Diffusion Tensor MR Imaging and Fiber Tractography: Theoretic Underpinnings. *American Journal of Neuroradiology.* 2008; 29(4):632-641.

98. Lin C-P, Wedeen VJ, Chen J-H, Yao C, Tseng W-YI. Validation of diffusion spectrum magnetic resonance imaging with manganese-enhanced rat optic tracts and ex vivo phantoms. *NeuroImage.* 2003; 19(3):482-495.

99. Basser PJ. Inferring microstructural features and the physiological state of tissues from diffusion-weighted images. *NMR in Biomedicine.* 1995; 8(7):333-344.

100. Tuch DS. Q-ball imaging. *Magnetic Resonance in Medicine.* 2004; 52(6):1358-1372.

101. Tournier JD, Calamante F, Connelly A. Improved probabilistic streamlines tractography by 2nd order integration over fibre orientation distributions. Paper presented at: Proceedings of the international society for magnetic resonance in medicine2010.

102. BASSER PJ. New Histological and Physiological Stains Derived from Diffusion-Tensor MR Images. *Annals of the New York Academy of Sciences.* 1997; 820(1):123-138.

103. Farquharson S, Tournier J-D, Calamante F, et al. White matter fiber tractography: why we need to move beyond DTI: Clinical article. *Journal of Neurosurgery JNS.* 2013; 118(6):1367-1377.

104. Jeurissen B, Leemans A, Tournier J-D, Jones DK, Sijbers J. Investigating the prevalence of complex fiber configurations in white matter tissue with diffusion magnetic resonance imaging. *Human Brain Mapping.* 2013; 34(11):2747-2766.

105. Tournier JD, Calamante F, Gadian DG, Connelly A. Direct estimation of the fiber orientation density function from diffusion-weighted MRI data using spherical deconvolution. *NeuroImage.* 2004; 23(3):1176-1185.

106. Tournier JD, Calamante F, Connelly A. Robust determination of the fibre orientation distribution in diffusion MRI: Non-negativity constrained super-resolved spherical deconvolution. *NeuroImage.* 2007; 35(4):1459-1472.

107. Healy DM, Hendriks H, Kim PT. Spherical Deconvolution. *Journal of Multivariate Analysis.* 1998; 67(1):1-22.

108. Hansen PC. REGULARIZATION TOOLS: A Matlab package for analysis and solution of discrete ill-posed problems. *Numerical Algorithms.* 1994; 6(1):1-35.

109. Wedeen VJ, Wang RP, Schmahmann JD, et al. Diffusion spectrum magnetic resonance imaging (DSI) tractography of crossing fibers. *NeuroImage.* 2008; 41(4):1267-1277.

110. Assaf Y, Freidlin RZ, Rohde GK, Basser PJ. New modeling and experimental framework to characterize hindered and restricted water diffusion in brain white matter. *Magnetic Resonance in Medicine.* 2004; 52(5):965-978.

111. Zhan W, Yang Y. How accurately can the diffusion profiles indicate multiple fiber orientations? A study on general fiber crossings in diffusion MRI. *Journal of Magnetic Resonance.* 2006; 183(2):193-202.

112. Behrens TEJ, Berg HJ, Jbabdi S, Rushworth MFS, Woolrich MW. Probabilistic diffusion tractography with multiple fibre orientations: What can we gain? *NeuroImage.* 2007; 34(1):144-155.

113. Hosey T, Williams G, Ansorge R. Inference of multiple fiber orientations in high angular resolution diffusion imaging. *Magnetic Resonance in Medicine.* 2005; 54(6):1480-1489.

114. Tuch DS, Reese TG, Wiegell MR, Makris N, Belliveau JW, Wedeen VJ. High angular resolution diffusion imaging reveals intravoxel white matter fiber heterogeneity. *Magnetic Resonance in Medicine.* 2002; 48(4):577-582.

115. Tournier J-D, Mori S, Leemans A. Diffusion tensor imaging and beyond. *Magnetic Resonance in Medicine.* 2011; 65(6):1532-1556.

116. Smith RE, Tournier J-D, Calamante F, Connelly A. Anatomically-constrained tractography: Improved diffusion MRI streamlines tractography through effective use of anatomical information. *NeuroImage.* 2012; 62(3):1924-1938.

117. Rubinov M, Sporns O. Complex network measures of brain connectivity: Uses and interpretations. *NeuroImage.* 2010; 52(3):1059-1069.

118. Calamante F, Tournier J-D, Jackson GD, Connelly A. Track-density imaging (TDI): Super-resolution white matter imaging using whole-brain track-density mapping. *NeuroImage.* 2010; 53(4):1233-1243.

119. Calamante F, Tournier J-D, Heidemann RM, Anwander A, Jackson GD, Connelly A. Track density imaging (TDI): Validation of super resolution property. *NeuroImage.* 2011; 56(3):1259-1266.

120. Shen X, Finn ES, Scheinost D, et al. Using connectome-based predictive modeling to predict individual behavior from brain connectivity. *Nature Protocols.* 2017; 12(3):506-518.

121. Volz LJ, Kocher M, Lohmann P, Shah NJ, Fink GR, Galldiks N. Functional magnetic resonance imaging in glioma patients: from clinical applications to future perspectives. *Q J Nucl Med Mol Imaging.* 2018; 62(3):295-302.

122. Bijsterbosch J, Smith SM, Beckmann C. *An introduction to resting state fMRI functional connectivity*: Oxford University Press; 2017.

123. Nimsky C, Bauer M, Carl B. Merits and Limits of Tractography Techniques for the Uninitiated. In: Schramm J, ed. *Advances and Technical Standards in Neurosurgery: Volume 43*. Cham: Springer International Publishing; 2016:37-60.

124. Essayed WI, Zhang F, Unadkat P, Cosgrove GR, Golby AJ, O'Donnell LJ. White matter tractography for neurosurgical planning: A topography-based review of the current state of the art. *NeuroImage: Clinical.* 2017; 15:659-672.

125. KRAMM CM, WAGNER S, VAN GOOL S, et al. Improved Survival after Gross Total Resection of Malignant Gliomas in Pediatric Patients from the HIT-GBM Studies. *Anticancer Research.* 2006; 26(5B):3773-3779.

126. Aerts H, Dhollander T, Marinazzo D. Evaluating the performance of 3-tissue constrained spherical deconvolution pipelines for within-tumor tractography. *bioRxiv.* 2019:629873.

127. Andrews-Hanna JR, Snyder AZ, Vincent JL, et al. Disruption of Large-Scale Brain Systems in Advanced Aging. *Neuron.* 2007; 56(5):924-935.

128. Broyd SJ, Demanuele C, Debener S, Helps SK, James CJ, Sonuga-Barke EJS. Default-mode brain dysfunction in mental disorders: A systematic review. *Neuroscience & Biobehavioral Reviews.* 2009; 33(3):279-296.

129. Park JK, Hodges T, Arko L, et al. Scale to Predict Survival After Surgery for Recurrent Glioblastoma Multiforme. *Journal of Clinical Oncology.* 2010; 28(24):3838-3843.

130. Pineda E, Domenech M, Hernández A, Comas S, Balaña C. Recurrent Glioblastoma: Ongoing Clinical Challenges and Future Prospects. *Onco Targets Ther.* 2023; 16:71-86.

131. Vaz-Salgado MA, Villamayor M, Albarrán V, et al. Recurrent Glioblastoma: A Review of the Treatment Options. *Cancers.* 2023; 15(17):4279.

132. Schaefer A, Kong R, Gordon EM, et al. Local-Global Parcellation of the Human Cerebral Cortex from Intrinsic Functional Connectivity MRI. *Cerebral Cortex.* 2017; 28(9):3095-3114.

133. Friedrich M, Filss CP, Lohmann P, et al. Structural connectome-based predictive modeling of cognitive deficits in treated glioma patients. *Neuro-Oncology Advances.* 2023; 6(1).

134. Friedrich M, Werner J-M, Steinbach JP, et al. Functional connectivity between tumor region and resting-state networks as imaging biomarker for overall survival in recurrent gliomas diagnosed by FET PET. *Neuro-Oncology Advances.* 2025.

135. Farrher E, Grinberg F, Kuo L-W, et al. Dedicated diffusion phantoms for the investigation of free water elimination and mapping: insights into the influence of T2 relaxation properties. *NMR in Biomedicine.* 2020; 33(4):e4210.

136. Pasternak O, Sochen N, Gur Y, Intrator N, Assaf Y. Free water elimination and mapping from diffusion MRI. *Magnetic Resonance in Medicine.* 2009; 62(3):717-730.

137. Dhollander T, Connelly A. *A novel iterative approach to reap the benefits of multi-tissue CSD from just single-shell (+b=0) diffusion MRI data*2016.

138. Dhollander T, Raffelt D, Connelly A. *Unsupervised 3-tissue response function estimation from single-shell or multi-shell diffusion MR data without a co-registered T1 image*2016.

139. Jeurissen B, Tournier J-D, Dhollander T, Connelly A, Sijbers J. Multi-tissue constrained spherical deconvolution for improved analysis of multi-shell diffusion MRI data. *NeuroImage.* 2014; 103:411-426.

140. Küpper H, Groeschel S, Alber M, Klose U, Schuhmann MU, Wilke M. Comparison of Different Tractography Algorithms and Validation by Intraoperative Stimulation in a Child with a Brain Tumor. *Neuropediatrics.* 2015; 46(01):072-075.

141. Gong S, Zhang F, Norton I, et al. Free water modeling of peritumoral edema using multi-fiber tractography: Application to tracking the arcuate fasciculus for neurosurgical planning. *PLOS ONE.* 2018; 13(5):e0197056.

142. Barajas RF, Hess CP, Phillips JJ, et al. Super-Resolution Track Density Imaging of Glioblastoma: Histopathologic Correlation. *American Journal of Neuroradiology.* 2013; 34(7):1319-1325.

143. Vul E, Harris C, Winkielman P, Pashler H. Puzzlingly High Correlations in fMRI Studies of Emotion, Personality, and Social Cognition. *Perspectives on Psychological Science.* 2009; 4(3):274-290.

144. Bosma I, Vos MJ, Heimans JJ, et al. The course of neurocognitive functioning in high-grade glioma patients1. *Neuro-Oncology.* 2007; 9(1):53-62.

145. Kazmi F, Soon YY, Leong YH, Koh WY, Vellayappan B. Re-irradiation for recurrent glioblastoma (GBM): a systematic review and meta-analysis. *Journal of Neuro-Oncology.* 2019; 142(1):79-90.

146. Salvati M, Pesce A, Palmieri M, Floriana Brunetto GM, Santoro A, Frati A. The Role and Real Effect of an Iterative Surgical Approach for the Management of Recurrent High-Grade Glioma: An Observational Analytic Cohort Study. *World Neurosurgery.* 2019; 124:e480-e488.

147. Weller M, Reifenberger G. Beyond the World Health Organization classification of central nervous system tumors 2016: what are the new developments for gliomas from a clinician's perspective? *Current Opinion in Neurology.* 2020; 33(6):701-706.

148. Weller M, van den Bent M, Preusser M, et al. EANO guidelines on the diagnosis and treatment of diffuse gliomas of adulthood. *Nature Reviews Clinical Oncology.* 2021; 18(3):170-186.

149. Witzmann K, Raschke F, Troost EGC. MR Image Changes of Normal-Appearing Brain Tissue after Radiotherapy. *Cancers.* 2021; 13(7):1573.

150. Ding Z, Zhang H, Lv X-F, et al. Radiation-induced brain structural and functional abnormalities in presymptomatic phase and outcome prediction. *Human Brain Mapping.* 2018; 39(1):407-427.

151. Zhang F, Daducci A, He Y, et al. Quantitative mapping of the brain's structural connectivity using diffusion MRI tractography: A review. *NeuroImage.* 2022; 249:118870.

152. Yeh F-C, Irimia A, Bastos DCdA, Golby AJ. Tractography methods and findings in brain tumors and traumatic brain injury. *NeuroImage.* 2021; 245:118651.

153. Rosen BQ, Halgren E. A Whole-Cortex Probabilistic Diffusion Tractography Connectome. *eneuro.* 2021; 8(1):ENEURO.0416-0420.2020.

154. Oken MM, Creech RH, Tormey DC, et al. Toxicity and response criteria of the Eastern Cooperative Oncology Group. *American Journal of Clinical Oncology.* 1982; 5(6):649-656.

155. Gilbert MR, Dignam JJ, Armstrong TS, et al. A randomized trial of bevacizumab for newly diagnosed glioblastoma. *N Engl J Med.* 2014; 370(8):699-708.

156. Robbins M, Greene-Schloesser D, Peiffer AM, Shaw E, Chan MD, Wheeler KT. Radiation-induced brain injury: A review. *Frontiers in Oncology.* 2012; 2.

157. Xi L, Moron F. Treatment-related MR imaging findings in patients with glioma after radiotherapy, chemotherapy, and biological therapy. *Clin Oncol.* 2016; 1(1103).

158. Terziev R, Psimaras D, Marie Y, et al. Cumulative incidence and risk factors for radiation induced leukoencephalopathy in high grade glioma long term survivors. *Scientific Reports.* 2021; 11(1):10176.

159. Aerts H, Fias W, Caeyenberghs K, Marinazzo D. Brain networks under attack: robustness properties and the impact of lesions. *Brain.* 2016; 139(12):3063-3083.

160. Stadlbauer A, Buchfelder M, Salomonowitz E, Ganslandt O. Fiber Density Mapping of Gliomas: Histopathologic Evaluation of a Diffusion-Tensor Imaging Data Processing Method. *Radiology.* 2010; 257(3):846-853.

161. Fekonja LS, Wang Z, Aydogan DB, et al. Detecting Corticospinal Tract Impairment in Tumor Patients With Fiber Density and Tensor-Based Metrics. *Frontiers in Oncology.* 2021; 10.

162. Liesche-Starnecker F, Prokop G, Yakushev I, et al. Visualizing cellularity and angiogenesis in newly-diagnosed glioblastoma with diffusion and perfusion MRI and FET-PET imaging. *EJNMMI Research.* 2021; 11(1):72.

163. Stadlbauer A, Pölking E, Prante O, et al. Detection of tumour invasion into the pyramidal tract in glioma patients with sensorimotor deficits by correlation of 18F-fluoroethyl-L-tyrosine PET and magnetic resonance diffusion tensor imaging. *Acta Neurochirurgica.* 2009; 151(9):1061-1069.

164. Stadlbauer A, Hammen T, Buchfelder M, et al. Differences in Metabolism of Fiber Tract Alterations in Gliomas: A Combined Fiber Density Mapping and Magnetic Resonance Spectroscopic Imaging Study. *Neurosurgery.* 2012; 71(2):454-463.

165. Nag S, Manias JL, Stewart DJ. Pathology and new players in the pathogenesis of brain edema. *Acta Neuropathologica.* 2009; 118(2):197-217.

166. Dubois LG, Campanati L, Righy C, et al. Gliomas and the vascular fragility of the blood brain barrier. *Frontiers in Cellular Neuroscience.* 2014; 8.

167. Szerlip N, Rutter C, Ram N, et al. Factors impacting volumetric white matter changes following whole brain radiation therapy. *Journal of Neuro-Oncology.* 2011; 103(1):111-119.

168. Duan F, Cheng J, Jiang J, Chang J, Zhang Y, Qiu S. Whole-brain changes in white matter microstructure after radiotherapy for nasopharyngeal carcinoma: a diffusion tensor imaging study. *European Archives of Oto-Rhino-Laryngology.* 2016; 273(12):4453-4459.

169. Chapman CH, Zhu T, Nazem-Zadeh M, et al. Diffusion tensor imaging predicts cognitive function change following partial brain radiotherapy for low-grade and benign tumors. *Radiotherapy and Oncology.* 2016; 120(2):234-240.

170. Chen W, Qiu S, Li J, et al. Diffusion Tensor Imaging Study on Radiation-induced Brain Injury in Nasopharyngeal Carcinoma during and after Radiotherapy. *Tumori Journal.* 2015; 101(5):487-490.

171. Ravn S, Holmberg M, Sørensen P, Frøkjær JB, Carl J. Differences in supratentorial white matter diffusion after radiotherapy – new biomarker of normal brain tissue damage? *Acta Oncologica.* 2013; 52(7):1314-1319.

172. Chapman CH, Nazem-Zadeh M, Lee OE, et al. Regional Variation in Brain White Matter Diffusion Index Changes following Chemoradiotherapy: A Prospective Study Using Tract-Based Spatial Statistics. *PLOS ONE.* 2013; 8(3):e57768.

173. Henderson F, Abdullah KG, Verma R, Brem S. Tractography and the connectome in neurosurgical treatment of gliomas: the premise, the progress, and the potential. *Neurosurgical Focus FOC.* 2020; 48(2):E6.

174. Dallabona M, Sarubbo S, Merler S, et al. Impact of mass effect, tumor location, age, and surgery on the cognitive outcome of patients with high-grade gliomas: a longitudinal study. *Neuro-Oncology Practice.* 2017; 4(4):229-240.

175. Habets EJJ, Hendriks EJ, Taphoorn MJB, et al. Association between tumor location and neurocognitive functioning using tumor localization maps. *Journal of Neuro-Oncology.* 2019; 144(3):573-582.

176. Hendriks EJ, Habets EJJ, Taphoorn MJB, et al. Linking late cognitive outcome with glioma surgery location using resection cavity maps. *Human Brain Mapping.* 2018; 39(5):2064-2074.

177. Dadario NB, Brahimaj B, Yeung J, Sughrue ME. Reducing the Cognitive Footprint of Brain Tumor Surgery. *Frontiers in Neurology.* 2021; 12.

178. Duffau H. Why brain radiation therapy should take account of the individual structural and functional connectivity: Toward an irradiation “à la carte”. *Critical Reviews in Oncology/Hematology.* 2020; 154:103073.

179. Herbet G, Duffau H. Revisiting the Functional Anatomy of the Human Brain: Toward a Meta-Networking Theory of Cerebral Functions. *Physiological Reviews.* 2020; 100(3):1181-1228.

180. Nieberlein L, Rampp S, Gussew A, Prell J, Hartwigsen G. Reorganization and Plasticity of the Language Network in Patients with Cerebral Gliomas. *NeuroImage: Clinical.* 2023; 37:103326.

181. Samuel N, Vetkas A, Pancholi A, et al. A Network-Based Approach to Glioma Surgery: Insights from Functional Neurosurgery. *Cancers.* 2021; 13(23):6127.

182. Grayson DS, Ray S, Carpenter S, et al. Structural and functional rich club organization of the brain in children and adults. *PLoS One.* 2014; 9(2):e88297.

183. Horn A, Ostwald D, Reisert M, Blankenburg F. The structural–functional connectome and the default mode network of the human brain. *NeuroImage.* 2014; 102:142-151.

184. Koch G, Casula EP, Bonnì S, et al. Precuneus magnetic stimulation for Alzheimer’s disease: a randomized, sham-controlled trial. *Brain.* 2022; 145(11):3776-3786.

185. de Lange SC, Scholtens LH, van den Berg LH, et al. Shared vulnerability for connectome alterations across psychiatric and neurological brain disorders. *Nature Human Behaviour.* 2019; 3(9):988-998.

186. Ojemann JG, Miller JW, Silbergeld DL. Preserved Function in Brain Invaded by Tumor. *Neurosurgery.* 1996; 39(2):253-259.

187. Skirboll SS, Ojemann GA, Berger MS, Lettich E, Winn HR. Functional Cortex and Subcortical White Matter Located within Gliomas. *Neurosurgery.* 1996; 38(4):678-685.

188. Mandal AS, Wiener C, Assem M, et al. Tumour-infiltrated cortex participates in large-scale cognitive circuits. *Cortex.* 2024; 173:1-15.

189. Aabedi AA, Lipkin B, Kaur J, et al. Functional alterations in cortical processing of speech in glioma-infiltrated cortex. *Proceedings of the National Academy of Sciences.* 2021; 118(46):e2108959118.

190. Schiffbauer H, Ferrari P, Rowley HA, Berger MS, Roberts TPL. Functional Activity within Brain Tumors: A Magnetic Source Imaging Study. *Neurosurgery.* 2001; 49(6):1313-1321.

191. Sharma P, Aaroe A, Liang J, Puduvalli VK. Tumor microenvironment in glioblastoma: Current and emerging concepts. *Neuro-Oncology Advances.* 2023; 5(1).

192. Winkler F, Venkatesh HS, Amit M, et al. Cancer neuroscience: State of the field, emerging directions. *Cell.* 2023; 186(8):1689-1707.

193. Monje M, Borniger JC, D'Silva NJ, et al. Roadmap for the Emerging Field of Cancer Neuroscience. *Cell.* 2020; 181(2):219-222.

194. Venkatesh Humsa S, Johung Tessa B, Caretti V, et al. Neuronal Activity Promotes Glioma Growth through Neuroligin-3 Secretion. *Cell.* 2015; 161(4):803-816.

195. Langen K-J, Stoffels G, Filss C, et al. Imaging of amino acid transport in brain tumours: Positron emission tomography with O-(2-[18F]fluoroethyl)-L-tyrosine (FET). *Methods.* 2017; 130:124-134.

196. Galldiks N, Lohmann P, Fink GR, Langen K-J. Amino Acid PET in Neurooncology. *Journal of Nuclear Medicine.* 2023; 64(5):693-700.

197. Kincade JM, Abrams RA, Astafiev SV, Shulman GL, Corbetta M. An Event-Related Functional Magnetic Resonance Imaging Study of Voluntary and Stimulus-Driven Orienting of Attention. *The Journal of Neuroscience.* 2005; 25(18):4593-4604.

198. Corbetta M, Shulman GL. Control of goal-directed and stimulus-driven attention in the brain. *Nature Reviews Neuroscience.* 2002; 3(3):201-215.

199. Johnson DR, Sawyer AM, Meyers CA, O'Neill BP, Wefel JS. Early measures of cognitive function predict survival in patients with newly diagnosed glioblastoma. *Neuro-Oncology.* 2012; 14(6):808-816.

200. Buckingham SC, Campbell SL, Haas BR, et al. Glutamate release by primary brain tumors induces epileptic activity. *Nature Medicine.* 2011; 17(10):1269-1274.

201. Campbell SL, Buckingham SC, Sontheimer H. Human glioma cells induce hyperexcitability in cortical networks. *Epilepsia.* 2012; 53(8):1360-1370.

202. Campbell SL, Robel S, Cuddapah VA, et al. GABAergic disinhibition and impaired KCC2 cotransporter activity underlie tumor-associated epilepsy. *Glia.* 2015; 63(1):23-36.

203. John Lin C-C, Yu K, Hatcher A, et al. Identification of diverse astrocyte populations and their malignant analogs. *Nature Neuroscience.* 2017; 20(3):396-405.

204. Belgers V, Numan T, Kulik SD, et al. Postoperative oscillatory brain activity as an add-on prognostic marker in diffuse glioma. *Journal of Neuro-Oncology.* 2020; 147(1):49-58.

205. Derks J, Wesseling P, Carbo EWS, et al. Oscillatory brain activity associates with neuroligin-3 expression and predicts progression free survival in patients with diffuse glioma. *Journal of Neuro-Oncology.* 2018; 140(2):403-412.

Danksagung

Diese Danksagung ist all jenen gewidmet, die an der vorliegenden Arbeit beteiligt waren, das Entstehen dieser Arbeit ermöglichten und mich auf dem Weg meiner Promotion begleitet haben.

Mein erster, ganz besonderer Dank gilt meinen hochgeschätzten Betreuern, Herrn Prof. Dr. Norbert Galldiks und Herrn Prof. Dr. Martin Kocher. Ich bin außerordentlich glücklich und dankbar, dass Sie sich bereit erklärten, mich auf dem Weg meiner Promotion zu begleiten und zu unterstützen! Mit all Ihrer Expertise und Erfahrung haben Sie den Weg geebnet und die Weichen für diese Arbeit gestellt. Ohne Sie wäre diese nicht möglich gewesen! Sie standen mir immer bei all meine Anliegen und Herausforderungen mit Rat und Tat zur Seite. Darüber hinaus haben Sie mich stets gefördert und mir Ihr Vertrauen geschenkt, so dass ich mich sowohl fachlich als auch persönlich immens weiterentwickeln konnte. An dieser Stelle möchte ich mich ganz herzlich bei Ihnen, Herrn Prof. Dr. Galldiks und Herrn Prof. Dr. Kocher, für Ihre großartige Unterstützung und Ihr enormes Engagement bedanken!

In diesem Sinne möchte ich mich auch ganz herzlich bei meinen beiden IPHS-Tutoren, Herrn Prof. Dr. Peter Weiss-Blankenhorn und Herrn Prof. Dr. Thilo van Eimeren, bedanken! Sie haben mich ebenfalls während meiner Promotion mit allerlei hilfreichen Anregungen und Ratschlägen im Bereich der Planung und Durchführung dieser Arbeit unterstützt. Insbesondere möchte ich mich nochmals in aller Form bei Herrn Prof. Dr. Weiss-Blankenhorn für seine umfassende Unterstützung während meiner gesamten Tätigkeit am INM-3 bedanken, herzlichen Dank!

Ein weiterer großer Dank geht an Herrn Prof. Dr. Gereon Fink für die Möglichkeit und die hervorragenden Rahmenbedingungen, die er mir an seinem Institut geboten hat, um diese Arbeit entstehen zu lassen. Es war mir eine große Freude, Teil des INM-3 zu sein! Ich habe die Arbeitsatmosphäre am Institut immer sehr geschätzt und als äußerst produktiv empfunden. Ich danke Ihnen für die freundliche Hilfsbereitschaft, die Sie mir jederzeit entgegengebracht haben! Auch Ihnen, lieber Herr Prof. Dr. Fink, ein herzliches Dankeschön!

Ich möchte mich außerdem ganz herzlich bei allen bedanken, die mich bei meiner Promotion unterstützt haben und an den einzelnen Forschungsprojekten beteiligt waren. Dabei möchte ich zwei Personen ganz besonders hervorheben, nämlich Herrn Prof. Dr. Karl-Josef Langen und Herrn Priv.-Doz. Dr. Philipp Lohmann. Sie haben mich immer mit viel Herzblut beraten und mir mit hervorragenden Anregungen weitergeholfen. An dieser

Stelle ist es mir ein besonderes Anliegen, mich noch einmal bei Herrn Prof. Dr. Langen zu bedanken, der mich auf meinem beruflichen Weg stets förderte und mich seinerzeit Herrn Prof. Dr. Galldiks als Doktorand empfahl. Auf diese Weise hat er mir die Promotion überhaupt erst ermöglicht, herzlichen Dank!

Ebenso möchte ich mich bei all denen bedanken, die zwar nicht direkt an meiner Arbeit beteiligt waren, mir aber eine schöne Zeit am Forschungszentrum bereitet haben. Besonders gerne erinnere ich mich an die vielen geselligen Mittagspausen, an die Konferenzen, die mir ermöglicht wurden, oder an die spaßigen Abende der INM-3-Retreats, die mir viel Freude bereitet haben.

Sehr am Herzen liegen mir meine letzten Danksagungen, die zum einen meiner Großmutter, Christa Friedrich und meinem verstorbenen Großvater, Peter Friedrich, gelten, ohne die ich heute nicht an diesem Punkt meines Lebens stehen würde. Sie haben immer an mich geglaubt und mich auf meinem Lebensweg ohne Zögern und auf so vielfältige Weise unterstützt. Ebenso möchte ich mich bei meiner Partnerin, Tabea Wieland, von ganzem Herzen dafür bedanken, dass Du mir immer zur Seite standest. Wie schon bei meiner Bachelor- und Masterarbeit hast Du mir den Rücken freigehalten und mich unterstützt, wo Du nur konntest, das weiß ich sehr zu schätzen! Ich liebe Dich mein Schatz und bin glücklich Dich in meinem Leben zu haben!

Geleistete Beiträge an den Publikationen

Die für die kumulative Dissertation verwendete Publikationen sind thematisch miteinander verknüpft und beschäftigen sich mit dem Einfluss von Hirntumoren auf die strukturelle und funktionelle Konnektivität im Gehirn. Im Folgenden werden die Beiträge der Mitautoren sowie mein eigener Beitrag zu den Veröffentlichungen im Einzelnen beschrieben:

Bei den zugrundeliegenden Publikationen handelt es sich um drei retrospektive Analysen basierend auf einem Patientenkollektivs, das von unserer Forschungsgruppe bereits in früheren Studien genutzt wurde. Die Studie zur funktionellen Konnektivität (3. Veröffentlichung) beschränkt sich dabei auf Patienten mit einem PET-positiven Tumor. Innerhalb aller drei Projekte konnte somit auf die bereits erhobenen MR- und PET-Rohbilddaten sowie auf die Befunde der Patienten zurückgriffen werden. Alle Patienten waren im Rahmen einer Nachuntersuchung mittels PET/MR-Hybridbildgebung mit der radioaktiv markierten Aminosäure FET an das Forschungszentrum Jülich überwiesen worden. Rekrutiert wurden sie seinerzeit von Herrn Prof. Dr. Fink, Herrn Prof. Dr. Kocher, Herrn Prof. Dr. Galldiks, Herrn Prof. Dr. Langen, Herrn Prof. Dr. Goldbrunner, Herrn Prof. Dr. Mottaghy, Herrn Prof. Dr. Ruge und Frau Dr. Weiss Lucas. Die Nachuntersuchungen wurden von Herrn Prof. Dr. Kocher, Frau Dr. Stoffels und Herrn Dr. Filss durchgeführt. Die dafür notwendigen MR- und PET-Messverfahren wurden von Herrn Prof. Dr. Langen, Herrn Prof. Dr. Shah, Herrn Priv.-Doz. Dr. Lohmann, Herrn Dr. Farrher und Herrn Dr. Lerche entwickelt und für die Scanner am Institut etabliert.

1. Publikation: *Alterations in white matter fiber density associated with structural MRI and metabolic PET lesions following multimodal therapy in glioma patients*, veröffentlicht am 14. November 2022 in Frontiers in Oncology (IF 5.7).

Die initiale Idee für das Forschungsprojekt stammte von meinem Betreuer, Herrn Prof. Dr. Kocher. In Absprache mit ihm und meinem zweiten Betreuer, Herrn Prof. Dr. Galldiks, habe ich das Projekt ausgearbeitet und umgesetzt. Abgesehen von der Hybrid PET/MR-Bildgebung habe ich die in der Publikation beschriebenen Methoden allesamt selbstständig angewendet. Besonders hervorheben möchte hierbei die von mir etablierte Traktografie-Pipeline zur Untersuchung der Faserdichte bei Patienten mit Hirntumoren, die ich sowohl bei den untersuchten Patienten als auch bei der Kontrollgruppe angewendet habe. Die dafür notwendigen Rohbilddaten der Kontrollgruppe stammen aus der am Forschungszentrum Jülich durchgeführten 1000Brains-Studie und wurden freundlicherweise von Frau Prof. Dr. Dr. Caspers zur Verfügung gestellt. Alle weiteren

Daten für das Projekt habe ich selbst erhoben, statistisch ausgewertet, interpretiert und abschließend beurteilt. Der erste Entwurf des Manuskripts, einschließlich aller Abbildungen, wurde von mir erstellt und nach entsprechender Korrektur durch Herrn Prof. Dr. Galldiks und Herrn Prof. Dr. Kocher fertiggestellt. Anschließend wurden noch kleinere Korrekturvorschläge der übrigen Koautoren eingearbeitet.

2. Publikation: *Structural connectome-based predictive modeling of cognitive deficits in treated glioma patients*, veröffentlicht am 15. November 2023 in Neuro-Oncology Advances (IF 3.5).

Die zweite Projektidee stammte ebenfalls von Herrn Prof. Dr. Kocher und wurde von mir erneut in Abstimmung mit meinen Betreuern geplant und realisiert. Das Projekt baut dabei auf die von mir im Rahmen des ersten Projekts erhobenen Konnektivitätsdaten auf. Um die Auswirkungen struktureller Konnektivitätsveränderungen auf die Kognition von behandelten Patienten mit Hirntumoren untersuchen zu können, habe ich das in der Arbeit vorgestellte Connectome-based Predictive Modeling (CPM) Verfahren eigenständig für die strukturellen Konnektivitätsdaten adaptiert und erweitert, so dass es zur Identifizierung kognitiv kritischer Verbindungen verwendet werden konnte. Alle Patienten wurden daraufhin von mir entsprechend den beschriebenen Methoden ausgewertet, statistisch analysiert und abschließend beurteilt. Ausgenommen sind die Messungen der PET/MR-Hybridbildgebung und die Bewertung der kognitiven Leistung der Patienten, die ich nicht selbst durchgeführt habe. Die kognitive Leistung der Patienten erfasste Herr Prof. Dr. Kocher am Tag der Nachuntersuchung anhand geeigneter Tests. Die zugehörigen Kontrolldaten gesunder Probanden stammen wiederum aus der 1000Brain-Studie und wurden von Frau Prof. Dr. Dr. Caspers zur Verfügung gestellt. Auch der erste Entwurf des zweiten Manuskripts, einschließlich aller Abbildungen, wurde von mir verfasst und, wie beim ersten Projekt, anschließend von Herrn Prof. Dr. Galldiks und Herrn Prof. Dr. Kocher korrigiert. Im Anschluss daran erhielten wieder alle weiteren Koautoren die Möglichkeit, das Manuskript zu korrigieren.

3. Publikation: *Functional connectivity between tumor region and resting-state networks as imaging biomarker for overall survival in recurrent gliomas diagnosed by FET PET*, veröffentlicht am 29. Januar 2025 in Neuro-Oncology Advances (IF 3.7).

Die dritte Projektidee wurde von Herrn Prof. Dr. Norbert Galldiks eingebracht und abermals gemeinsam mit Herrn Prof. Dr. Kocher konzipiert und schließlich von mir umgesetzt. Alle im Rahmen dieser Studie neu gewonnenen Daten wurden von mir selbst erfasst. Einschließlich der funktionellen Konnektivität zwischen Tumorregion und Ruhezustandsnetzwerken unter Verwendung der „Seed-based Dual Regression

Analysis“, einer modifizierten Version der „Seed-based Correlation Analysis“, die von mir eigenständig für die untersuchten Patienten etabliert und durchgeführt wurde. Ebenso wie die anschließende statistische Auswertung (einschließlich der Überlebensanalyse), Interpretation und abschließende Beurteilung aller Daten. Die zugrunde liegenden Überlebensdaten stammen aus insgesamt fünf Universitätskliniken und wurden von Herrn Prof. Dr. Steinbach (Frankfurt), Herrn Prof. Dr. Sabel (Düsseldorf), Herrn Prof. Dr. Herrlinger (Bonn), Herrn Prof. Dr. Piroth (Wuppertal) und Herrn Dr. Werner (Köln) bereitgestellt. Die Rohfassung des Manuskripts, samt aller Abbildungen, wurde von mir erstellt und von Herrn Prof. Dr. Galldiks und Herrn Prof. Dr. Kocher korrigiert und ergänzt. Geringfügige Korrekturen der anderen Koautoren wurden nachträglich eingearbeitet.

Lebenslauf

Praxiserfahrung

04/2021 - 03/2025 **Doktorand, Arbeitsgruppe Translationale Bildgebung in der Neuro-Onkologie, Institut für Neurowissenschaften und Medizin 3, Forschungszentrum Jülich GmbH, Jülich, Deutschland**

Erstellung meiner Dissertation zum Thema Konnektivität bei Patienten mit Gliomen sowie die Mitarbeit an weiteren Forschungsprojekten

04/2020 - 03/2021 **Masterstudent, Arbeitsgruppe Hirntumore, Institut für Neurowissenschaften und Medizin 4, Forschungszentrum Jülich GmbH, Jülich, Deutschland**

Anfertigung meiner Masterarbeit „Structural connectivity changes in malignant glioma patients“; Note: 1,3

03/2019 - 08/2019 **Wissenschaftlicher Mitarbeiter, Labor Medizinische Physik, Fachhochschule Aachen, Jülich, Deutschland**

Auslegung eines Gammastrahlendetektorsystems für die Sondierung mit Neutronen zur Detektion von Sprengstoffen in Zusammenarbeit mit der P-H-Röhll NRW GmbH

03/2018 - 08/2018 **Wissenschaftlicher Mitarbeiter, Arbeitsgruppe Hirntumore, Institut für Neurowissenschaften und Medizin 4, Forschungszentrum Jülich GmbH, Jülich, Deutschland**

Assistenz bei der präklinischen Evaluierung eines PET-Tracers, einschließlich histologischer Färbungen, Mikroskopie und Pflege von Versuchstieren

09/2017 - 02/2018 **Bachelorstudent, Arbeitsgruppe Hirntumore, Institut für Neurowissenschaften und Medizin 4, Forschungszentrum Jülich GmbH, Jülich, Deutschland**

Anfertigung meiner Bachelorarbeit „Vergleich zwischen einer Template- und Transmissions-Schwächungskorrektur für einen Hybrid PET/MRT Scanner unter dem Aspekt der Hirntumordiagnostik“; Note: 1,3

03/2017 - 08/2017 **Praktikant, Arbeitsgruppe Hirntumore, Institut für Neurowissenschaften und Medizin 4, Forschungszentrum Jülich GmbH, Jülich, Deutschland**

Assistenz bei histologischen Färbungen, Kultivierung von Tumorzellen, Autoradiographie und PET-Messungen

08/2014 - 09/2014 **Praktikant, MHS-Medizintechnik, Mönchengladbach, Deutschland**

Wartung und Vertrieb von medizinischen Beatmungsgeräten

07/2014 - 08/2014 **Praktikant, Städtische Kliniken Mönchengladbach, Mönchengladbach, Deutschland**

Ausübung von pflegerischen und medizinischen Maßnahmen direkt am Patienten

Ausbildung

04/2021 - 09/2025 **Universität zu Köln, Köln, Deutschland**
Doktor/PhD in Health Sciences (Doktorandenprogramm „Interdisciplinary Program Health Sciences“ [IPHS]), Juli 2025, Abschlussnote: magna cum laude (0,3)

09/2018 - 03/2021 **Fachhochschule Aachen, Jülich, Deutschland**
Master of Science in „Nuclear Applications“, Schwerpunkt Medizinphysik, Februar 2021, Abschlussnote: 1,4

09/2014 - 03/2018 **Fachhochschule Aachen, Jülich, Deutschland**
Bachelor of Engineering in „Biomedizinische Technik“ mit Praxissemester, Februar 2018, Abschlussnote: 2,1

08/2005 - 07/2014 **Gesamtschule Espenstraße, Mönchengladbach, Deutschland**
Allgemeine Hochschulreife, Juni 2014, Abschlussnote: 1,9

Konferenzbeiträge

11/2024 **Vortrag**, **29. Jahrestagung - Society for Neuro-Oncology (SNO), Houston, USA**
Referiert über funktionelle Tumorkonnektivität und ihre Bedeutung für das Gesamtüberleben von Patienten

10/2024 **Vortrag, 19. Jahrestagung - European Association of Neuro-Oncology (EANO), Glasgow, Großbritannien**
Referiert über funktionelle Tumorkonnektivität und ihre Bedeutung für das Gesamtüberleben von Patienten

11/2023 **Vortrag**, **28. Jahrestagung - Society for Neuro-Oncology (SNO), Vancouver, Kanada**
Referiert über den Zusammenhang zwischen struktureller Hirnkonnektivität und kognitiven Defiziten bei Patienten mit Gliomen

09/2023 **Vortrag und Poster, 18. Jahrestagung - European Association of Neuro-Oncology (EANO), Rotterdam, Niederlande**
Referiert über den Zusammenhang zwischen struktureller Hirnkonnektivität und kognitiven Defiziten bei Patienten mit Gliomen

09/2022 **Zwei Vorträge, 17. Jahrestagung - European Association of Neuro-Oncology (EANO), Wien, Österreich**
Referiert über die Auswirkungen des Medikaments „Cilengitide“ auf das Auftreten bestimmter behandlungsbedingter Hirnveränderungen sowie über die veränderte strukturelle Hirnkonnektivität von Patienten mit Gliomen

Auszeichnungen

11/2023 **Auszeichnung für herausragende Leistungen im Bereich „Neurology of Cancer“, 28. Jahrestagung - Society for Neuro-Oncology (SNO), Vancouver, Kanada**
In Anerkennung meines auf der 28. Jahrestagung vorgestellten Abstracts

Vereine

seit 08/2021 **SNO - Society for Neuro-Oncology**
Bietet Mitgliedern u.a. die Möglichkeiten zum Austausch von Forschungsergebnissen, Zugang zu Bildungsressourcen und Maßnahmen zur Karriereförderung

Publikationsliste

01/2025 **Friedrich, M.**, Werner, J.-M., Steinbach, J. P., Sabel, M., Herrlinger, U., Piroth, M., Stoffels, G., Filss, C. P., Lohmann, P., Shah, N. J., Ruge, M. I., Mottaghy, F. M., Goldbrunner, R., Langen, K.-J., Fink, G. R., Kocher, M., & Galldiks, N. (2025). Functional connectivity between tumor region and resting-state networks as imaging biomarker for overall survival in recurrent gliomas diagnosed by FET PET. *Neuro-Oncology Advances*.

06/2024 Galldiks N., Lohmann P., **Friedrich M.**, Werner J.-M, Stetter I., Wollring M., Ceccon G., Stegmayr C., Krause S., Fink G.R., Law I., Langen K.-J., & Joerg-Christian Tonn J.-T. (2024). PET imaging of gliomas: Status quo and quo vadis?. *Neuro-Oncology.*

01/2024 Flies, C. M., **Friedrich, M.**, Lohmann, P., van Garderen, K. A., Smits, M., Tonn, J.-C., Weller, M., Galldiks, N., & Snijders, T. J. (2024). Treatment-associated imaging changes in newly diagnosed *MGMT* promoter-methylated glioblastoma undergoing chemoradiation with or without cilengitide. *Neuro-Oncology*, *26*(5), 902-910.

11/2023 **Friedrich, M.**, Filss, C. P., Lohmann, P., Mottaghy, F. M., Stoffels, G., Weiss Lucas, C., Ruge, M. I., Shah, N. J., Caspers, S., Langen, K.-J., Fink, G. R., Galldiks, N., & Kocher, M. (2023). Structural connectome-based predictive modeling of cognitive deficits in treated glioma patients. *Neuro-Oncology Advances*, *6*(1).

02/2023 Heinzel, A., Mottaghy, F. M., Filss, C., Stoffels, G., Lohmann, P., **Friedrich, M.**, Shah, N. J., Caspers, S., Lucas, C. W., Ruge, M. I., Galldiks, N., Fink, G. R., Langen, K.-J., & Kocher, M. (2023). The impact of brain lesions on health-related quality of life in patients with WHO CNS grade 3 or 4 glioma: a lesion-function and resting-state fMRI analysis. *Journal of Neuro-Oncology*, *161*(3), 643-654.

12/2022 Galldiks, N., Wollring, M., Werner, J.-M., **Friedrich, M.**, Fink, G. R., Langen, K.-J., & Lohmann, P. (2022). An updated review on the diagnosis and assessment of post-treatment relapse in brain metastases using PET. *Expert Review of Neurotherapeutics*, *22*(11-12), 915-921.

11/2022 **Friedrich, M.**, Farrher, E., Caspers, S., Lohmann, P., Lerche, C., Stoffels, G., Filss, C. P., Weiss Lucas, C., Ruge, M. I., Langen, K.-J., Shah, N. J., Fink, G. R., Galldiks, N., & Kocher, M. (2022). Alterations in white matter fiber density associated with structural MRI and metabolic PET lesions following multimodal therapy in glioma patients. *Frontiers in Oncology*, *12*.

Eidesstattliche Versicherung

Hiermit versichere ich an Eides statt, dass ich die vorliegende Dissertationsschrift selbstständig und ohne die Benutzung anderer als der angegebenen Hilfsmittel angefertigt habe. Alle Stellen - einschließlich Tabellen, Karten und Abbildungen -, die wörtlich oder sinngemäß aus veröffentlichten und nicht veröffentlichten anderen Werken im Wortlaut oder dem Sinn nach entnommen sind, sind in jedem Einzelfall als Entlehnung kenntlich gemacht. Ich versichere an Eides statt, dass diese Dissertationsschrift noch keiner anderen Fakultät oder Universität zur Prüfung vorgelegen hat; dass sie - abgesehen von unten angegebenen Teilpublikationen - noch nicht veröffentlicht worden ist sowie, dass ich eine solche Veröffentlichung vor Abschluss der Promotion nicht ohne Genehmigung der / des Vorsitzenden des IPHS-Promotionsausschusses vornehmen werde. Die Bestimmungen dieser Ordnung sind mir bekannt. Die von mir vorgelegte Dissertation ist von Herrn Univ.-Prof. Dr. med. Norbert Galldiks und Herrn Prof. Dr. med. Martin Kocher betreut worden.

Darüber hinaus erkläre ich hiermit, dass ich die Ordnung zur Sicherung guter wissenschaftlicher Praxis und zum Umgang mit wissenschaftlichem Fehlverhalten der Universität zu Köln gelesen und sie bei der Durchführung der Dissertation beachtet habe und verpflichte mich hiermit, die dort genannten Vorgaben bei allen wissenschaftlichen Tätigkeiten zu beachten und umzusetzen.

Übersicht der Publikationen:

1. *Alterations in white matter fiber density associated with structural MRI and metabolic PET lesions following multimodal therapy in glioma patients, veröffentlicht am 14. November 2022 in Frontiers in Oncology (IF 5.7).*
2. *Structural connectome-based predictive modeling of cognitive deficits in treated glioma patients, veröffentlicht am 15. November 2023 in Neuro-Oncology Advances (IF 3.5).*
3. *Functional connectivity between tumor region and resting-state networks as imaging biomarker for overall survival in recurrent gliomas diagnosed by FET PET, veröffentlicht am* 29. Januar 2025 *in Neuro-Oncology Advances (IF 3.7).*

Ich versichere, dass ich alle Angaben wahrheitsgemäß nach bestem Wissen und Gewissen gemacht habe und verpflichte mich, jedmögliche, die obigen Angaben betreffenden Veränderungen, dem IPHS-Promotionsausschuss unverzüglich mitzuteilen.

15.07.2025	Michel Friedrich .....
Datum	*Unterschrift*